ASSESSMENT OF HEALTH-COST EXTERNALITIES OF AIR POLLUTION CAUSED BY TRANSIT SHIP TRAFFIC IN ISTANBUL

by

Oğuz Sarıgül

B.Sc. in Chemical Engineering, İstanbul Technical University, 2010

Submitted to the Institute of Environmental Sciences

in partial fulfillment of the requirements for the degree of

Master of Science

in

Environmental Technology

Boğaziçi University

2019

ASSESSMENT OF HEALTH-COST EXTERNALITIES OF AIR POLLUTION
CAUSED BY TRANSIT SHIP TRAFFIC IN ISTANBUL

APPROVED BY:

Prof. Dr. Nadim Copty ....
Thesis Advisor

Assist. Prof. Dr. İrem Daloğlu Çetinkaya ....

Assist. Prof. Dr. Yiğit Can Altan ....

DATE OF APPROVAL: 03/12/2019

ACKNOWLEDGEMENTS

I would like to express my sincere gratitude to my advisor Prof. Dr. Nadim Copty for his valuable support, persistent help and most imporatantly his patience. Without him this thesis would never be completed.

I would also like to express my gratitude to my jury members Assist. Prof. Dr. İrem Daloğlu and Assist. Prof. Dr. Yiğit Can Altan for their help and suggestions. And special thanks to Prof. Dr. Emre Otay for his valuable comments and suggestions.

I would like to thank my friends from the Chemical Engineering Faculty and the Institute of Environmental Sciences F. Öykü Sefiloğlu, Batuhan Burç Türkoğlu and Özgücan Eken Türkoğlu for their friendship and support throughout my higher education.

Finally, I would like to express my very profound gratitude to my beloved family and Hande Coşkun who always believed in me, always were there and will always be whenever I need them. I owe you everything.

ABSTRACT

ASSESSMENT OF HEALTH-COST EXTERNALITIES OF AIR POLLUTION CAUSED BY TRANSIT SHIP TRAFFIC IN ISTANBUL

Air pollution has become a leading environmental concern as a result of rapid urbanization in recent decades. The pollutants of most concern relating to the burning of fossil fuels include sulphur dioxide (SO_2), nitrogen oxides (NO_2) carbon monoxide (CO) and particulate matter (PM). The purpose of this study is to evaluate the contribution of transit marine traffic through the Bosphorus (Istanbul Strait) on the air quality of Istanbul. Atmospheric emissions originating from ships passing through the Bosphorus were computed and the EPA-approved CALPUFF atmospheric dispersion modelling computer program was used to estimate the air pollutant concentration distributions resulting from maritime traffic. The corresponding health impacts and related health costs due to emissions from maritime traffic are estimated using the EVA (Economic Valuation of Air pollution) methodology.

The results show that, ship emissions have major effect on the overall air quality. Along the Bosphorus strait, the yearly average impact due to ship emissions is upto 60 % of the SO_2 Turkish air quality standard, nearly 35 % of the NO_2 Turkish air quality standard and approximately 2.5 % of the PM_{10} Turkish air quality standard. The corresponding health impacts expressed in morbidity and premature mortality estimates as significant. It is estimated the transit maritime traffic through the Bosphorus is causing about 2,540,000 adverse health incidents, the vast majority are asthma. More severe morbidity impacts include 47 cases of lung cancer and 116 cases of congestive heart failure. The model also estimates 69 cases of acute death and 2255 of YOLL (years of life lost). The total associated health-related costs are estimated to be 83.3 million euros. Given the proximity of large populations to the Bosphorus strait and the large volume of maritime traffic that passes thorugh it, there is a need to impose stricter standards on ship stack emissions.

ÖZET

İSTANBUL'DA TRANSİT GEMİ TRAFİĞİNİN SEBEP OLDUĞU HAVA KİRLİLİĞİNİN SAĞLIK VE MALİYET AÇISINDAN DEĞERLENDİRİLMESİ

Hava kirliliği, son yıllarda hızlı kentleşmenin bir sonucu olarak önde gelen çevresel bir sorun haline gelmiştir. Fosil yakıtların yanmasıyla ilgili en fazla önem taşıyan kirleticiler arasında kükürt dioksit (SO_2), azot oksitler (NO_2) karbon monoksit (CO) ve partikül madde (PM) bulunur. Bu çalışmanın amacı, İstanbul Boğazı'ndaki transit deniz trafiğinin İstanbul'un hava kalitesine olan etkisini değerlendirmektir. Boğaz'dan geçen gemilerden kaynaklanan atmosferik emisyonlar hesaplanmıştır. Deniz trafiğinden kaynaklanan hava kirletici konsantrasyon dağılımını tahmin etmek için EPA onaylı CALPUFF atmosferik dağılım modelleme bilgisayar programı kullanılmıştır. Deniz trafiğinden kaynaklanan emisyonların sağlık etkileri ve buna bağlı sağlık maliyetleri, EVA metodolojisi kullanılarak tahmin edilmiştir.

Sonuçlar, gemilerin genel SO_2 emisyonlarının % 60'ına, NO_2 emisyonlarının yaklaşık % 35'ine ve yıllık PM_{10} emisyonlarının yaklaşık % 2,5'ine kadar önemli bir paya sahip olmasıyla toplam hava kalitesi üzerinde büyük bir etkiye sahip olduğunu göstermektedir. Deniz trafiğinin yaklaşık 2,540,000 sağlık vakasına neden olduğu tahmin edilmektedir, ve bunların büyük çoğunluğu astımdır. Daha ciddi morbidite etkileri 47 akciğer kanseri ve 116 kalp-damar tıkanıklığı vakasını içerir. Model ile ayrıca, 69 akut ölüm vakası ve 2255 erken ölümlere bağlı kaybedilmiş yıl olduğu tahmin edilmiştir. Sağlıkla ilgili toplam maliyetin 83,3 milyon Euro olduğu tahmin edilmiştir. Boğaza yakın yaşayan nüfus yoğunluğunun fazlalığı ve deniz trafiğinin hacmi boyutu göz önüne alındığında, gemi baca emisyonlarına daha katı standartlar getirilmesine ihtiyaç bulunmaktadır.

TABLE OF CONTENTS

LIST OF FIGURES

LIST OF TABLES

LIST OF SYMBOLS/ABBREVIATIONS

Symbol	Explanation
NO_2	Nitrogen Dioxide
NO_2	Nitrogen Dioxide
H_2S	Hydrogen Sulfide
CH_3SCH3	Dimethyl sulfide
CS_2	Carbon disulfide
OCS	Carbonyl Sulfide
SO_2	Sulfur dioxide
N_2O	Dinitrogen monoxide
NO	Nitric Oxide
NO_2	Nitrogen dioxide
HNO_3	Nitric Acid
CO	Carbon Monooxide
CO_2	Carbon diooxide
HCFC	Hydrochlorofluoro carbons
CFC	Chlorofluro carbon
HFC	Hydrofluoro carbons

Abbreviation	Explanation
µm	Micrometer
µm	Micrometer
kW	Kilowatt
T	Temperature
P	Power Engine
LF	Load Factor
GT	Gross Tonnage
FC	Fuel Consumption
ST	Steam Turbine
GT	Gas Turbine
RO	Residuel Oil
HFO	High Fuel Oil

MDO	Marine Diesel Oil
MGO	Marine Gasoline Oil
AE	Auxilary Engine
SSD	Slow Speed Diesels
MSD	Medium Speed Diesels
HSD	High Speed Diesels
SFC	Specific Fuel Consumption
WHO	The World Health Organization
IHME	Institute for Health Metric and Evaluation
PM	Particulate Matter
IHD	Ischaemic Heart Disease
COPD	Chronic Obstructive Pulmonary Disease
ALRI	Acute Lower Respiratory Infection
MassDEP	Massachusetts Department of Environmental
CTDMPLUS	Complex Terrain Dispersion Model Plus
EPA	Environmental Protection Agency
PRIME	Plume Rise Model Enhancements
NWP	Numerical Weather Prediction
DEHM	Eulerian Hemispheric Model
EVA	Economic Valuation of air pollution
GEOS	Goddard Earth Observing System
CMAQ	The Community Multi-scale Air Quality
ENTEC	Environmental Engineering Consultancy
STEAM	Ship Traffic Emission Assessment Model
TurkStat	Turkish Statistical Institute
CTDMPLUS	Complex Terrain Dispersion Model
USGS	United States Geological Survey
NCDC	National Center for Atmospheric Research
ESRL	Earth System Research Laboratory
SECA	SulfurEmissionControlArea
YOLL	Years of life lost
WRF	Weather Reseach and Forecasting

1. INTRODUCTION

Air pollution is defined as the contamination of the atmosphere with emission of substances in quantities which can have adverse effects on human health, the environment or property. Air pollution can be caused by both human activities and natural sources. Some of the human activities-also called anthropogenic activities- that cause air pollution are power plants, transportation, industry, incineration of solid wastes, landfills, farms/agricultural sources. On the other hand, natural phenomena leading to atmospheric pollution include forest fires, volcanic eruptions, meteors, and emission from oceans or the soil.

Air pollutants can be broadly categorized according to its content into the following categories:

- Sulfur containing compounds, such as H_2S, CH_3SCH3, CS_2, OCS and SO_2
- Nitrogen containing compounds, such as N_2O, NO, NO_2 HNO_3 and NH_3
- Carbon containing compounds, such as CH_4, volatile organic compounds, CO and CO_2
- Halogen containing compounds, such as: Chloroflurocarbons (CFCs), Hydrochlorofluorocarbons (HCFCs), Hydrofluorocarbons (HFCs), Perhalocarbons, and Halons
- Ozone
- Particulate matter (aerosols)

Exposure to pollution has evolved into a dominant risk factor worldwide. The World Health Organization (WHO) reports that air pollution is a major threat to human health and the ecosystem. The Lancet Commission on pollution and health data estimate that exposure to pollution was responsible for an estimate of 9 million premature deaths in 2015, placing it in the first place among the major risk factor and causes (Figure 1.1.) (Landrigan et al., 2018). Using data from the Institute for Health Metric and Evaluation (IHME), The Lancet Commission on pollution and health report also states that the air pollution has the largest contribution to global number of premature deaths compared to other pollution risk factors (Figure 1.2.). Premature deaths attributed to $PM_{2.5}$ (particulate matter of size 2-5 μm) only was estimated to be 4.2 million in 2015 and is estimated to increase to 6.6 million in 2050 globally (Landrigan et al., 2018). Exposure to air pollution, both indoor or urban, increases the risk of diseases such as, ischaemic heart disease (IHD), stroke, chronic obstructive pulmonary disease (COPD), lung cancer, and acute lower respiratory infection (ALRI) in children (WHO (World Health Organization), 2018).

Urban air pollution has become an important concern as a result of the rapid growth of cities. More than half of the world's population is living in cities where energy consumption, industrial activities and traffic is concentrated. These building blocks of urban areas are the main sources of air pollution; as a result, studying health impacts from air pollution, particularly in urban areas, gained importance in recent years.

Air pollution is not only associated with health risks, it also has an economic burden. Air pollution causes productivity losses and healthcare costs. Productivity losses consist of time lost from work or school and decreased economic productivity. Healthcare costs includes, hospital, physician, medication costs and other services like management and insurance costs. Productivity and health costs can also cause significant emotitional and societal costs. Assessment of the levels of air pollution, their health and costs impacts is crucial for taking the optimal action to alleviate the impacts of this problem. In order to increase the functional worth of the assessments of health-related external costs caused by air pollution, both mortality and non-mortal impacts must be included into the assessment. The burden of the negative health impact should be expressed in a unit that also can be used for assessing the benefits of any interventions, thus allowing for unbiased independent evaluation of any intervention. Air pollution analysis for urban areas is particularly important, since urban areas are responsible for 85% of global economic activities (Murray and Lopez, 1997).
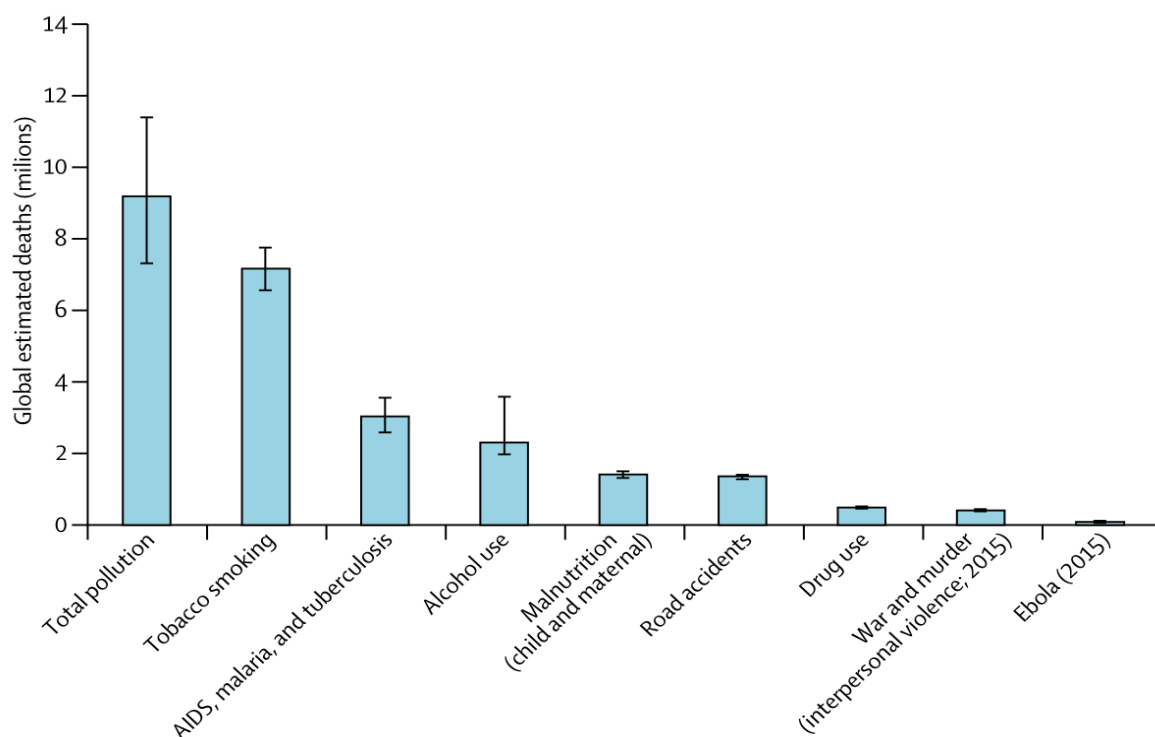
Figure 1.1. Global estimated premature deaths by major risk factors and causes in 2015 (Landrigan et al., 2018).

Furthermore, in addition to adverse effects to human health and economy, air pollution causes several environmental problems such as, acid rain, haze, eutrophication, ozone depletion, crop and forest damage and global climate change (MassDEP (Massachusetts Department of Environmental Protection, 2016).
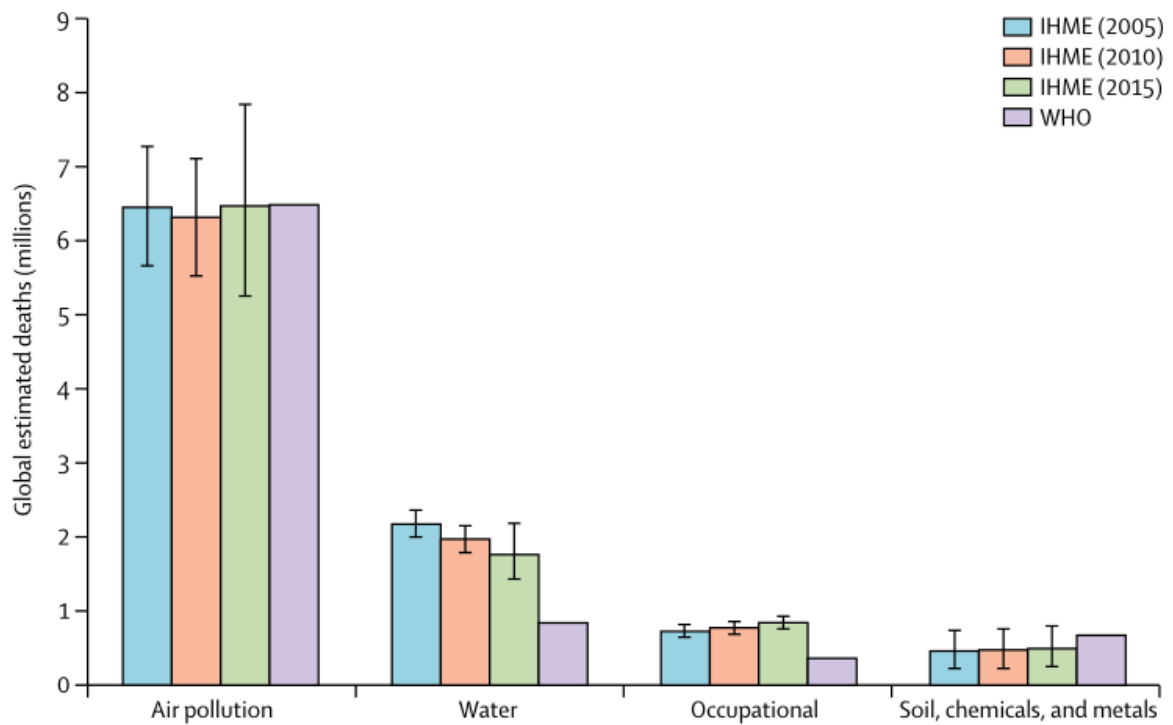
Figure 1.2. Global estimated deaths by pollution risk factor in 2015 (Landrigan et al., 2018).

Atmospheric dispersion modelling is an important step in estimating air pollution levels due to pollutant emissions into the atmosphere. Dispersion models identify potential pathways between pollution sources and human or environmental receptors and quantify the impact of these sources at the receptors. These mathematical models simulate dispersion and advection transport processes and the chemistry and reactions of pollutants in the atmosphere.

The burning of fossil fuels is the most significant source of atmospheric pollution. Fossil fuel burning is used mostly for vehicular, maritime and air transport, heating, energy generation and industrial activity. The pollutants of most concern relating to the burning of fossil fuels include sulphur dioxide (SO_2), nitrogen oxides (NO_2) carbon monoxide (CO) and particulate matter (PM). The purpose of this study is to evaluate the contribution of transit marine traffic through the Bosphorus (Istanbul Strait) on the air quality of Istanbul. The specific objectives that were performed to achieve this goal are:

- estimate air pollutant emissions of ships passing through the Bosphorus.
- use atmospheric dispersion modelling to estimate air pollutant concentrations resulting from the traffic through the Bosphorus. The dispersion model selected for this purpose is the EPA-approved CALPUFF computer program (Bennett et al., 2002) (Levy et al., 2002) (Zhou et al., 2003).
- Estimate the health impacts due to emissions originating from maritime traffic. The health costs are estimated using the EVA methodology (Brandt et al., 2013).

The findings from this study can be used for developing effective regulatory actions relating to maritime traffic.

2. THEORETICAL BACKGROUND

This chapter is organized as follows. Section 2.1 reviews the various approaches available for modelling the disersion of atmospheric pollutants. Section 2.2 reviews different methods for estimating emissions from ships which is needed to evaluate the effect of maritime traffic through the Bosphorus. Section 2.3 describes the EVA methodology that was used to estimate the health effects of air pollution originating from ships passing through the Bosphorus. Section 2.4 reviews some recent air pollution studies that focused specifically on the city of Istanbul.

2.1. Air Pollution Modeling

The processes governing the fate and transport of pollutants in the atmosphere are highly complex, requiring the construction of a well-integrated mathematical model. A well-constructed mathematical model must accurately account for individual processes like chemistry, transport and removal and their interactions (Seinfeld and Pandis, 2006). In the past 2 decades a wide range of atmospheric models have been developed. These models can be separated into 3 general categories by the approach they use, namely: Gaussian, Lagrangian and Eulerian models. Each of these approaches are described below.

2.3.1. Gaussian Dispersion Models

The main equation of Gaussian dispersion models is the continuity equation which describes the conservation of mass principle applied to the pollutants of concern (Christensen, 1997):

$$\frac{\partial C}{\partial t} = -\left(u\frac{\partial C}{\partial x} + v\frac{\partial C}{\partial y} + \sigma\frac{\partial C}{\partial \sigma}\right) + K_x\frac{\partial^2 C}{\partial x^2} + K_y\frac{\partial^2 C}{\partial y^2} + \frac{\partial}{\partial \sigma}\left(K_\sigma\frac{\partial C}{\partial \sigma}\right) + P(C,t) - L(C,t) \quad (1)$$

where

C is the concentration, t is time, u, v, and σ are the wind velocity in x, y and $\sigma^\cdot$ directions respectively, P and L are emission and removal fluxes respectively and K_x, K_y and K_σ are eddy diffusivities.

The above partial differential equation can be solved analytically or numerically. In order to derive an analytical solution to the partial differential equation, a number of simplifying assumptions are required which typically include the following (Stockie, 2011):

- Contaminant is released from a single point source (or few points sources) at height H, at a constant rate.
- The wind velocity is constant in space and time and is in the, positive x direction, $\vec{u} = (u, 0, 0)$.
- Solution is under steady state conditions.
- The eddy diffusivities are function of the travel distance and the stability of the atmosphere.
- The wind velocity is large enough to ignore diffusion in the x direction, $K_x \frac{\partial^2 C}{\partial x^2}$. Only advection takes place on the $x\ axis$.
- Ground surface height changes are negligible; the ground surface elevation is taken as plane $z = 0$.
- The contaminant does not penetrate the ground. Surface boundary conditions are typically
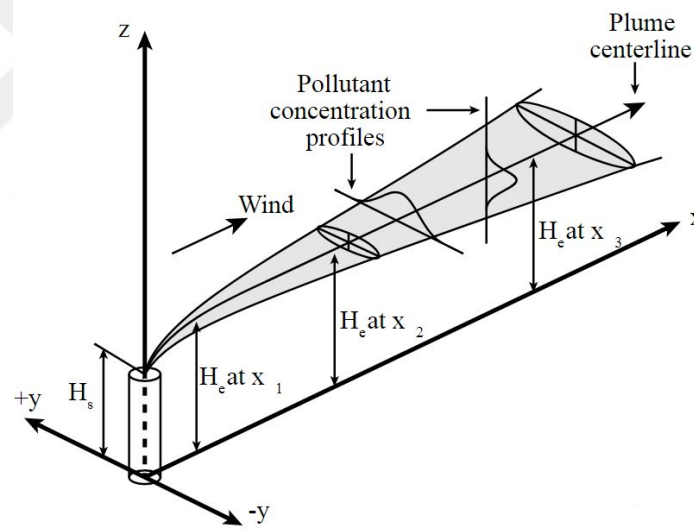
Figure 2.1 Plume emitted from a continuous point source (Seinfeld and Pandis, 2006).

As a result of the above assumptions, the continuity equation reduces to the following equation:

$$u\frac{\partial C}{\partial x} = K\frac{\partial^2 C}{\partial y^2} + K\frac{\partial^2 C}{\partial z^2} + Q\delta(x)\delta(y)\delta(z - H) \qquad (2)$$

The source term is defined with a Dirac delta function. Figure 2 shows the plume emitted from a continuous point source and the height is represented as the effective height which is the sum of stack height and the plume rise caused by buoyant effects, $H_e = H_s + \delta h$.

After simplifications the following suitable boundary conditions are used:

- $C(0, y, z) = 0$
- $C(\infty, y, z) = 0$
- $C(x, \pm\infty, z) = 0$
- $C(x, y, \infty) = 0$
- Two types of boundary conditions that are defined at the ground surface, either fully absorbing which means that pollutants reaching the ground surface are removed from the atmosphere or fully reflective which reflects the pollutants back to the atmosphere. The latter leads to higher atmospheric concentrations.

The above conditions essentially imply that the model domain is unbounded and hence the concentration at the boundary remains infinitely small. Finally, using either Green's functions (Crank, 1975) or Laplace transforms, the well-known Gaussian Plume Solution is obtained:

$$C(x, y, z) = \frac{Q}{2\pi\sigma_y\sigma_z u} exp\left(\frac{y^2}{2\sigma_y^2}\right)\left(exp\left(\frac{-(z-h)^2}{2\sigma_z^2}\right) + exp\left(\frac{-(z+h)^2}{2\sigma_z^2}\right)\right) \qquad (3)$$

C is the concentration at position x downwind, y crosswind and z vertical direction. The Release height is represented by h and u is wind speed. Crosswind and vertical mixing of pollutant are described by standard deviations σ_y and σ_z which are function by the stability of the atmosphere and the travel distance from the source This model is referred to as the Gaussian model because of the Gaussian plume shape that it predicts. Gaussian plume shape is represented in Figure 2.1.

Slightly modified forms of the above solution can also be found in the literature for other source types. For example, similar solutions can also be developed for multiple point sources or for line sources such as that due to traffic from highways.

Gaussian models can be used to calculate concentrations very rapidly since only a single Gaussian plume equation is solved and no differential equation is involved in the process. However,

Gaussian model performance diminishes at low wind speeds since the diffusion effects takes important role under such conditions. Such situations are important since stable or low level of inversions often lead to the highest concentrations and hence are the most critical cases to consider during decision making. In order to overcome this problem, the turbulence parameterizations and meteorological data preprocessing must be extended, but these processes increase the computational cost. Increasing computational power of modern computers allowed development of more sophisticated parameterization methods and helped increasing the accuracy of Gaussian dispersion models.

Several Gaussian dispersion models are available for computation, including AERMOD, Complex Terrain Dispersion Model Plus (CTDMPLUS), ADMS model, CALINE3, OCD, BLP, ISC and ALOHA.

In particular, AERMOD modeling system is developed by the US Environmental Protection Agency (EPA) and The American Meteorological Society, in order to bring in the planetary boundary layer concepts into regulatory dispersion models (Cimorelli et al., 2005). In AERMOD, the Monin-Obuklov theory (Venkatram, 1980) has been used for turbulence parameterization and for complex terrain flows including dividing streamline concept (Snyder et al., 1985). AERMOD also incorporates Plume Rise Model Enhancements (PRIME) for complex turbulence process like downwash effect. These properties of AERMOD make it an important and widely used tool for impact analysis for existing/proposed industrial facilities and agricultural areas.

CTDMPLUS is also another Gaussian model developed by EPA for elevated sources that do not consider intermediate scale flow field calculations (Perry et al., 1989) (Perry, 1992). In Europe ADMS model (Kalhor and Bajoghli, 2017) is widely used for air quality assessments and regulatory purposes. ADMS can be used for complicated processes like complex terrain, radioactive decay and wet/dry deposition processes (Carruthers et al., 1994) different modules have been developed for ADMS, leading to increased functionality of the model. For example, Urban module (developed by Cambridge Environmental Research Consultants) focuses on a chemistry model where the complex interactions between plumes of different sources in an urban area is calculated (Leelőlssy et al., 2014).

Moreover, there are Gaussian models developed for specific conditions, for example; CALINE3 (Benson, 1992) can be used for highway pollution, OCD (DiCristofaro and Hanna, 1991) is specific for coastal regions while ALOHA (Jones et al., 2013) is designed for accidental releases. All of these models are being used for impact and risk analysis by authorities worldwide.

2.3.2.   Lagrandian Models

Although, Gaussian models are often used for local scale impact analysis, they are less valid for continental scale dispersion studies. As a result, other models have been developed for such impact assessments (Suh, Han et al., 2009) (Piedelièvre et al., 1991) (Shuen et al., 1983). The models generally adopt Lagrangian and Eulerian approaches which combine Numerical Weather Prediction (NWP) models, gridded meteorological data and modern computers processing power (Leelőlssy et al., 2014) for more accurate long range prediction of pollutant transport predictions.

Lagrangian models describe concentration changes relative to the moving fluid. The trajectory of the pollutant is calculated using ordinary differential equations rather than partial differential equations in the original continuity equation. This way, computation requirements decrease, and also spatial truncation errors are averted.

In the Lagrangian approach the dispersed phase is assumed as an ensemble of many single point particles and particle dynamics are represented with modeled equations instead of exact instantaneous equations. Mean quantities (velocity, turbulent kinetic energy and concentration etc.) are calculated by ensemble averaging over a large number of particles which increases the computational cost. However, the increasing computation capacity in recent years allows these trajectory models to become important atmospheric dispersion computation tools.

Turbulent particle dispersion is a very complex and hard task because it is affected by both particle properties and turbulence properties. In order to overcome this complexity, a stochastic particle dispersion model is often used (Shuen et al., 1983). Lagrangian methods decomposes the driving fluid velocity into a mean term and a fluctuating term. Estimate of the mean and the turbulent properties of continuous phase are needed for this stochastic representation. The mean velocity part is interpolated at particle location and the fluctuating part is calculated by a Lagrangian model (Pozorski and Minier, 1998). With a large amount of particle trajectories, random sampling method can be used to determine particle motion.

2.1.2.1.   *Continuous Phase*

Turbulence properties of the continuous phase are calculated with the model transport equations for turbulence kinetic energy, k, and dissipation rate, ϵ:

$$\frac{\partial u}{\partial x} = \frac{1}{r}\frac{\partial}{\partial r}(rv) = D(u) = D(C) = 0 \tag{4}$$

$$D(k) = \mu_t \left(\frac{\partial u}{\partial r}\right)^2 - \rho\epsilon \tag{5}$$

$$D(\epsilon) = C_{\epsilon 1}\mu_t \left(\frac{\epsilon}{k}\right)\left(\frac{du}{dr}\right)^2 - C_{\epsilon 2}\frac{\rho\epsilon}{k} \tag{6}$$

Where

$$D(\emptyset) = \rho u \left(\frac{d\emptyset}{dx}\right) + \rho v \left(\frac{d\emptyset}{dr}\right) - \frac{1}{r}\frac{d}{dr}\left(r\frac{\mu_t}{\rho_\emptyset}\frac{d\emptyset}{dr}\right) \tag{7}$$

For $\emptyset = u,\ k,\epsilon$. With u denoting the mean axial velocity of gas, v being mean radial gas velocity, μ_t turbulent viscosity, and C_i is the turbulence model constant. All the dependent variables in the above equations are time averaged quantities.

Boundary conditions for the above equations are as follows (Shearer et al., 1979):

- $r = 0$
- $\frac{d\emptyset}{dr} = 0$ for $r \to \infty$
- $\emptyset = 0$

And model constants in the turbulent model are given in Table 2.1.

Table 2.1. Turbulent model constants (Lockwood and Naguib, 1975)

Constant	Value
$C_{\epsilon 1}$	1.44
$C_{\epsilon 2}$ (constant density flow)	1.89
$C_{\epsilon 2}$ (variable density flow)	1.84

In the conservation equation for particle concentration, it is assumed that the particles' local mean velocity and turbulent diffusivity values are equal to the gas phases. This means locally homogeneous flow approximation can be set for this equation (Shearer et al., 1979).

Also mean value of any scalar quantity, θ, (except k, ϵ, μ_t) can be calculated by:

$$\theta = \int_0^1 \theta(f)P(f)df \tag{8}$$

Where the $\theta(f)$ is obtained from equation of state and $P(f)$ is the probability density function for f. In this equation a Gaussian probability density function is assumed (Lockwood and Naguib, 1975).

2.1.2.2. *Particle Motion*

Particle trajectories are calculated using a Lagrangian formulation of the governing equation:

$$\frac{\partial u_{pi}''}{\partial t} = \left(\frac{3\rho C_D}{4d_p \rho_p}\right)(u_i'' - u_{pi}'')|\overrightarrow{u''} - \overrightarrow{u_p''}| + g_i \quad for \ i = 1,3 \tag{9}$$

where u_i'' is instantaneous value of mean axial velocity of particle, u_i'' represents instantaneous value of mean axial velocity of gas and g is the gravitational acceleration.

The position of the particle is calculated from:

$$\frac{\partial x_{pi}''}{\partial t} = u_{pi}'' \quad for \ i = 1,3 \tag{10}$$

In the above two equations, Lagrangian formulation of the governing equation and position of the particle equation are integrated to calculate particle trajectories then averaged to yield dispersion properties.

2.1.2.3. <u>*Particle Dispersion*</u>

Studies have shown that turbulent dispersion of particles can be calculated to a reasonable extend using the stochastic approach (Gosman and loannides, 1983). Initially eddy-life time method has been proposed where the fluid particle fluctuation velocity is being sampled from the Gaussian distribution of zero mean and variance of mean square turbulent velocity (Gosman and loannides, 1983). The sampled velocity is retained constant for a timespan of T that coincide to typical timescale of the energy containing eddies. Later, the time interval between subsequent velocity changes considered as an exponentially-distributed random variable with mean value T. The usage of Poisson process can account for discontinous velocity changes (Pozorski and Minier, 1998). The following stochastic differential equation called Langevin equation which defines the Brownian motion originally has been proposed:

$$dv = v(t + dt) - v(t) = -\frac{v}{T_L}dt + \sigma_f \sqrt{\frac{2}{T_L}}dW \qquad (11)$$

In this equation dW is the Wiener process with zero mean and variance equal to time interval, σ_f is vertical turbulent velocity fluctuation and T_L is the Lagrangian timescale. T_L is either given explicitly (Williams and Yamada, 1990) or can be calculated from velocity fluctuations (Stohl et al., 2005).

Numerous Lagrangian models are available for computation of environmental dispersion. The US EPA recommended CALPUFF Modeling system is a non-steady state Lagrangian puff dispersion model that computes the pollution transport. CALPUFF is widely used for scientific and regulatory purposes (Bennett et al., 2002) (Levy et al., 2002) (Zhou et al., 2003). The Danish RIMPUFF uses the Lagrangian model for the areas close to the source to compute the dispersion, it is a part of the RODOS decision support system (Brandt et al, 1996). Specifically, for the heterogeneous surface conditions, The RAPTAD model is being used for industrial and urban applications (Yamada et al., 1992). HYSPLIT, developed by NOAA, is another computer model used for computing air parcel trajectories and dispersion of air pollutants (Stein et al., 2015). Also, the UK Met Office developed two models, NAME atmospheric pollution dispersion model which is mostly used for predicting the dispersion and deposition of radioactive gases and materials into the atmosphere (Jones et al., 2007) and FLEXPART which is a model for the simulation of a large range of atmospheric transport

processes (Stohl et al., 1998). Apart from prediction of pollutants in the atmosphere, trajectory models can be used to locate the source region of the pollution by following the trajectory backward.

2.3.3. Eulerian Models

Like Lagrangian models, Eulerian models describe the concentration change relative to the moving fluid. The point of the Eulerian models is to compute the continuity equation which defines the conservation of mass in fluid motion:

$$\frac{\partial C}{\partial t} = -\left(u\frac{\partial C}{\partial x} + v\frac{\partial C}{\partial y} + \sigma\frac{\partial C}{\partial \sigma}\right) + K_x\frac{\partial^2 C}{\partial x^2} + K_y\frac{\partial^2 C}{\partial y^2} + \frac{\partial}{\partial \sigma}\left(K_\sigma\frac{\partial C}{\partial \sigma}\right) + P(C,t) - L(C,t) \quad (12)$$

where C is the concentration, t is time, u, v, and σ are the wind velocity in x, y and σ directions respectively, E and L are emission and removal fluxes respectively and K_x, K_y and K_σ are eddy diffusivities.

For the solution of the dispersion equation, first, spatial discretization is performed using one of the several methods (e.g. finite difference method, finite volume method, finite element method or spectral and pseudo-spectral method) which reduces the partial differential equation into a system of ordinary differential equation. Secondly, the temporal integration of the derived equation is performed.

There are several Eulerian models available for atmospheric dispersion studies. The Danish Eulerian Hemispheric Model (DEHM) is an atmospheric chemistry-transport model that is developed initially for sulphur and sulphate transport into the Arctic (Christensen, 1997). However, the chemical scheme model has been expanded to 58 chemicals, 9, primary particles and 122 chemical reactions (Jørgen Brandt et al., 2012). Moreover, DEHM model is coupled with the EVA (Economic Valuation of air pollution) model system which assesses the health impacts of air pollution and their economical valuations (Brandt et al., 2013). Another Eulerian model is the GEOS-Chem model which is a three-dimensional chemical transport model that incorporates Goddard Earth Observing System (GEOS) meteorological observations and operate at global scale (Bey et al., 2001). The Community Multi-scale Air Quality (CMAQ) modeling system is an air quality modeling tool that focuses on solving a wide range of air quality problems, for example aerosol and acid depositions, tropospheric ozone (Byun and Schere, 2006).

2.2. Ship Inventory and Emissions

There are two types of methodologies available for calculation of ship emission, top-down and bottom-up methods (Miola and Ciuffo, 2011). The top-down method combines fuel sales data and emissions factors to calculate emissions from ships; on the other hand, the bottom-up method calculates ship emissions through the modeling of fuel consumption by considering operating conditions of ships.

In this study, a bottom-up method is used for ship emissions calculation since this method is shown to be more accurate compared to top-down method (Chen et al., 2016). The bottom-up calculations would require an inventory of ships. There are several inventory methodologies available for the estimation of ship emission factors which are the emissions from individual ship types including: Environmental Engineering Consultancy (ENTEC) (Whall et al., 2010), Ship Traffic Emission Assessment Model (STEAM) (Jalkanen et al., 2009), TNO model by Netherlands Organization for Applied Scientific Research (van der Gon and Hulskotte, 2010), model by Endresen and co-workers (Endresen et al., 2007), model by Eyring and co-workers. (Eyring et al., 2005) are examined. Figure 2.2 shows the flow diagram for the bottom-up models to calculate ship emissions. Effective power of vessel is calculated from multiplication of main and auxiliary engine power with load factors. The time a vessel spends at the bert and sea is calculated from the route of the ship and the velocity data. Lastly, emissions by vessel are calculated with the multiplication of energy output of the vessel and determined emission factors according to fuel and engine type.
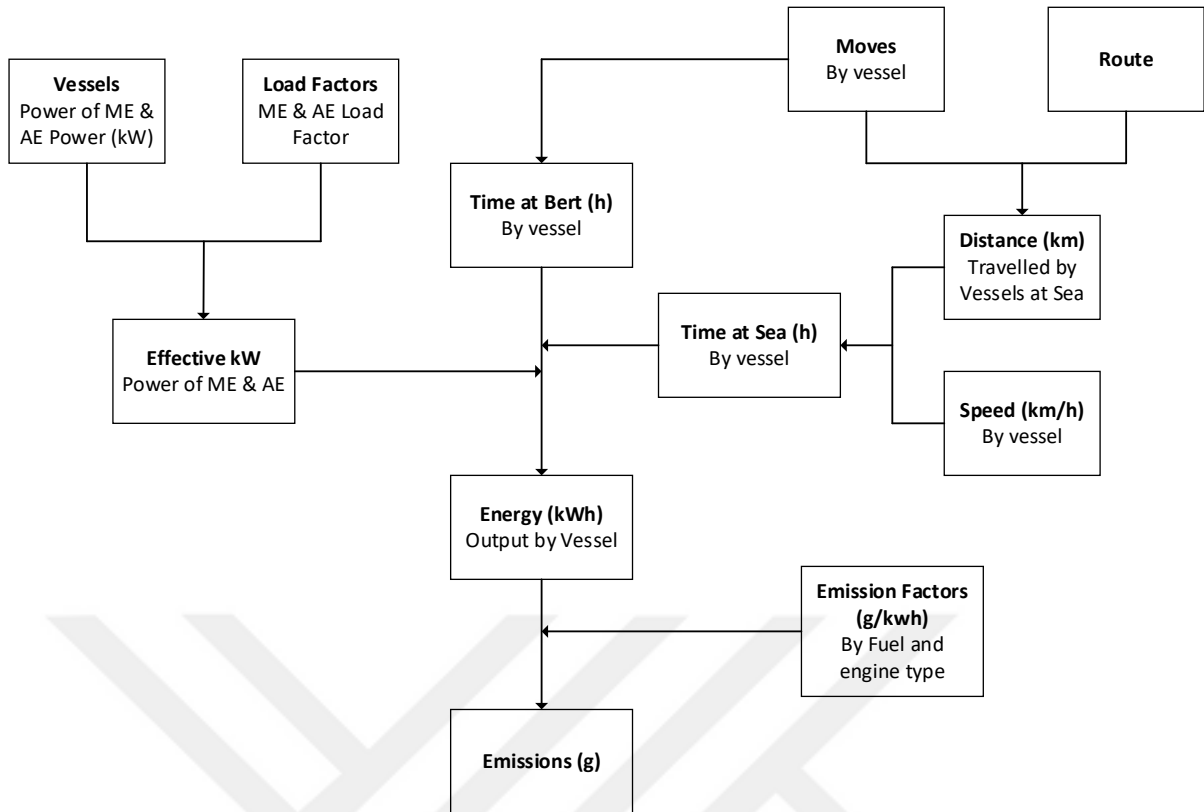
Figure 2.2. Summary of methodology for estimating ship emissions (Whall et al., 2010)

The consumption of fuel by ship is commonly modelled using the following equation:

$$FC = \sum_{engine} SFC \left(\frac{g}{kWh}\right) x \ P(kW) x \ LF \ (\%) x \ T(h) \tag{13}$$

where FC is the fuel consumption, SFC is specific fuel consumption, P is engine power, LF is load factor and T is time respectively.

And pollutant emissions are calculated using the equation:

$$Emission = \sum_{engine} EF \left(\frac{g}{kWh}\right) x \ P(kW) x \ LF \ (\%) x \ T(h) \tag{14}$$

where EF represents emission factor.

SFC depends on the load factor, the fuel and the engine age. Table 2.2 summarizes the fuel consumption calculation of three widely used models ENTEC, TNO and STEAM. As can be seen from the table not every model takes into account every parameter in order to make the emissions

calculations and preparation of the input data simple. For example, while engine age is a parameter for TNO model fuel consumption calculations, ENTEC and STEAM models only consider engine type and fuel type. Also, Table 2.3 summarizes the emission factor calculation of ENTEC, TND and STEAM models.

Table 2.2. Comparison of of fuel consumption calculation for three commonly used ship emission models in terms (European Environment Agency, 2013).

Fuel Consumption		ENTEC	TNO	STEAM
Main engine	Installed power	Lloyd's register	Lloyd's register	Lloyd's register and ship owners
	Load factor	At sea: 80 % Manoeuvring: 20 % At berth: 20 %	Cruising: 85 % Reduced speed: 65 % Manoeuvring: 10–40 % At berth: 0 %	$LF = 0.8 \times (V_{transient}/(V_{design}+V_{safety}))^3$ $V_{transient}$: speed from AIS data V_{design}: design speed from Lloyds Register V_{safety}: 0.5 kilotonnes Correction for wave height and direction
	Delivered power	$P (kW) = LF \times P_{installed}$	$P (kW) = LF \times P_{installed}$	$P (kW) = 0.8 \times P_{installed} \times (V_{transient}/(V_{design}+V_{safety}))^3$
	SFC	SFC taking into account: engine type fuel type	SFC considering: the engine type load factor fuel type build year	SFC from engine manufacturers Default SFC = 200 g/kWh
Auxiliary engine	Installed power	Lloyd's register	Lloyd's register	Lloyd's Register as upper limit for power estimate
	Load factor	At sea: 30 % Manoeuvring: 50 % At berth: 40 %	n/a	n/a
	Power		For each ship type from port survey (GT)	Power depends on ship type and activity
SFC = specific fuel consumption; SSD = slow-speed diesels; MSD = medium speed diesels; HSD = high speed diesels; ST = steam turbine***; GT = gas turbine***; AE = Auxiliary engine; MDO = marine diesel oil; MGO = marine gasoline oil; HFO = heavy fuel oil; RO = residuel oil.				

Table 2.3. Comparison in terms of emission factor calculation of three commonly used ship emission models (European Environment Agency, 2013).

Emissions factors	ENTEC	TNO	STEAM
NO_x	Depends on 5 engine types, 3 fuel types and activity (at sea, at berth) Post-2000: IMO NO_X Technical Code	Depends on engine type, build year and load	Engine manufacturer information Default: IMO Tier I Curve
SO_x	Depends on sulphur content and eventual exhaust gas after treatment (scrubber)	Depends on sulphur content and eventual exhaust gas after treatment (scrubber)	Depends on sulphur content and eventual exhaust gas after treatment (scrubber)
PM	Depends on engine type, fuel type and activity (at sea, at berth) and sulphur content: $PM_{2.5}$: 90 % of PM PM_{10}: 95 % of PM	Sulphur content, fuel type, engine type EFs for PM1, $PM_{2.5}$ and PM_{10}	Depends on engine type, sulphur content and engine load EF for organic carbon (OC)

2.3. Health Related Economic externalities of air pollution

In this study, the integrated model system EVA (Brandt et al., 2013) was used to assess the health-related economic externalities of air pollution. Although there are several methods to calculate health effects and their associated costs applicable to Europe, there is a lack of studies specifically applicable to Turkey. Thus in the current study, we applied exposure-response coefficients from the EVA (Economic Valuation of Air Pollution) model for the estimation of health effects due to emissions from maritime traffic through the Bosphorus. Details of the exposure-response coefficients from EVA are summarized in the Table 2.4. below.

The health effects and mortality associated with the different scenarios were calculated from population statistics and the dispersion model output as follows:

$$Number\ of\ case = [pollutant\ concentration]\ x\ [affected\ population]\ x\ [exposure\text{-}response\ coefficient] \tag{14}$$

Pollutant concentration refers to the average annual pollutant concentration calculated by the air dispersion model for Istanbul. Population and demographic datasets were retrieved from the national

official data provider, Turkish Statistical Institute (TurkStat). Exposure-response coefficients where adopted from the EVA (Economic Valuation of Air Pollution) modelling system which was applied previously for Denmark, Europe and USA. The EVA methodology is based on an extensive cohort study conducted in year 2000 with updates in 2004 and 2005 for over 500,000 individuals. The study was supported by the WHO and applicable for European conditions. As indicated in Table 2.4, it gives detailed health effects, classifies mortality into acute and chronic and allows for the estimates of associated health costs.

Table 2.4. Exposure-response coefficients used in this study (Brandt et al., 2013).

Health effects (compounds)	Exposure-response coefficient ( )
	Morbidity
Chronic bronchitis (PM)	8.2×10^{-5} cases/µg/ m^3 (adults)
Restricted activity days (PM)	$=8.4 \times 10^{-4}$ days/µg m^3 (adults)
	-3.46×10^{-5} days/µg m^3 (adults)
	-2.47×10^{-4} days/µg m^3 (adults>65)
	-8.42×10^{-5} days/µg m^3 (adults)
Congestive heart failure (PM)	3.09×10^{-5} cases/µg m^3
Congestive heart failure (CO)	5.64×10^{-7} cases/µg m^3
Lung cancer (PM)	1.26×10^{-6} cases/µg m^3
	Hospital Admissions
Respiratory (PM)	3.46×10^{-6} cases/µg m^3
Respiratory (SO2)	2.04×10^{-6} cases/µg m^3
Cerebrovasculat (PM)	8.42×10^{-6} cases/µg m^3
	Asthma, children (7.6%<16 tr)
Bronchodilator use (PM)	1.29×10^{-1} cases/µg/m^3
Cough (PM)	4.46×10^{-1} cases/µg/m^3
Lower respiratory symptoms (PM)	1.72×10^{-1} cases/µg/m^3
	Asthma, adults (5.9 %<15 tr)
Bronchodilator use (PM)	2.72×10^{-1} cases/µg/m^3
Cough (PM)	2.8×10^{-1} cases/µg/m^3
Lower respiratory symptoms (PM)	1.01×10^{-1} cases/µg/m^3
	Mortality
Acute mortality (SO2)	$7.85 \times 10\text{-}6$ cases/µg/m^3
Acute mortality (O3)	$3.27 \times 10\text{-}6$ SOMO35 cases/µg/m^3
Chronic mortality, YOLL (PM)	$1.138 \times 10\text{-}3$ YOLL/µg/m^3 (>30 yr)
Infant mortality (PM)	$6.68 \times 10\text{-}6$ cases/µgm^3 (>9 months)

Brandt et al. (2012) used EVA model system to evaluate health-cost externalities of air pollution in Europe that is contributed by international ship traffic. Total air pollution levels in Europe were represented by the years 2000, 2007, 2011 and 2020. The study focused especially on ship traffic in the Baltic and North seas, since the special regulatory actions on sulphur emissions are introduced,

SECA (sulfur emission control area). Results of this study shows that, SECA regulatory efforts have significant reduction in the health-related external costs of international shipping.

Brandt et al. (2013) used the EVA model system to assess contribution of ten major emission sectors in Europe and Denmark to the health-cost externalities of air pollution. The authors used a newly developed tagging method which can calculate the contribution from specific emission source or sector to the overall air pollution levels. Results showed that the main contributors to health-related external costs are power production, agriculture, road traffic, and nonindustrial domestic combustion, including wood combustion (Brandt et al., 2013). EVA system uses an impact-pathway chain which is schematically shown in Figure 2.3.
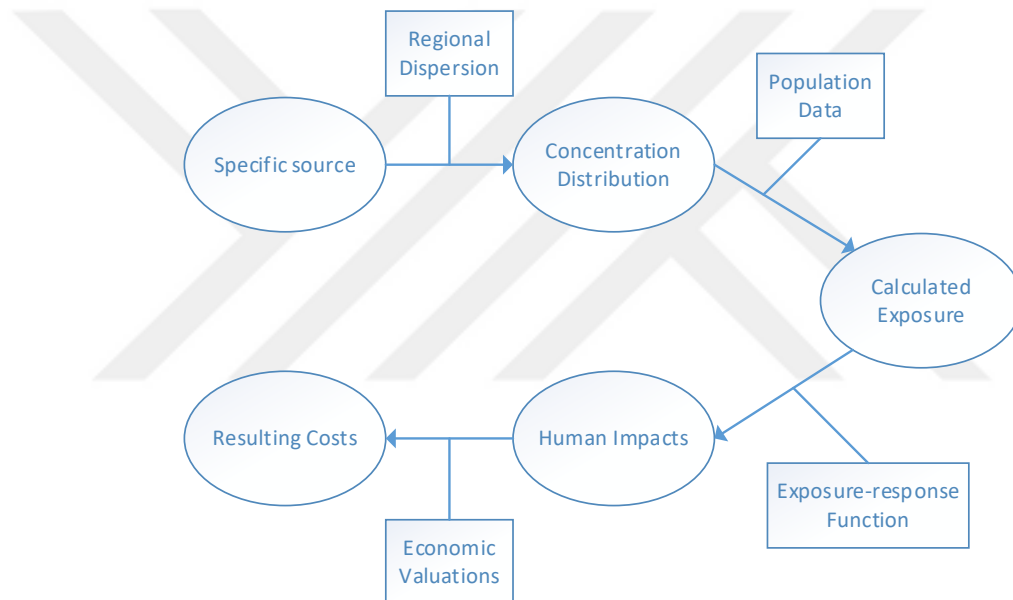
Figure 2.3. Impact-pathway methodology schematic diagram (Brandt et al., 2013).

2.4. Air dispersion studies for the city of Istanbul

This section reviews air pollution studies focusing on the city of Istanbul. The section also includes some recent studies that have specifically examined the impact of martime traffic on air quality which is the focus of this study.

Elbir, Mangır and Kara (2015) modeled the air quality dispersion Istanbul using the CALPUFF Modeling System. The results revealed that industry was responsible for the 83% of the SO2 emissions, with residential heating contributing 51% of the total PM_{10} emissions (Elbir et al., 2015). Bozyazi et al. (2000) used GIS spatial analysis to simulate air pollution in Istanbul. The study

included the pollutants SO_2 and total suspended particulate matter emissions. Their main finding is that air pollution in Istanbul is primarily connected to land use type (Bozyazi et al., 2000).

Elbir, et al. (2010), developed a decision support system for urban air quality management for the city of Istanbul. Emission inventory, air quality modeling and air quality mapping were calculated by GIS. CALPUFF dispersion modeling system has been used along with CALMET for the air quality modeling part of the system. The system estimates air quality anywhere and anytime in the study area, however, since the studies in Turkey have low spatial resolution, it cannot take the full advantage of GIS (Elbir et al., 2010).

Akkoyunlu and Ertürk (2002) investigated the SO_2 and PM_{10} concentration distributions in order to assess air pollution in Istanbul. The effect of natural gas and coal consumption in residential areas on air pollution levels was also examined. The Method of kriging by spherical interpolation was used to calculate the concentration distribution of these pollutants. Obtained pollution map in this study showed that, high quality fuel usage, in houses and industry results in improved air quality (Akkoyunlu and Erturk, 2002). Erturk (1986), used a modified version of ATDL urban dispersion model to estimate annual SO_2 and suspended particulate concentrations in the golden horn region of İstanbul. The emissions were categorized as area sources defined over a 3 km square grid pattern and point sources such has industrial sources. The study considers four different scenarios to obtain the impact on average annual SO_2 and suspended particulate levels. The proposed scenarios were mainly focuses on improving fuel quality and using better separation equipment in industry (Erturk, 1986).

3. METHODOLOGY

This chapter describes in detail the methodology used to compute the effect of transit maritime traffic in the Bosphorus strait on air quality and human health in Istanbul. Section 3.1 describes the CALPUFF model which was used for the atmospheric air pollution. Sction 3.2 presents the calculation used to estimate ship emissions.

3.1. Model Overview of CALPUFF Modeling System

The CALPUFF Modeling System consists of three components: CALMET, CALPUFF and CALPOST. An overview of the CALPUFF system is given in Figure 3.1. CALMET is a meteorological model that creates hourly wind and temperature fields on a three-dimensional gridded domain which also includes two dimensional fields such as mixing height, surface characteristics and dispersion properties. CALPUFF is a transport and dispersion model that advects "puffs" of material emitted from modeled sources, simulating dispersion and transformation processes along the path. Either on a gridded as in CALMET domain or non-gridded domain. CALPOST is a program that creates tabulations that summarizes the results of the output files, produced by CALPUFF. The output of CALPUFF can be used for the generation of air pollutant concentration maps.
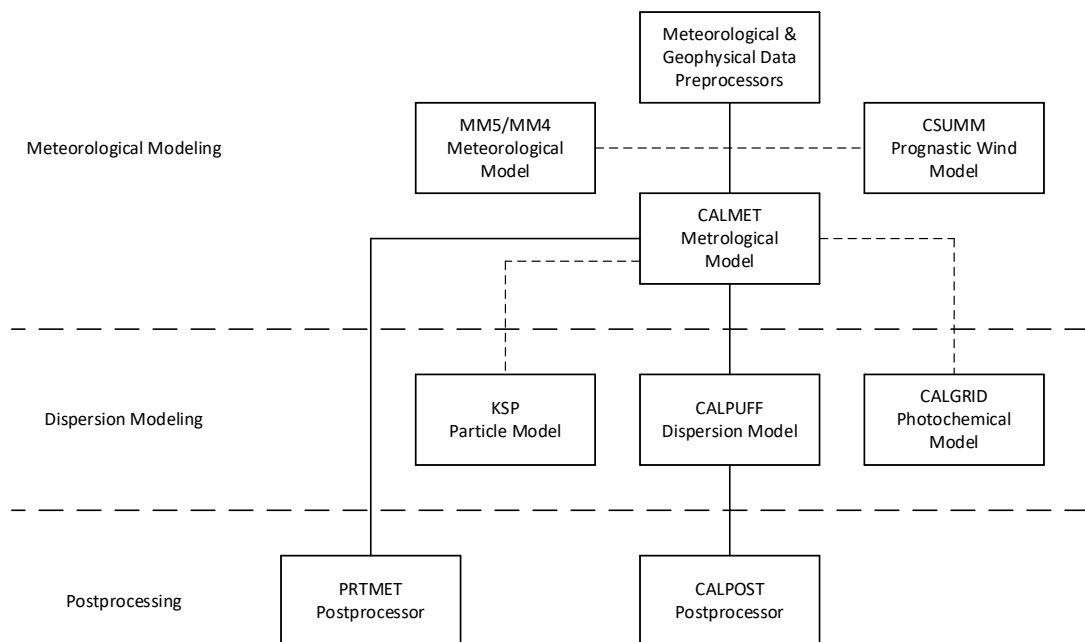

Figure 3.1. Overview of the program elements in the CALMET/CALPUFF modeling system (Scire, Strimaitis, and Yamartino, 1990)

3.2. CALMET

The components of CALMET include diagnostic wind field module and micro-meteorological modules for overwater and overland boundary layers (Scire et al., 1990).

3.3.1.   Major Features

In this part major features of CALMET is explained. Major features of the CALMET are shown in the Table 3.1.

Table 3.1. Major Features of the CALMET Meteorological Models (Scire et al., 1990).

Boundary Layer Modules of CALMET	Overland Boundary Layer - Energy Balance Method	
	Overwater Boundary Layer - Profile Method	
	Produces Gridded Field of:	Surface Friction Velocity
		Convective Velocity Scale
		Monin-Obukov length
		Mixing Height
		PGT Stability Class
		Air Temperature (3-D)
		Precipitation Rate
Diagnostic Wind Field Module of CALMET	Slope Flows	
	Kinematic Terrain Effects	
	Terrain Blocking Effects	
	Divergence Minimization	
	Produces Gridded Field of U, V, W Wind Components	
	Input Include Domain-Scale Winds, Observations, and (optionally) Coarse-Grid Prognostic Model Winds	
	Lambert Conformal Projection Capability	

Wind fields are computed according to a two-step approach. In the first step an initial-guess wind field called Step 1 wind field is adjusted for kinematic effects of terrain, slope flows, and terrain blocking effects. For the calculation of kinematic terrain effect on terrain forced vertical velocity, domain scale winds are used for calculation of a decay function which is function of stability. The kinematic terrain effect on the horizontal wind components is calculated by implementing diverge minimization scheme on the initial guess wind field (Liu and Yocke, 1980). Slope flows are calculated with buoyancy driven flows that are balanced by advective of weaker momentum, surface drag and entrainment at the top of the slope flow layer. Slope flow can be characterized in terms of terrain slope, distance to the crest and local sensible heat flux. Blocking effect of terrain on the wind flow is

characterized with Froude number. Wind direction of a grid is adjusted when the Froude number is less than a threshold value and the wind gas an uphill component (Allwine and Whiteman, 1985). In the second step, observational data are introduced into Step 1 wind field to form Step 2 wind field. At the grids with no observation data, Step 1 wind field has more influence. An inverse distance scheme is used to compute larger weight for the observational data around the vicinity of observational station (Douglas and Kessler, 1988). There is the option of smoothing wind field vertical velocities are smoothed with divergence minimization to form the final Step 2 wind field (O'Brien, 1970).

There exist two boundary layer models in the CALMET to implement for overland and overwater grid cells. For the over land surfaces, houry gridded fields of sensible heat flux, surface friction velocity, Monin-Obukhov length, and convective velocity scale are calculated using the energy balance method (Holtslag and Van Ulden, 1983). Modified Carson method is used to calculate the mixing heights from the computed hourly surface heat fluxes and observed temperatures (Carson, 1973). Gridded fields of PGT (Pasquiil-Gifford-Turner) stability class are also calculated by the model. For the overwater boundary layer, CALMET uses a profile technique, using the temperature difference between air and sea to calculate micrometeorological parameters in the marine boundary layer.
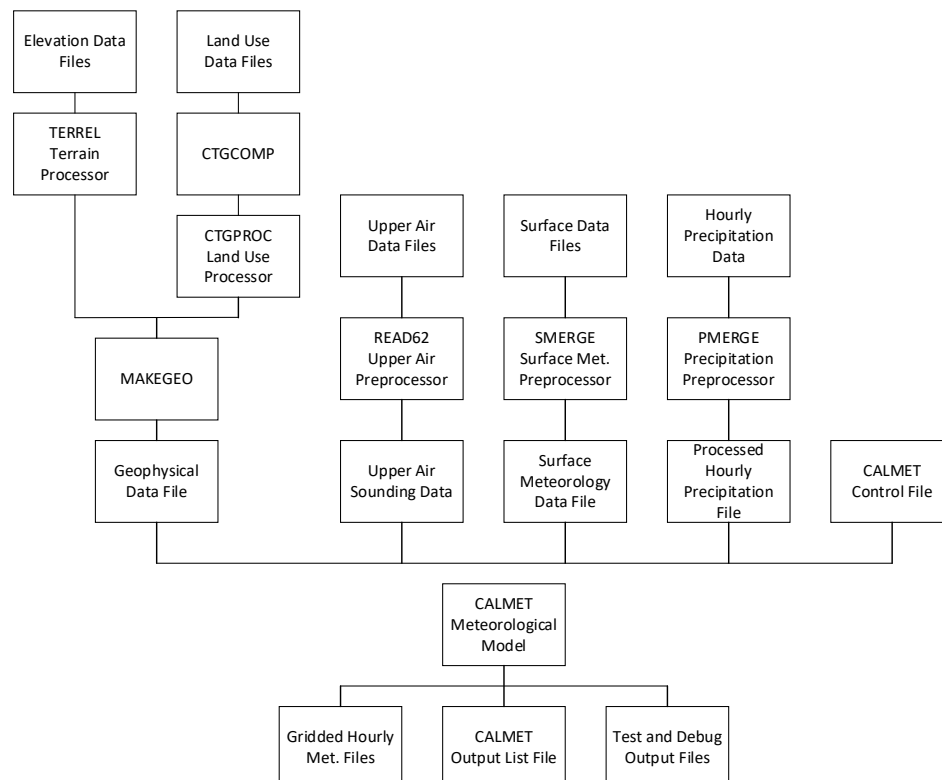

Figure 3.2. CALMET modeling flow diagram, based on (Scire, Insley, et al., 1990)

3.3.2.   Data Requirements

Figure 3.2 shows the flow diagram for the system inputs and preprocessing steps to make data usable with CALMET. The program is designed in a way that, it only requires commonly available surface and upper air meteorological observations data.. Also, the detailed input data requirements of the CALMET model are shown in Table 3.2.

Table 3.2. Data requirements of CALMET (Scire, Insley, et al., 1990).

Geophysical Data			
Gridded field of:	Terrain elevations		
	Land use categories		
	Surface roughness length (optional)		
	Albedo (optional)		
	Bowen ration (optional)		
	Soil heat flux constant (optional)		
	Antropogenic heat flux (optional)		
	Vegetative leaf area index (optional)		
Surface Meteorological Data			
Hourly observation of:	Wind speed	Hourly precipitation data:	Precipitation rates
	Wind direction		Precipitation type code
	Temperature		
	Cloud cover		
	Ceiling height		
	Surface pressure		
	Relative humidity		
Upper Air Data			
Twice-daily observed vertical profiles of:	Wind speed	Hourly gridded wind fields (optional):	MM4/MM5 output
	Wind direction		CSUMM output
	Temperature		
	Pressure		
	Elevation		
Overwater Observations (optional)			
Air-sea temperature difference			
Air temperature			
Relative humidity			
Overwater mixing height			
Wind speed			
Wind direction			
Overwater temperature gradients above and below mixing height			

3.3. CALPUFF

The US EPA-recommended CALPUFF Modeling system is a non-steady state Lagrangian puff dispersion model that computes the pollution transport, transformation and removal with the effect of time and space varying meteorological conditions. Figure 3.3 shows the flow diagram for the system input and output data for CALPUFF.
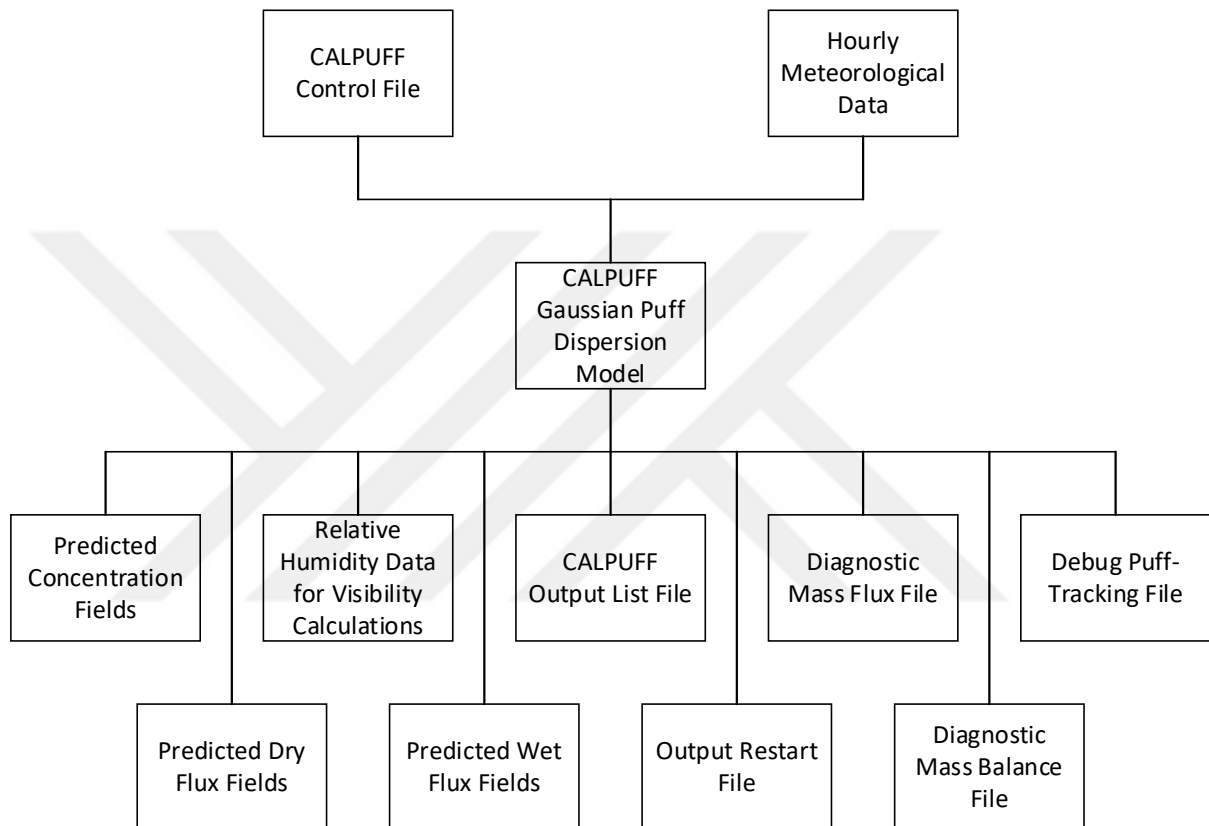
Figure 3.3. CALPUFF modeling flow diagram (adopted from Scire, Strimaitis et al., 1990).

3.3.3. Major Features

3.2.3.1. *Dry Deposition*

Dry deposition is the aggregation and deposition of particulate matter. The rate of dry deposition depends on the geophysical parameters incorporated into a full resistance model . CALPUFF also has the option that of user-specified deposition velocities or entirely disable the feature.

3.2.3.2. <u>*Wet Deposition*</u>

CALPUFF calculates the depletion and wet deposition fluxes caused by precipitation scavenging by an empirical scavenging coefficient approach.

3.2.3.3. <u>*Chemical Transformation*</u>

There are three different parameterizing chemical transformation in CALPUFF, a five species scheme employed in MESOPUFF II model, a six-species scheme adopted from RIVAD/ARM3 method or user specified varying transformation rates. In the simulations conducted in this study, the ARM3 method was used to compute the transformation of NOx emissions into nitrate particulate matter. This model requires aonium and ozone background concentrations, which are neede for the progression of the chemical reactions.

3.2.3.4. <u>*Subgrid Scale Complex Terrain*</u>

Pollutants deflected around the sides of a subgrid scale hills are calculated using the approach in the Complex Terrain Dispersion Model (CTDMPLUS) (Perry et al., 1989). Because the available Istanbul topography was relatively low, this feature was not accounted for in the model.

4. STUDY AREA AND SOURCE CHARACTERISTICS

This chapters describes the data used in the atmospheric dispersion model. Section 4.1 and 4.2 presents the topographic and meteorological data, respectively which are used in the CALMET program. Section 4.3 describes the calculation of the emissions sources.

4.1. Topographical Data

Istanbul, located in the north-west of Turkey, is a transcontinental city straddling the Bosporus strait which separates Europe and Asia. The Bosphorus strait (alos called Strait of Istanbul) is one of the most used waterways in the world.

The area covered in the model is 80 by 80 km centering around the Bosphorus Strait. The model domain extends from 624 to 704 km E in UTM zone 35 and 4516 to 4596 km N in UTM zone 35. The simulation area is divided into 80 x 80 x 10 grids. In the x and y directions grids are uniform with a spacing of 1 km and in the vertical direction it has a varying spacing. The domain discretization is the vertical direction was: 0, 20, 40, 80, 100, 200, 400, 600, 800, 1000 meters and the ceiling value of 1500 meters. The gridded receptor option is used in CALPUFF with 80 x 80 ground-level grids covering all the modeling area, resulting into 6400 receptors.

The terrain elevation are read from GTOPO30 global digital elevation model (Danielson and Gesch, 2011) (Gesch et al., 1999), with a horizontal grid spacing of approximately 1 kilometer. The terrain elevation of the model domain are shown in the Figure 4.1, and a three-dimensional surface plot of the domain can be seen in Figure 4.2

The land use types of the domain is retrieved from the United States Geological Survey (USGS) Global Land Cover Characterization survey (United States Geological Survey, n.d.). The land use type of the modeling domain for each grid is plotted and shown in the Figure 4.3. Table 4.1 shows the land use categories present in the Istanbul area. The majory of the model domain is classified as agricultural land. In the northern section, some forest areas are present. The Shoreline in the Bosphors is defined as urban area.
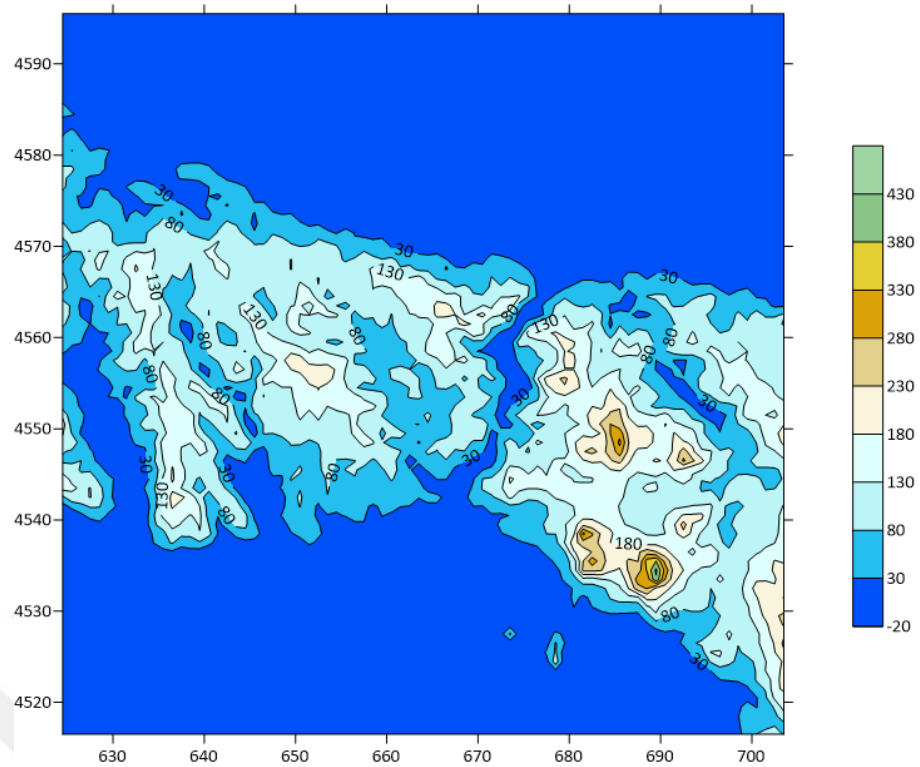
Figure 4.1. Terrain elevation of Istanbul, Turkey (in meters)
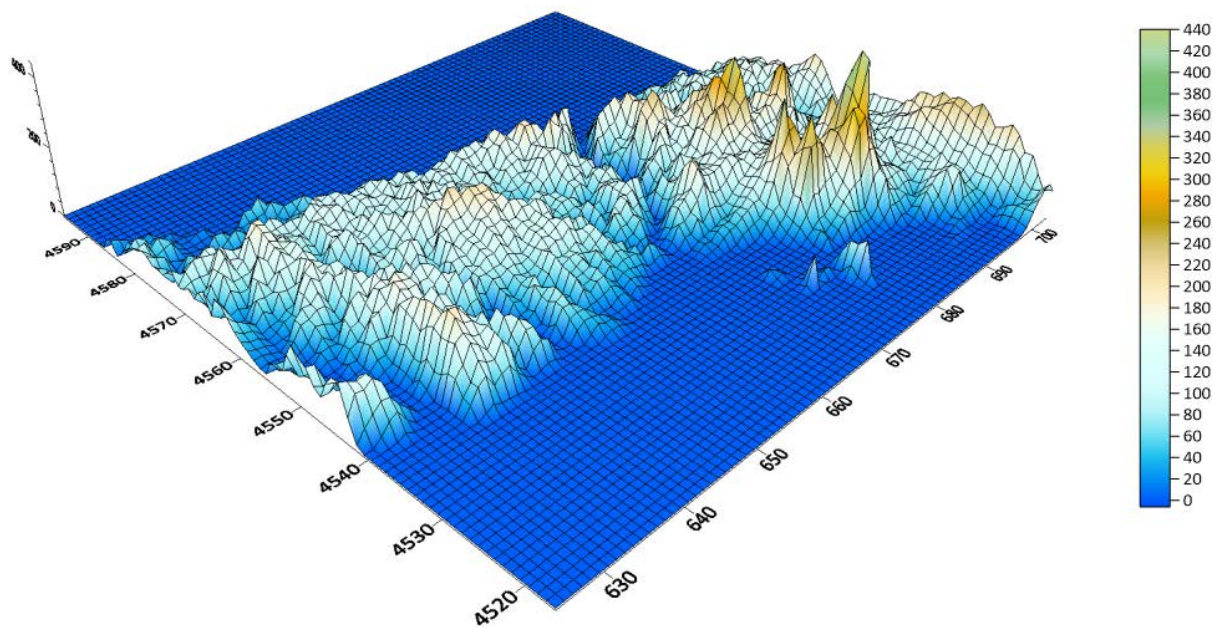

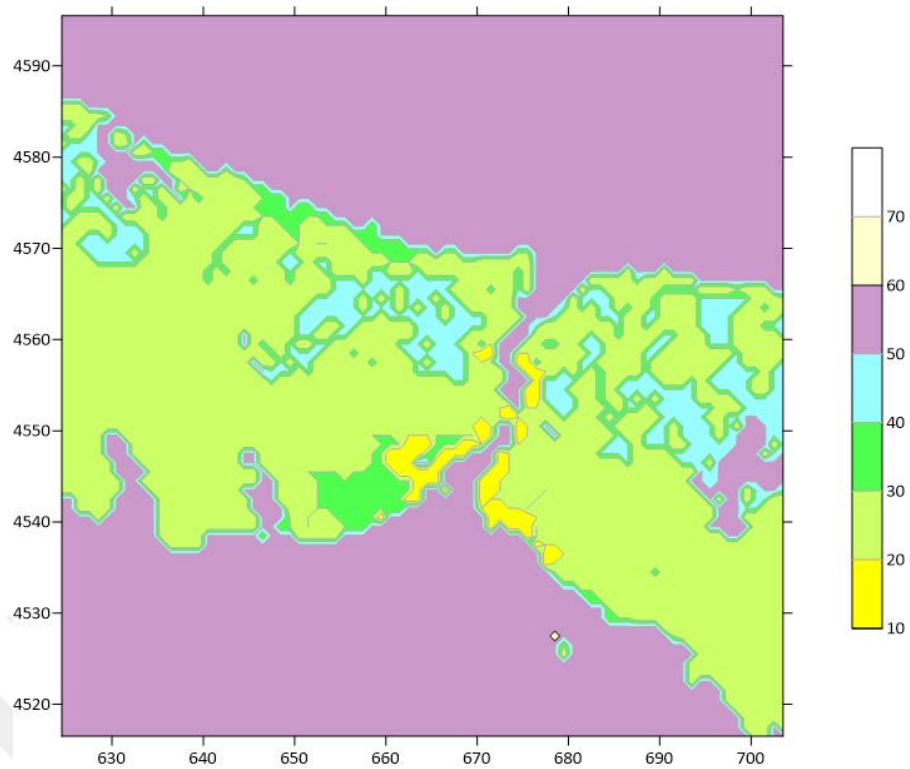Figure 4.2. 3D terrain elevation of Istanbul, Turkey (in meters).

Figure 4.3. Land use domain of Istanbul, Turkey.

Table 4.1. CALMET land use categories.

Level	Land use category
10-20	Urban or built-up land
20-30	Agricultural land
30-40	Rangeland
40-50	Forest land
50-60	Water
60-70	Wetland
70-80	Barren Land
80-90	Tundra
90-99	Perennial snow, ice

4.2. Meteorological Data

Six meteorological stations located in the Istanbul region were used for the definition of the hourly surface data implement to CALMET. Table 4.2 lists the names and coordinates of these stations. Surface meteorological data consist of temperature, wind speed, wind direction, relative humidity, surface pressure, cloudiness, and precipitation information. The surface observation data were obtained from the NCDC (National Center for Atmospheric Research) for the year 2017 (NCDC TD3505 Integrated Surface Hourly Data, 2005).

CALMET program needs upper level meteorological data to define the 3D wind field. Upper air radiosonde data is normally taken two times a day, one at midnight and the other at noon. Radiosonde collect upper air data includes wind speed and direction, pressure, humidity and height values as it travels upward. In the Istanbul area, there is only 1 location at Kartal where upper air data are collected on regular daily basis. The data at this station were acquired from ESRL (Earth System Research Laboratory Radiosonde Database) for 2017.

Initial wind field and other meteorological parameters are very important for air pollution dispersion studies. For this reason, initially latest version of state of art program WRF (Weather Research and Forecasting) Model was initially used. WRF Model numerically predicts the atmospheric parameters in the domain, however EPA-approved version of CALPUFF was unable to process the input files taken from WRF Models latest version.

As a result of the incompatibility of the WRF Model output files with EPA-approved version of CALPUFF, we used CALMET module with only observational data taken from surface stations. For this reason we used 6 different surface observation station. However, there were no observation station on the sea. Since a large portion of the modeling domain was sea, CALMET only used interpolations and extrapolations to prepare the meteorological parameters over the sea covered area in the domain.

Another limitation was the missing informations from the surface observation station. CALMET requires at least one surface observation to be available for each time period of the simulation. There were some cases where all 6 of the observation stations have no data. For these period of times, we replace the data with the previous days.

It is important to note that calibration of air dispersion models such as CALPUFF is often not possible. For these models to accurately match observed pollutant concentrations, the meteorological conditions should be known precisely at a very fine grid which is generally not possible when observed meteorological data are interpolated over a large model domain. Second, all pollutant sources should be accurately defined including thse originating outside the domain of interest. This is beyond the scope of many studies such as this where the focus is one one particular source of pollution. To compensate for this, models are generally simulated on small time steps (e.g., hourly or less) for long periods of time such as 1 year or more. The simulated concentrations can then be used to for regulatory purposes such as comparing the simulated concentrations corresponding to different exposure times to air quality regulations.

Table 4.2. Meteorological stations used in the model.

Station ID	Station Name
17060099999	Atatürk Airport
17063099999	Sabiha Gökçen Airport
17059099999	Kumköy
17061099999	Sarıyer
17119099999	Yalova
17066199999	İzmit

4.3. Source Characterization

The source pollution considered in this study is the transit maritime traffic in the strait of Istanbul. Detailed maritime traffic, passing through the Turkish Straits data were collected from 2017 to 2018 (Altan, 2017). Available traffic data consists of:

- Passing time from North and South bound
- Identity (MMIS number)
- Overall length
- Beam
- Draugh
- Speed over ground
- Course over ground of the ships

First, hourly number of ships passing through strait in the year 2017 were calculated from the data. Time series plot of hourly number of ships passing through the Bosporus are shown in Figure 4.4(a). To reduce the noise in the data, the series was smoothened with localized regression (loess), as shown in Figure 4 part b. The smoothened data was used in the calculation of the pollutant emissions). Also, in order to group the data and to see the seasonal intervals, monthly ship traffic is examined. Figure 4.5 represents the monthly distributed values as box plot. The box plots show the mean, upper and lower 25 percentiles and range It can be seen from the graphs that, traffic in the Bosporus was higher during February and March with nearly 9 ships per hour passing through the strait. Traffic was somewhat stable throughout rest of the year with a rate of approximately 6 ships per hour passing.
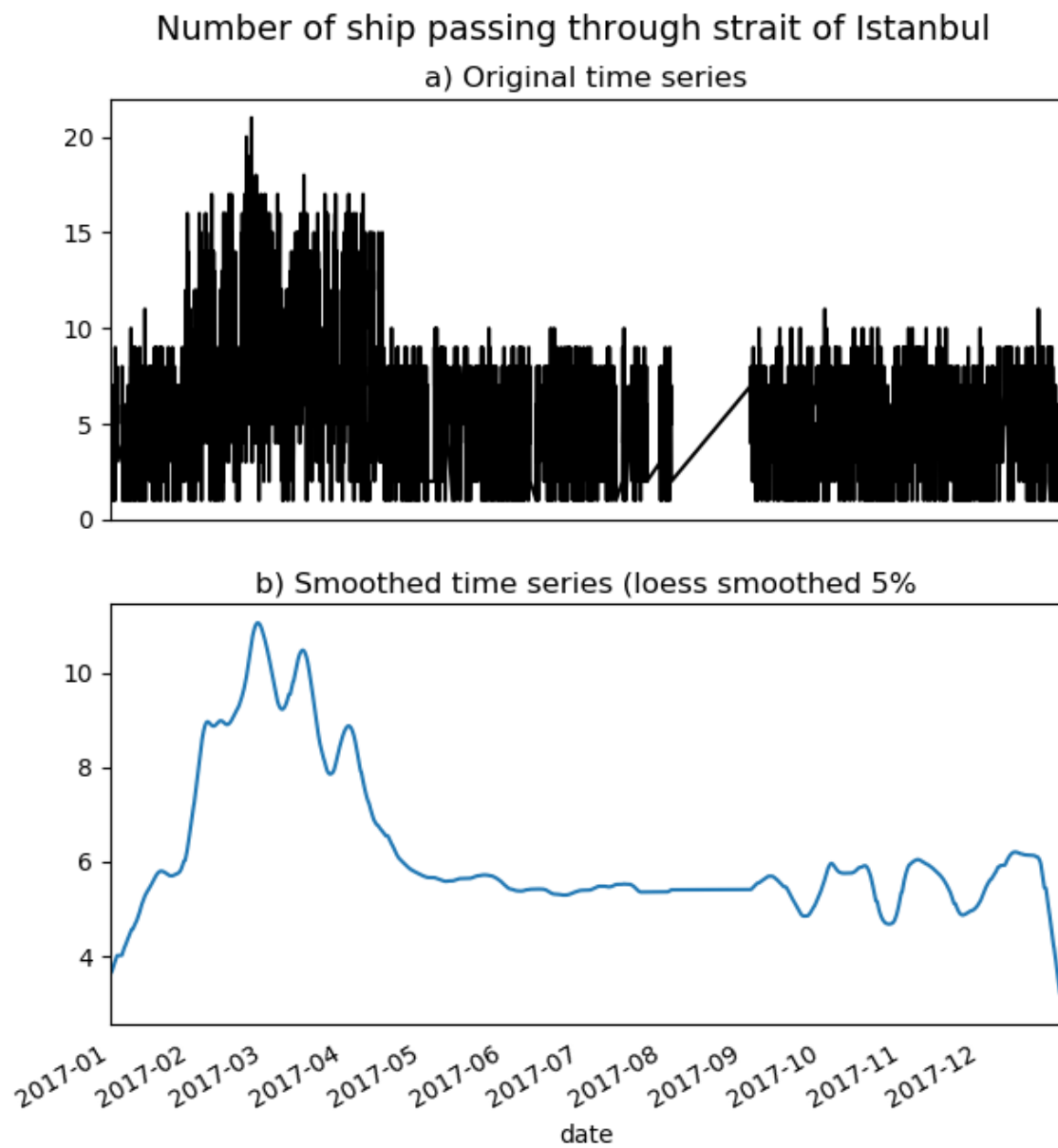
Figure 4.4. Hourly number of ships passing through strait of Istanbul.

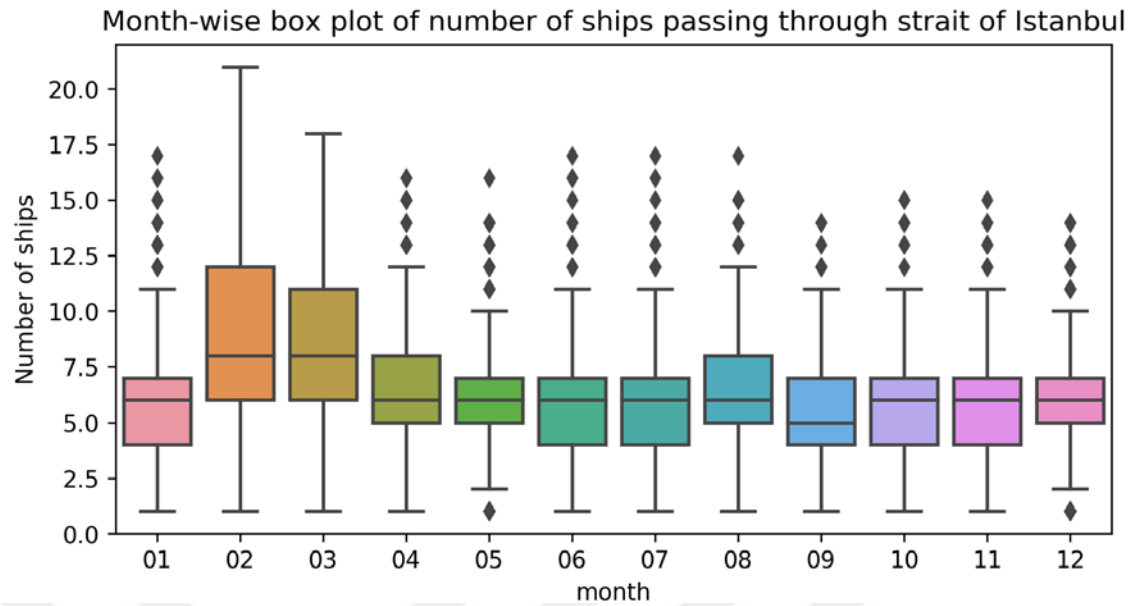Month-wise box plot of number of ships passing through strait of Istanbul

Figure 4.5. Month-wise box plot of number ships passing through strait of Istanbul.

In order to calculate the emissions from ships, the following information are required for each ship:

- Traveling distance of the ship
- Average speed of the ship
- Installed main engine power
- Installed auxiliary engine power
- Average load factor of main engine at sea
- Average load factor of auxiliary engine at sea
- Emission factors assigned to each vessel, which requires the following information:
  - Fuel type
  - Engine speed

The determination of each of these parameters is described below.

4.3.1.   Traveling Distance

It is assumed that ships will travel along a line through the Bosphorus, and hence the source type is defined as a line source. This assumption was deemed appropriate as width of the Bosphorus is much smaller than the model domain extent. However, since the Bosphorus not a straight line, involving several sharp bends and in order for the source not to pass overland, The line source was divided into six straight line segments for the model simulation. Figure 4.6 illustrates the line sources superimposed over the modle domain.
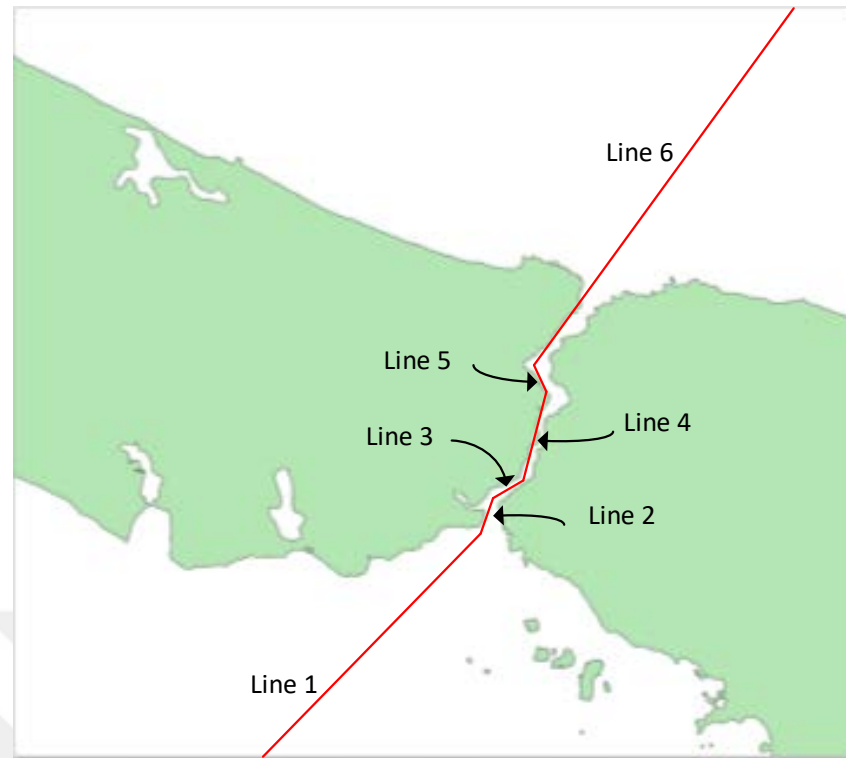
Figure 4.6. Line source representation for the domain.

    Table 4.3 given the coordinates and length information of the modelled line segment sources. It can bee seen that total length of the route is approximately 95.3 km long which includes also the ship routes through the Marmara and Black seas in the vicinity of the Bosphorus entrances/exit. This distance is used in the emission calculation and the emission rates from each segment are divided proportional to segment length.

Table 4.3. Line source coordinates and length.

	Beginning		Ending		
	X (km)	Y (km)	X (km)	Y (km)	Length (km)
Line 1	640.000	4516.000	667.166	4540.863	36.83
Line 2	667.166	4540.863	668.381	4544.063	3.42
Line 3	668.381	4544.063	671.704	4546.484	4.11
Line 4	671.704	4546.484	674.400	4555.151	9.08
Line 5	674.400	4555.151	672.906	4558.140	3.34
Line 6	672.906	4558.140	4558.140	680.000	38.52

4.3.2. **Average Ship Speed**

Maximum allowable ship speed by legislation by Kıyı Emliyeti Genel Müdürlüğü is 18.52 km/h (Türk Boğazları Gemi Geçiş İstatistikleri, 2017). This speed was used to simulate the average ship speed in the simulation.

4.3.3. **Installed Main and Auxiliary Engine Power**

Installed main and auxiliary power for each ship type is calculated from the ENTEC data which has a dataset of 14255 vessels. More detail on the engine sizes can be seen in the Table 4.4.

Table 4.4. Total main/auxiliary engine power for each vessel type (Whall et al., 2010).

Ship type	Number of ships	AE total power (kW)	ME total power (kW)	Average AE (kW)	Average ME (kW)
Bulk Carrier	846	1,627,555	7,595,982	1,924	8,979
Container Ship	521	2,822,373	12,611,795	5,418	24,207
Fishing	86	105,685	165,481	1,229	1,925
General Cargo	1,811	1,777,232	5,467,977	982	3,020
Others	250	152,445	522,972	610	2,092
Passenger	37	58,431	166,526	1,580	4,501
Ro-Ro Cargo	211	532,972	1,765,660	2,526	8,369
Tanker	1,118	2,736,512	10,115,796	2,448	9,049
AE: Auxiliary engine ME: Main engine					

In order to distribute engine size according to vessel type, first, vessel type statistics were examined (Türk Boğazları Gemi Geçiş İstatistikleri, 2017). This data includes the number of vessels passing though the Istanbul strait with their vessel type, on a monthly basis. From this data, monthly ship type distributions are assumed to be the same with the monthly vessel type distribution used in this study.

Using the ship distribution data from Türk Boğazları Gemi Geçiş İstatistikleri, (2017), the hourly ship data from Altan (2017) were randomly matched with a vessel type, hence engine size. Figure 4.7 illustrates the data usage for each reference below.
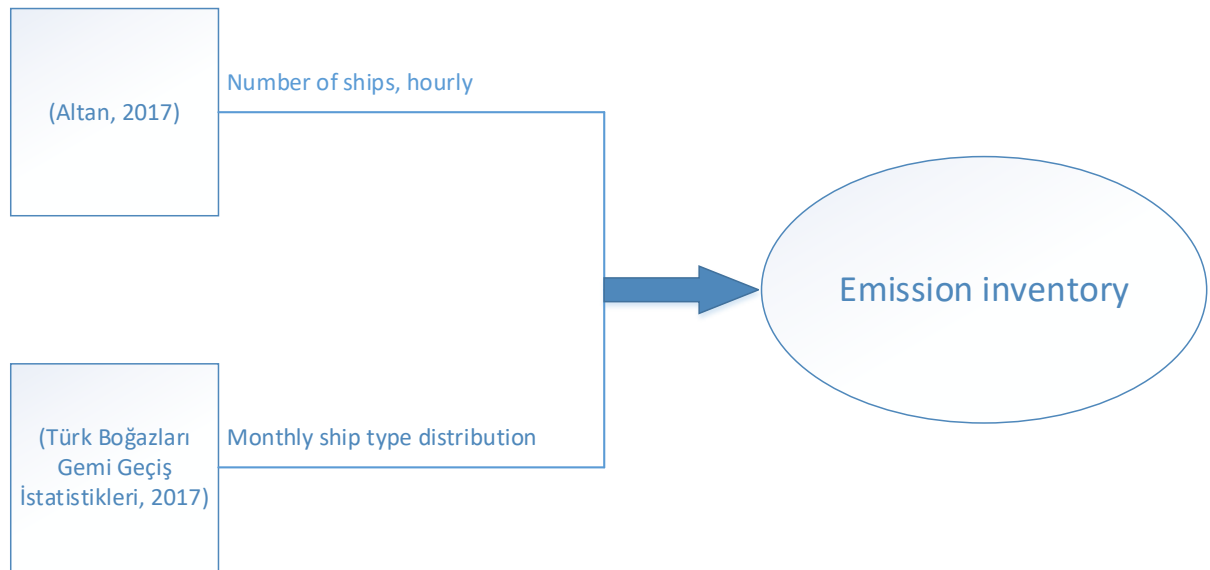
Figure 4.7. Data used for the emission inventory

4.3.4. Average Load Factor for Main and Auxiliary Ship Engines

Average load factor for engines was retrieved from ENTEC model (Whall et al., 2010). Load factors for main and auxiliary engines in this study are implemented as 0.8 and 0.3 respectively (Whall et al., 2010). These values are needed in the calculation of the pollutant emissions (Equation 14).

4.3.5. Emission Factors Assigned to Each Vessel

In order to assign emission factors to each vessel, fuel type used and engine speed must be known. In this study, fuel type has been assumed to be residual oil. This is the most used fuel type for large size vessels.

There are three main categories available for the ship engine speed, slow-speed, medium-speed and high-speed diesel engines. In order to find the engine speed of the vessel it is required to calculate the gross tonnage of the ship. For this purpose, gross tonnage of each ship is calculated using a non-linear regression model for engine power and gross tonnage of ships (Trozzi, 2010).

Table 4.5. Distribution of number of vessels according to gross tonnage and engine speed (Whall et al., 2010).

Vessel category	<=5000 GT			5000-25000 GT			>25000 GT		
	High	Medium	Slow	High	Medium	Slow	High	Medium	Slow
Bulk Carrier	0	44	4	0	29	633	1	11	1094
Container Ship	0	67	0	1	233	161		2	634
Fishing	27	256	4	0	8	1			
General Cargo	129	1494	121	0	298	510			82
Tanker	28	348	91	5	238	558	3	12	901
Passanger	37	28	5	8	60	8	1	41	14
Ro-Ro cargo	8	31	2	2	154	38		22	286
Others	295	546	23	5	90	7		1	6
Category Total	524	2814	250	21	1110	1916	5	89	3017
Overall %	14.60	78.43	6.97	0.69	36.68	63.32	0.16	2.86	96.98

Table 4.5 represents the number of ships and their engine type according to their gross tonnage (GT). Figure 4.8 illustrates the distribution of number of vessels according to three gross tonnage groups and engine speed. From the table and graph, it can be seen that nearly 80 % of ships with less than 5000 GT has medium-speed diesel engine, more than 60 % of ships having GT between 5000 and 25000 uses slow-speed diesel engine and lastly more than 95 % of ships that has GT of larger than 25000 uses slow-speed diesel engine. In this study, it is assumed that if gross tonnage of ship is less than 5000, it employs medium speed diesel engine and if gross tonnage of ship is larger than 5000 it employs slow speed diesel engine. Figure 4.9 below illustrates the flow diagram of the emission factor calculation.
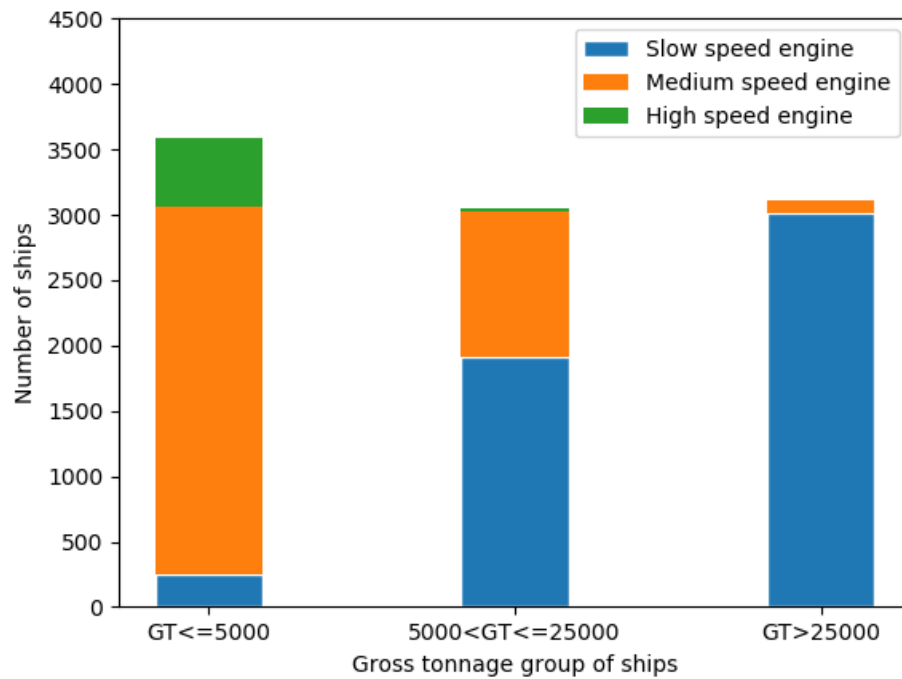
Figure 4.8. Distribution of number of vessels according to three gross tonnage groups and engine speed, data retrieved from (Whall et al., 2010).
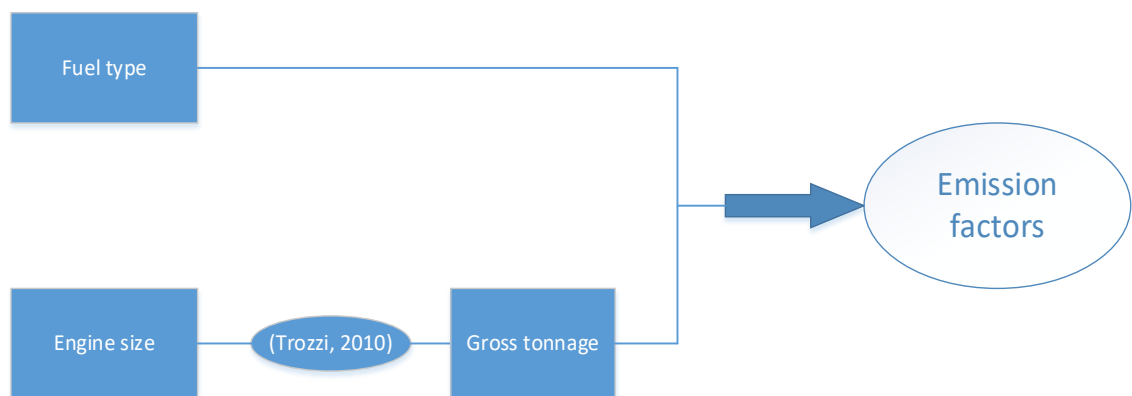

Figure 4.9. Flow diagram of the emission factor calculation.

Table 4.6. Emission factors depending on vessel gross tonnage used in this study.

	Emission factors, NO_x (g/kWh)	Emission factors, SO_2 (g/kWh)	Emission factors, PM (g/kWh)
Gross tonnage of <=5000	13.1	11.5	0.8
Gross tonnage of >5000	17	10.5	1.7

As indicated above, calculated emission rates are implemented into the CALPUFF as line sources, consist of six segments. Also, stack diameter of 1.5 meters and stack height of 35 meters is assumed. Flue gas emitted is assumed to leave the stack tip at 100 °C with a velocity of 5 m/s. Table 4.7 below summarizes the ship stack characteristics used in this study.

Table 4.7. Ship stack characteristics used in this study.

Stack tip exit velocity	m/s	5
Stack tip exit Temperature	°C	100
Stack height	m/s	35
Stack diameter	m/s	1.5

By employing the above assumptions, the emission inventory for the the Strait of Istanbul was calculated on hourly basis, for pollutants SO_2 NO_x and Particulate matter, (PM), the three atmospheric pollutants that are associated with fossil fuel burning. Table 4.8 below summarizes the monthly emission rates of the inventory created in this study.

Table 4.8. Emission summary table for each pollutants, monthly basis.

Months	Sum of Emission NO_x (g/s)	Sum of Emission SO_2 (g/s)	Sum of Emission PM (g/s)
January	53.3	35.4	5.0
February	100.1	66.4	9.3
March	103.4	68.8	9.6
April	70.3	47.1	6.5
May	45.5	30.5	4.2
June	45.3	30.4	4.2
July	35.1	23.4	3.2
August	5.8	3.8	0.5
September	46.3	30.8	4.3
October	52.0	35.0	4.8
November	56.0	37.3	5.2
December	52.3	34.9	4.8
Grand Total	**665.3**	**443.8**	**61.6**

5. RESULTS

5.1. Atmospheric Pollutant Concentrations

CALMET and CALPUFF were used to simulate 8735-hour period, starting from January 1, 2017 at 02:00, to December 31, 2017 00:00. In total eight pollutants were modelled: three of them emitted in the simulation period (SO_2, NO_x and PM_{10}), while the additional modeled species include SO_4, HNO_3, NO and CO. These additional species are needed for the reactive module of CALPUFF which calculates the formation of secondary PM in the atmosphere. The model also required the definition of background ammonium and ozone which are also needed in the reaction module. The monthly emission rates defined in Table 4.8 were incorporated in the model.

In order to assess the effect of the ship emissions on the air quality, the simulated concentrations were compared to the EU's air quality directives (2008/50/EC directive on Ambient Air Quality and Cleaner Air for Europe) and Turkish regulations. Table 5.1 summarizes the air quality standards set by the EU Air Quality Directive and Turkish regulations. The Turkish regulations, passed in 2008 call for a gradual decrease in the air concentrations to make it inline with the EU regulations. Depending on the exposure time, the regulations allow a certain number of exceedances as indicated in Table 5.1.

Table 5.1. Summary of the threshold set by the EU Air Quality Directive and Turkish regulations.

Pollutant	Exposure Time	Turkish Regulation Concentration ($\mu g/m^3$)	EU Regulation Concentration ($\mu g/m^3$)
Sulfur Dioxide (SO2)	1 hour (a)	350	350
	24 hour (b)	125	125
	Annual	20	
Nitrogen Dioxide (NO2)	1 hour (c)	200	200
	Annual	40	40
Particulate Matter (PM10)	24 hour (d)	50	50
	Annual	40	40
Remarks: (a) Can be exceeded up to 24 times per year			
(b) Can be exceeded up to 3 times per year			
(c) Can be exceeded up to 18 times per year			
(d) Can be exceeded up to 35 times per year			

In order to compare the concentrations calculated with the regulations, simulated hourly pollutant concentrations at each grid are averaged for the exposure periods (1 hour, 24 hour, annual) indicated in Table 5.1. For these averaging periods, third, eighteenth, twenty forth and thirty-fifth highest value for each grid is plotted depending on the pollutant. For example, for SO_2, the exposure times are 1 hour, 1 day and annual. Moreover, the regulations allow for 24 exceedances of the hourly limit (350 µg/m^3) and 3 exceedances of the daily limit (125 µg/m^3). Therefore at each receptor, the following data were extracted from the CALPUFF output: 25th highest hourly value, 4th highest daily value and the average annual value and compared to the relevant regulations. It is important to note that this comparison is done for each receptor separately. Hence, the 25th highest hourly value, 4th highest daily value at two receptors may not necessary occur at the same time.

The figures presented in the following section show both meteorological and highest pollutant concentration plots as predicted by the modeling system. The specific dates indicated in the plots are listed below:

Sulfur dioxide (SO_2):
- 03.03.2017 – 21:00, which is the time when the 24th highest hourly SO_2 concentration occured.
- 24th highest hourly SO_2 concentration at each receptor (as noted above, these values can occur at different times).
- 25th highest hourly SO_2 concentration at each receptor (these values can occur at different times).
- 20.03.2017, which is the day when the 3rd highest 24-hour SO_2 concentration occured.
- 3rd highest 24-hour SO_2 concentration at each receptor (these values can occur at different times).
- 4rd highest 24-hour SO_2 concentration at each receptor (these values can occur at different times).
- Maximum hourly SO_2 concentration at each receptor (these values can occur at different times).
- Maximum 24-hour SO_2 concentration at each receptor (these values can occur at different times).
- Annually average SO_2 concentration for year 2017.

Nitrogen dioxide (NO_2):
- 24.04.2017 – 14:00, which is the time when the 18th highest hourly NO_2 concentration occured.
- 18th highest hourly NO_2 concentration at each receptor (these values can occur at different times).
- Maximum hourly NO_2 concentration at each receptor (these values can occur at different times).

- Maximum 24-hour NO_2 concentration at each receptor (these values can occur at different times).
- Annually averaged NO_2 concentration for year 2017.

Particuate Matter (PM)

- 23.11.2017, which is the day when the 35th highest 24-hour primary PM10 concentration occured.
- 35th highest 24-hour primary PM10 concentration at each receptor (these values can occur at different times).
- 36th highest 24-hour primary PM10 concentration at each receptor (these values can occur at different times).
- Maximum hourly primary PM10 concentration at each receptor (these values can occur at different times).
- Maximum 24-hour primary PM10 concentration at each receptor (these values can occur at different times).
- Annually averaged primary PM10 concentration for year 2017 (these values can occur at different times).
- Annually averaged secondary PM concentration for year 2017 (these values can occur at different times). These secondary PM is the particulate matter formed in the atmosphere as a result of chemical reactions (please refer to Chapter 3). Secondary PM is considered to be in the size category PM2.5.
- Annually averaged total PM2.5 concentration for year 2017 (these values can occur at different times). The total PM2.5 consists of the portiton of primary PM that is smaller than 2.5 µm and all secondary PM.
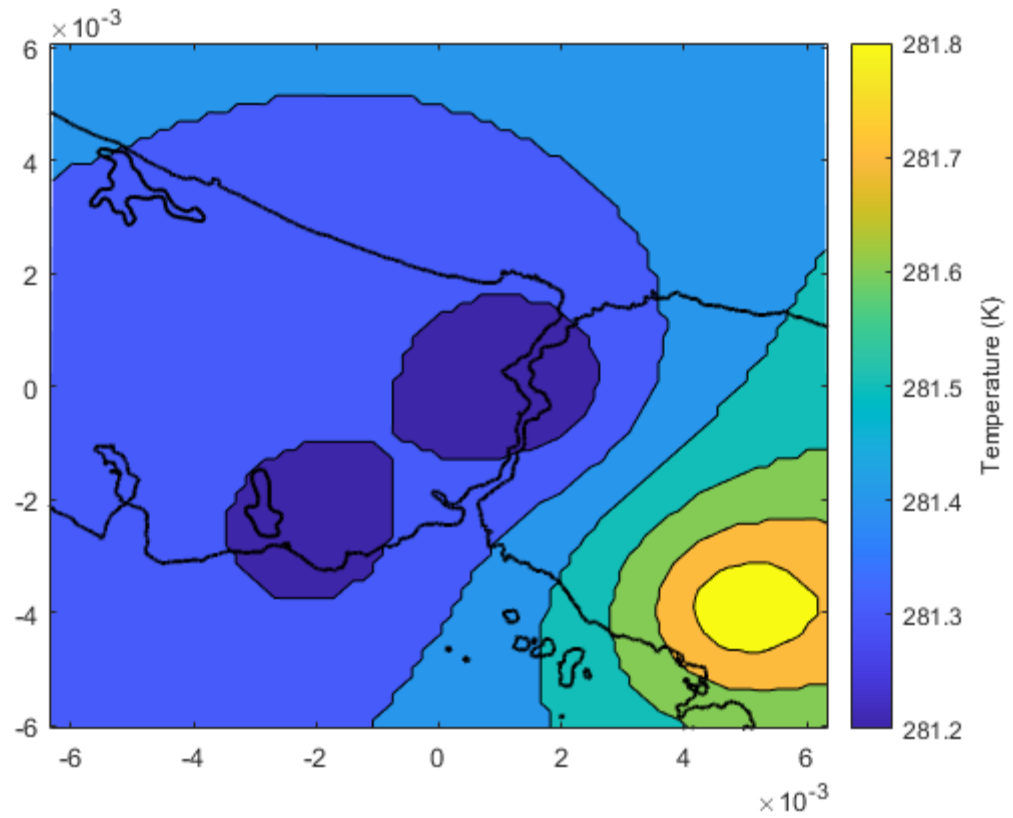
Figure 5.1. Temperature contour in the Bosphorus region, date, time: 03.03.2017, 21:00.
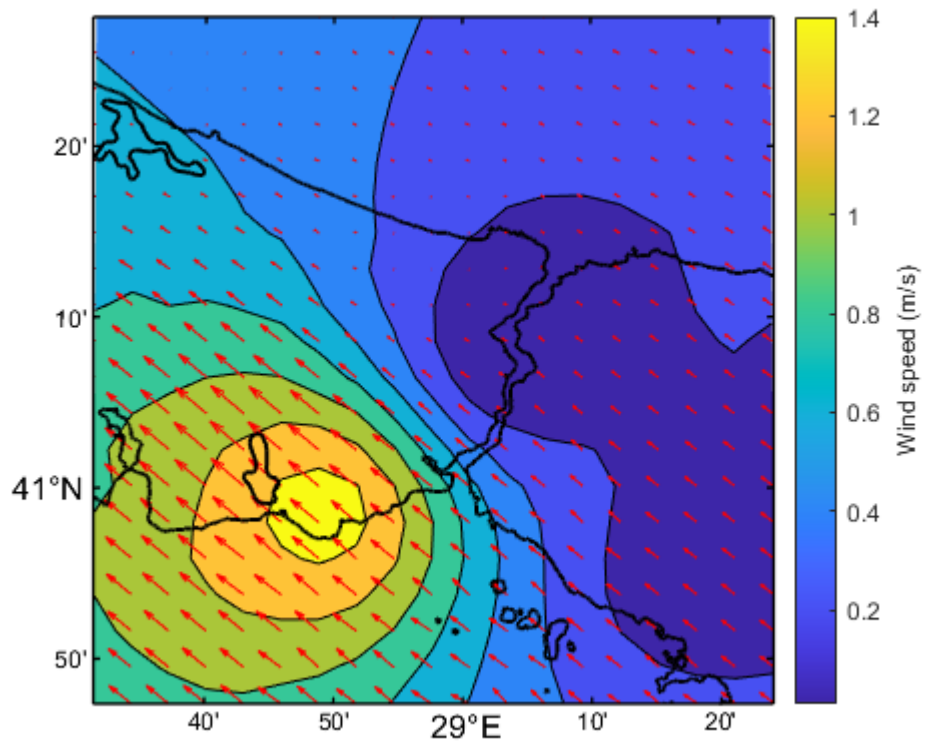
Figure 5.2. Wind plot in the Bosphorus region, date, time: 03.03.2017, 21:00.
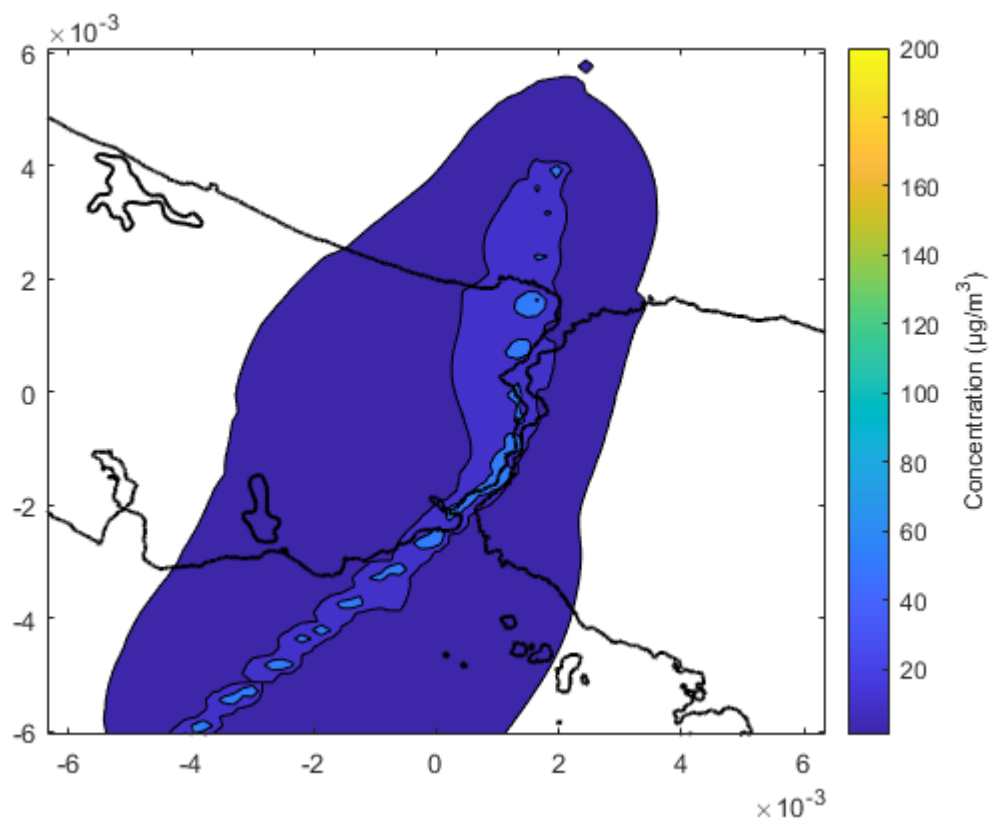
Figure 5.3. SO$_2$ contour plot at 03.03.2017 – 21:00, the time when the 24th highest hourly SO$_2$ concentration occured.
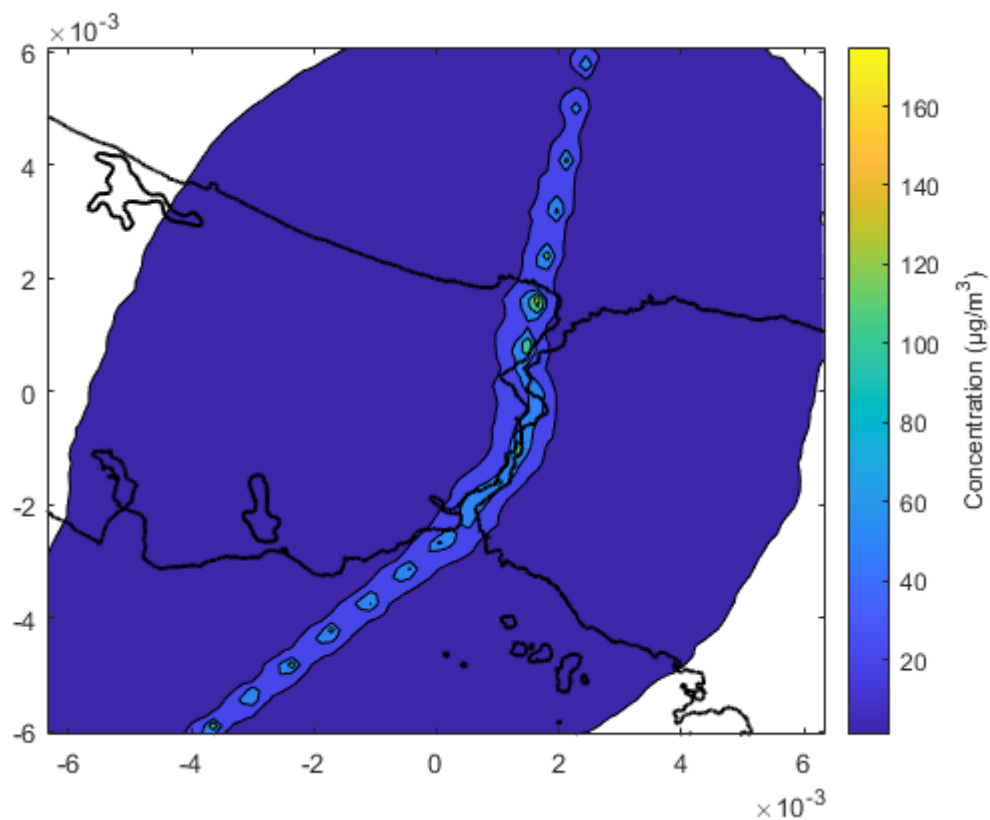

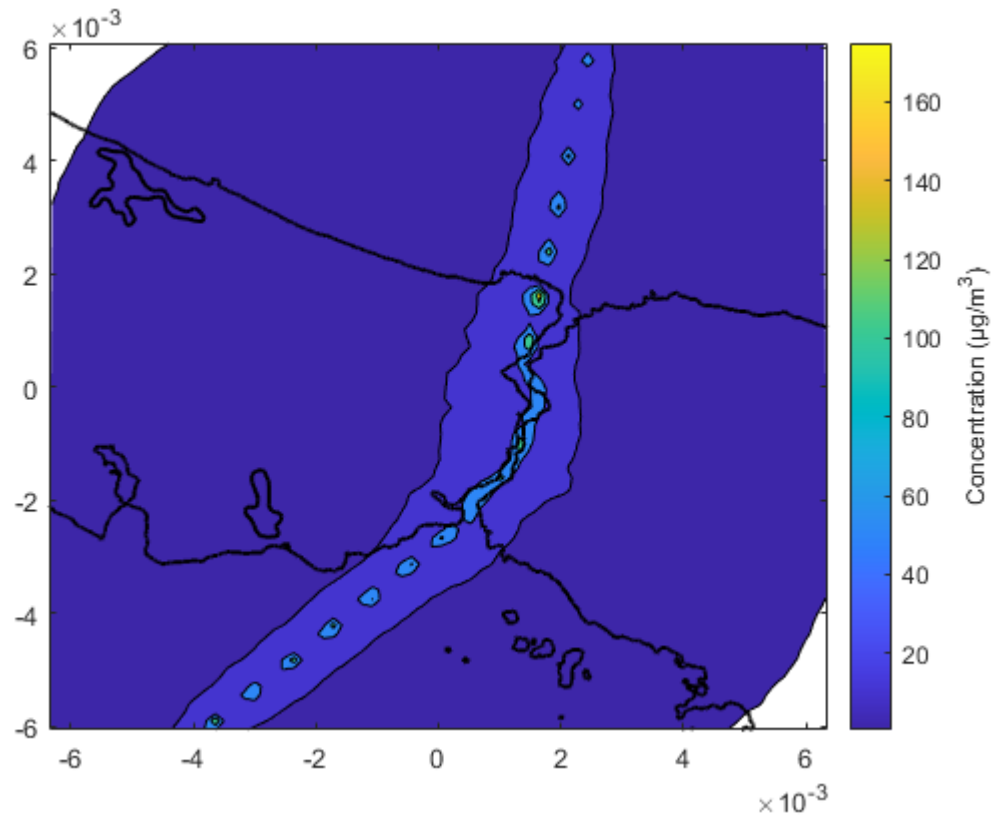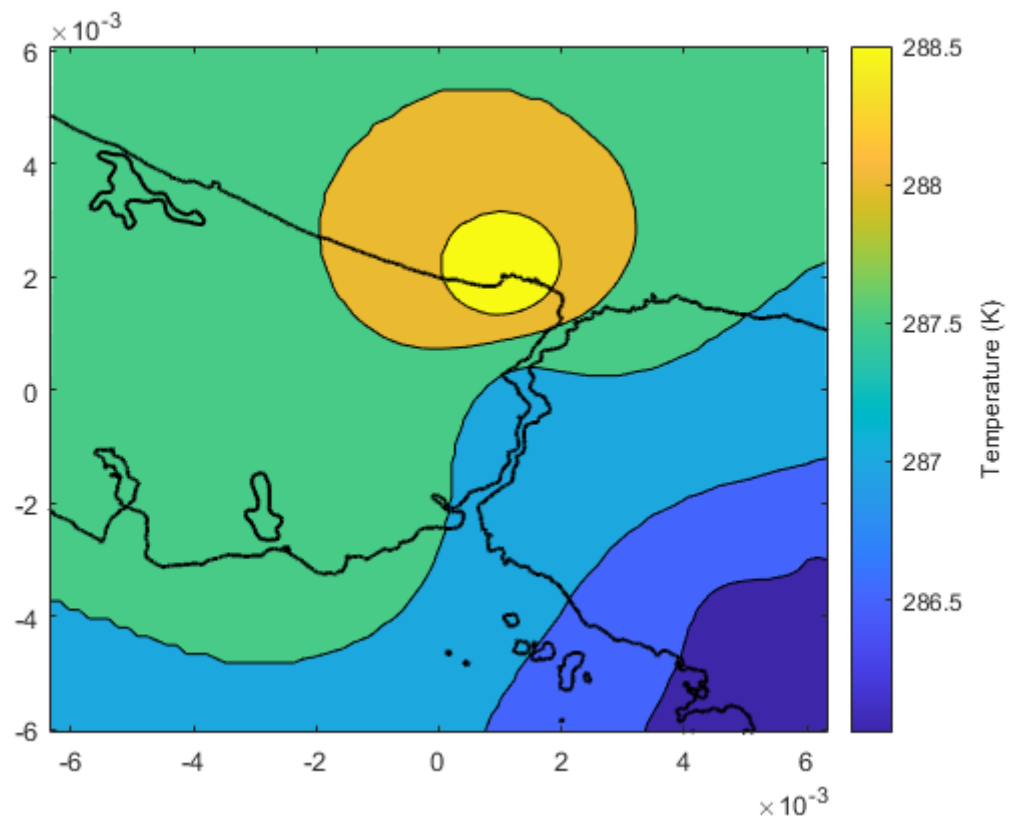Figure 5.4. Contour plot of the 24th highest hourly SO$_2$ concentration at each receptor.

Figure 5.5. Contour plot of 25th highest hourly SO$_2$ concentration at each receptor.

Figures 5.1 and 5.2 shows the air temperature and wind behaviour during the hour when the 24th highest hourly concentration of SO$_2$ occurs. CALMET simulation shows that on March 3, 2017, 21:00, winds are south-easterly. Very low wind speed of nearly 0.4 m/s and 1.4 m/s were observed at the northern and the southern part of the simulated area respectively.

Figure 5.3. shows that, the highest SO$_2$ concentrations are observed on the Bosphorus, around the emission source as expected and with the south-easterly winds, spreads more on the European side of the Istanbul. Concentration spread decreases from the south to north as the wind speed decreases from south to north in the simulated area.

Figure 5.4. and Figure 5.5. shows the 24th and 25th highest hourly SO$_2$ concentration observed at each receptor, during the simulation period. It is observed that, the spread of SO$_2$ is similar on the Asian and European sides of Istanbul, since the wind direction over a 1 year period cover all directions.
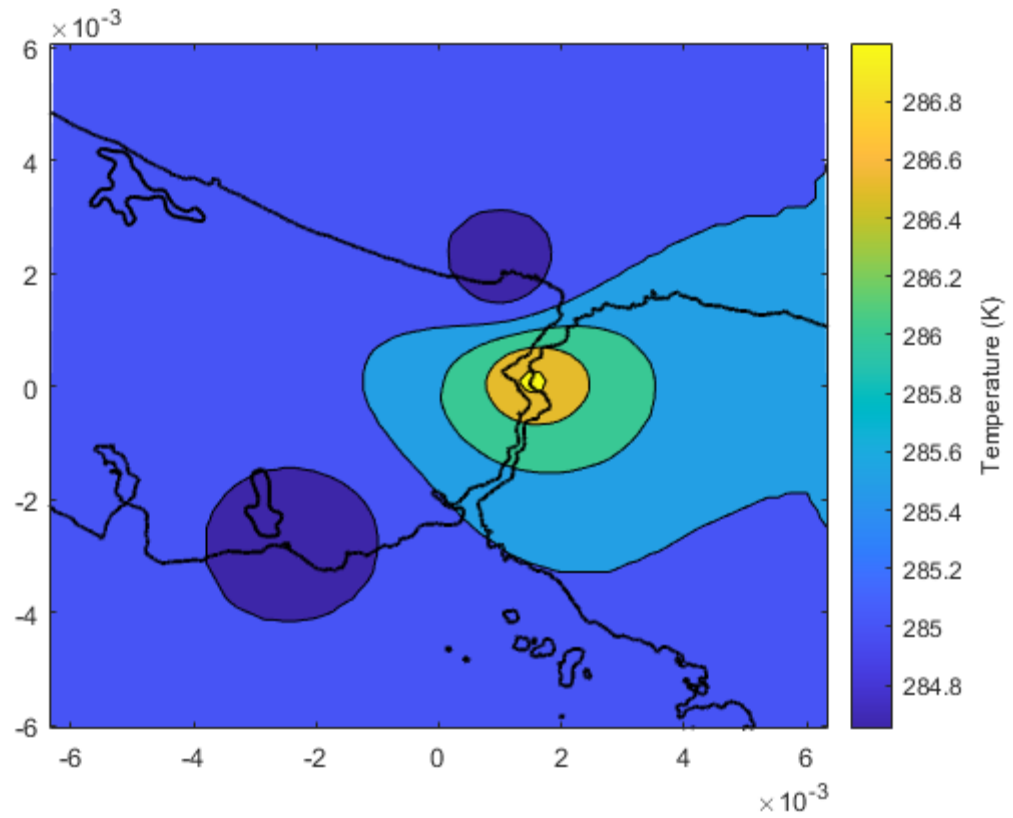
Figure 5.6. Temperature contour of the Bosphorus region, date, time: 20.03.2017, 09:00.

Figure 5.7. Temperature contour of the Bosphorus region, date, time: 20.03.2017, 15:00.
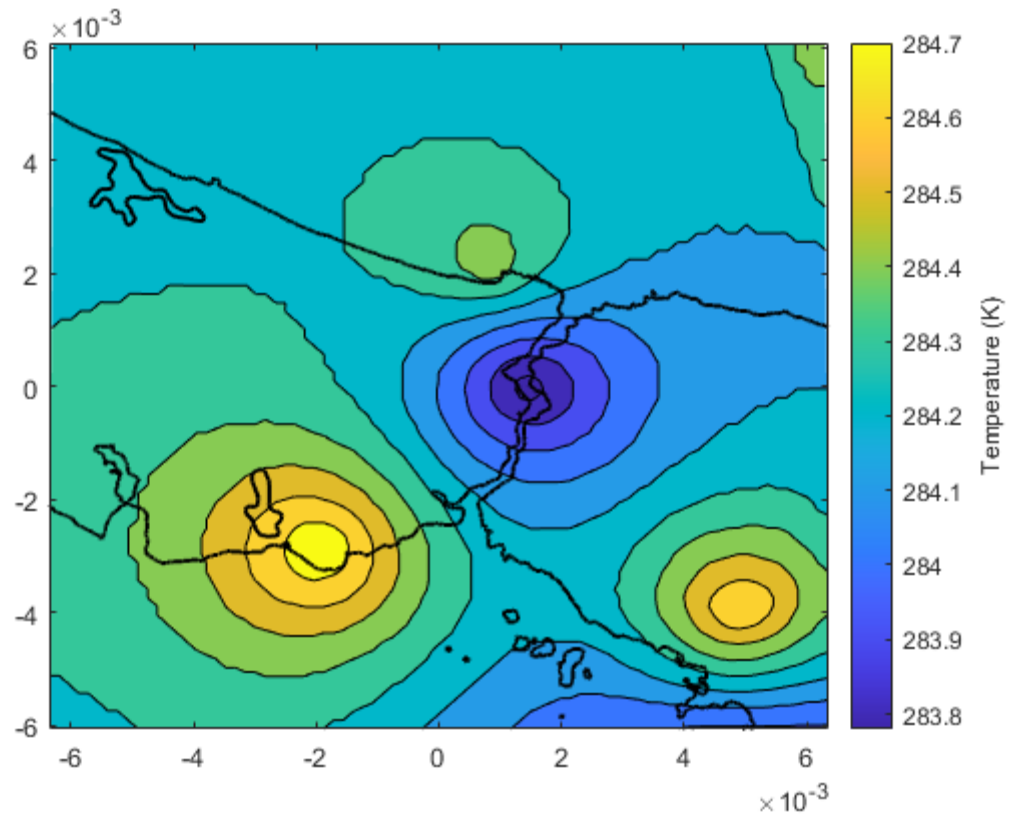
Figure 5.8. Temperature contour of the Bosphorus region, date, time: 20.03.2017, 21:00.
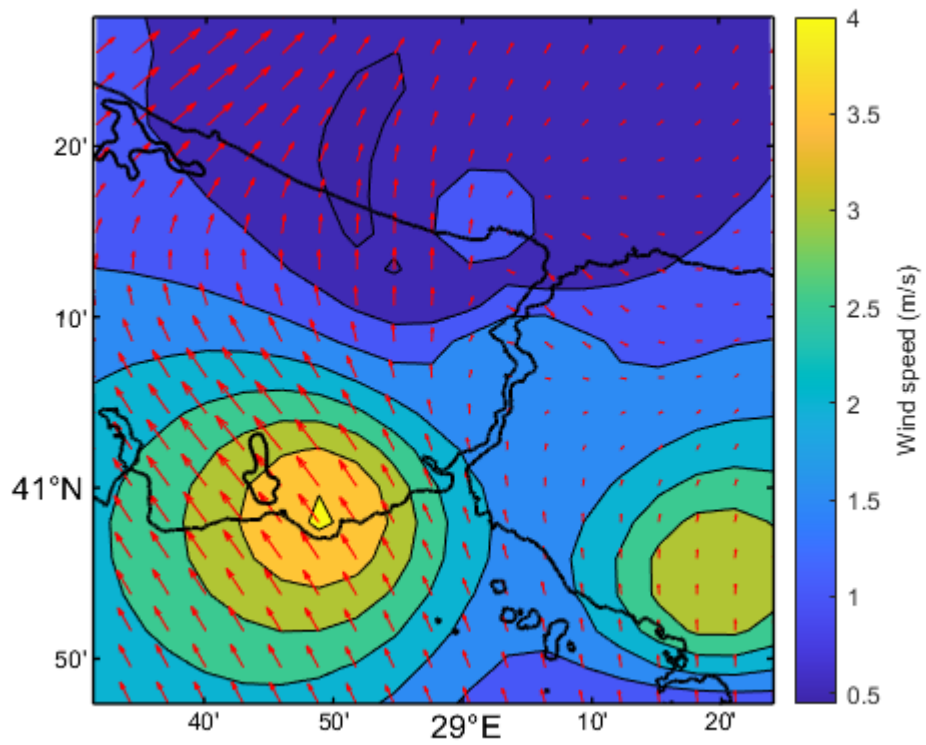

Figure 5.9. Wind plot of the Bosphorus region, date, time: 20.03.2017, 09:00.
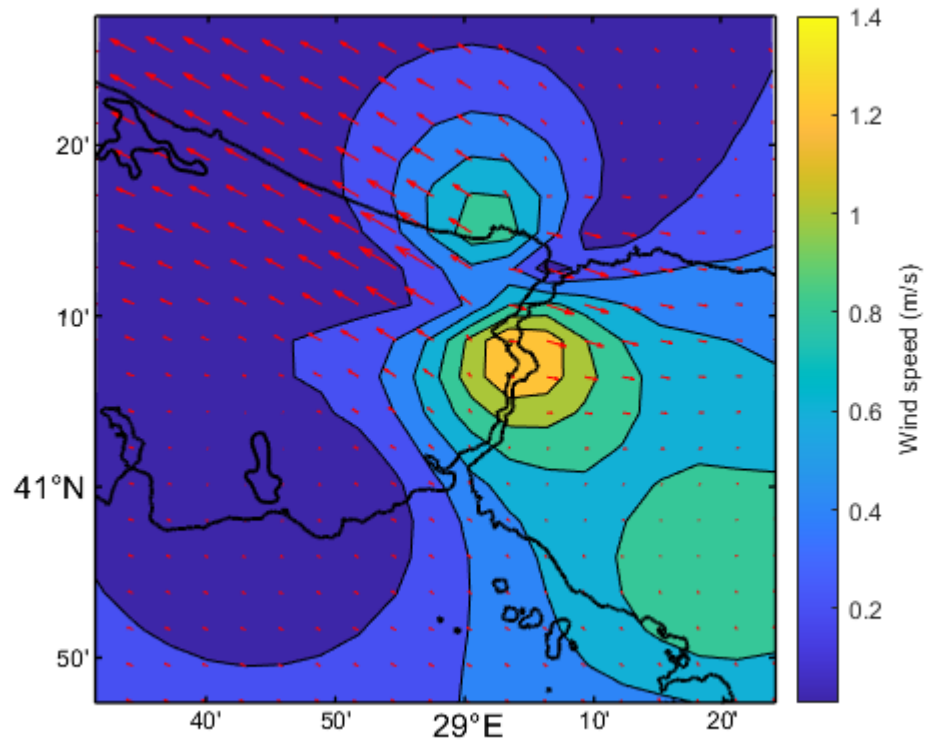
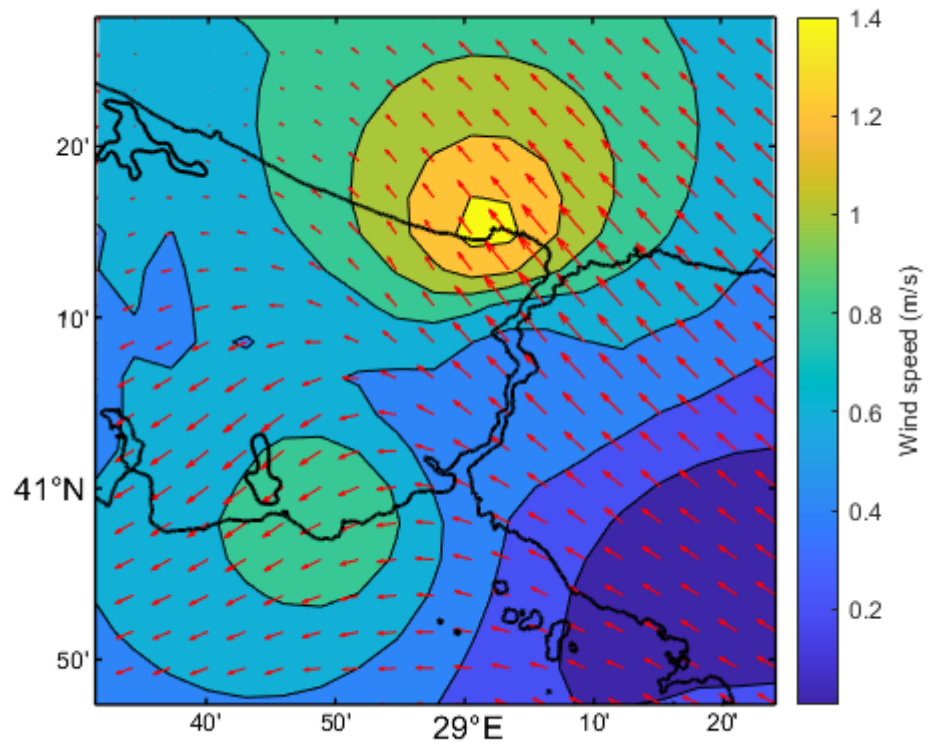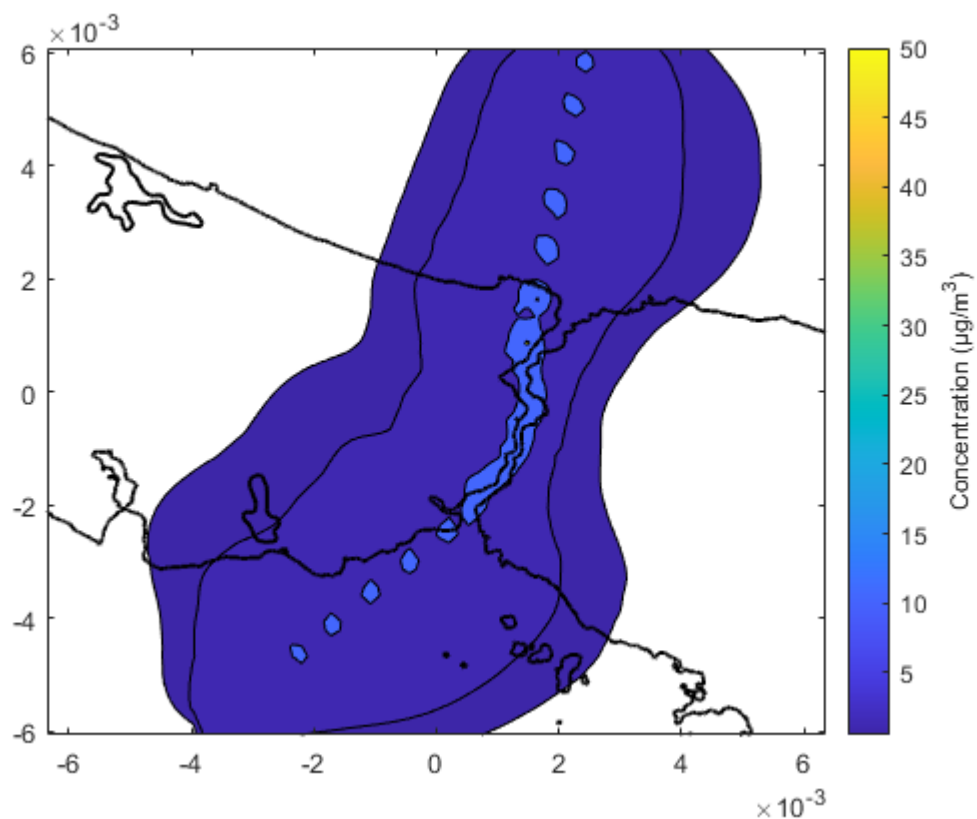Figure 5.10. Wind plot of the Bosphorus region, date, time: 20.03.2017, 15:00.

Figure 5.11. Wind plot of the Bosphorus region, date, time: 20.03.2017, 21:00.

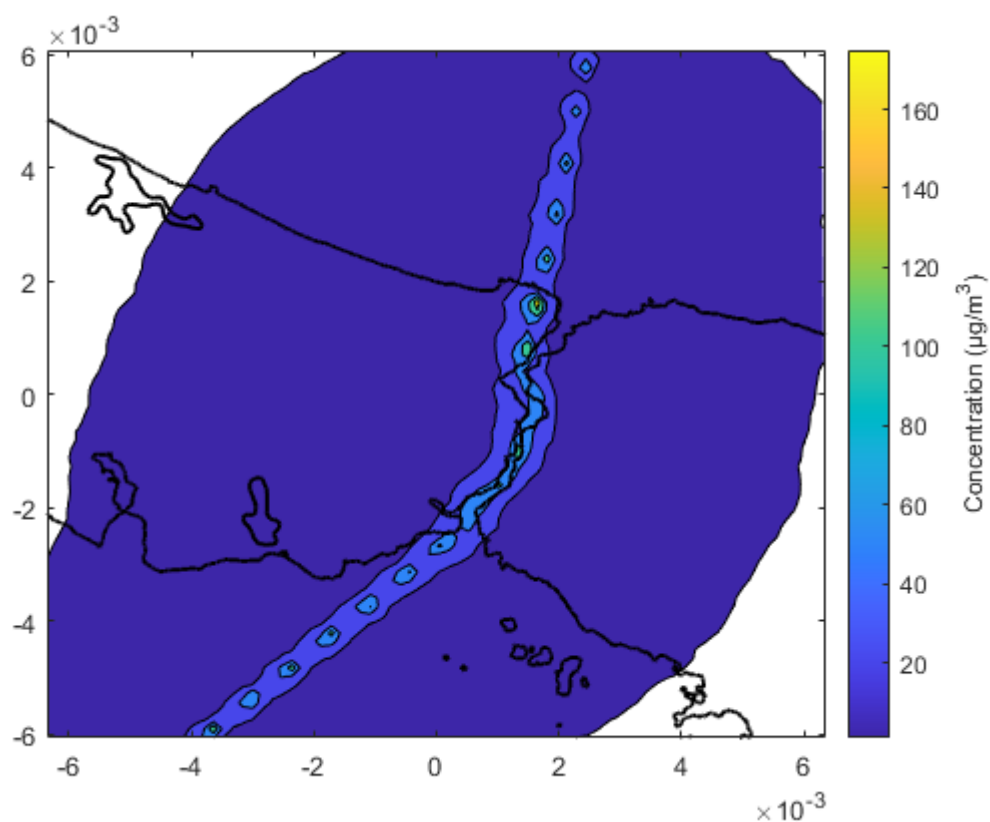Figure 5.12. SO$_2$ contour plot on 20.03.2017, when the 3rd highest 24-hour SO$_2$ concentration occurs.

Figure 5.13. SO$_2$ contour plot of the 3rd highest 24-hour SO$_2$ concentration at each receptor.
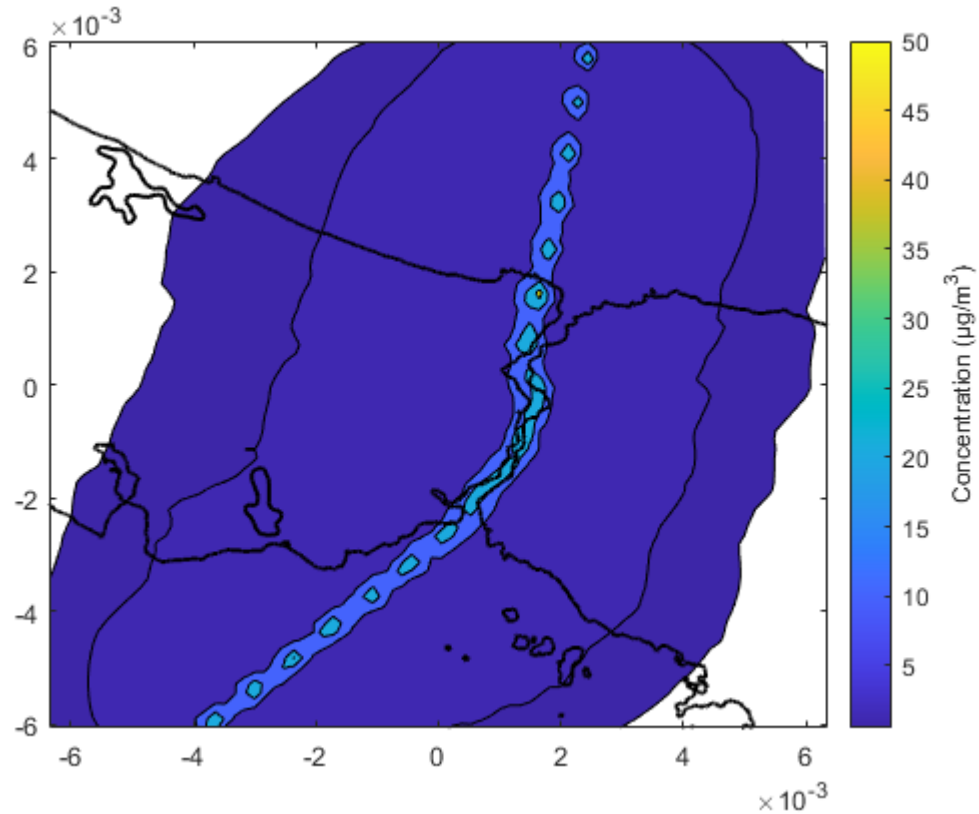
Figure 5.14. SO$_2$ contour plot of the 4th highest 24-hour SO$_2$ concentration at each receptor.

Figures 5.6., 5.7., 5.7., 5.8., 5.9., 5.10. and 5.11. show the air temperature and wind distribution during the episode, when the 3rd highest concentration of SO$_2$ with an exposure time of 24 hour occurs. CALMET simulation shows that on March 20, 2017, winds blew from south in the morning and changed direction to south-easterly in the afternoon. A meaningful decrease in wind speed to values below 0.5 m/s has been observed compared to 3.5 m/s in the morning.

Figure 5.12. shows that, the highest SO$_2$ concentrations are observed as expected along the Bosphorus, which is the emission source location. The concentration contour for SO$_2$ in the southern part of Istanbul is observed to be spread more compared to north. This is attributed to the stronger south-easterly winds in the morning. Concentration spreads are more dominant on the European side of Istanbul. The concentration spread decreases from the south to north as the wind speed decreases in the simulated area .

Figures 5.13. and 5.14. show the 3rd and 4th highest 24-hour SO$_2$ concentration observed at each receptor, during the simulation period. It is observed that, the spread of SO$_2$ is similar on the Asian and European sides of Istanbul, since the wind direction changes throughout the year.
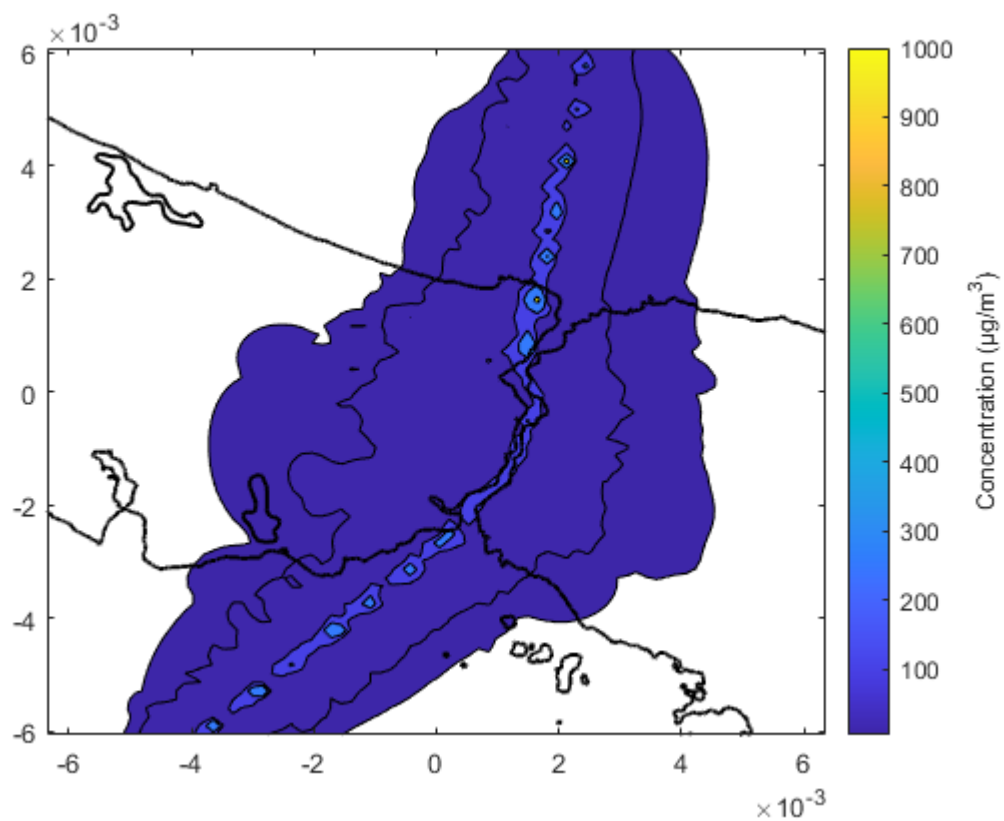
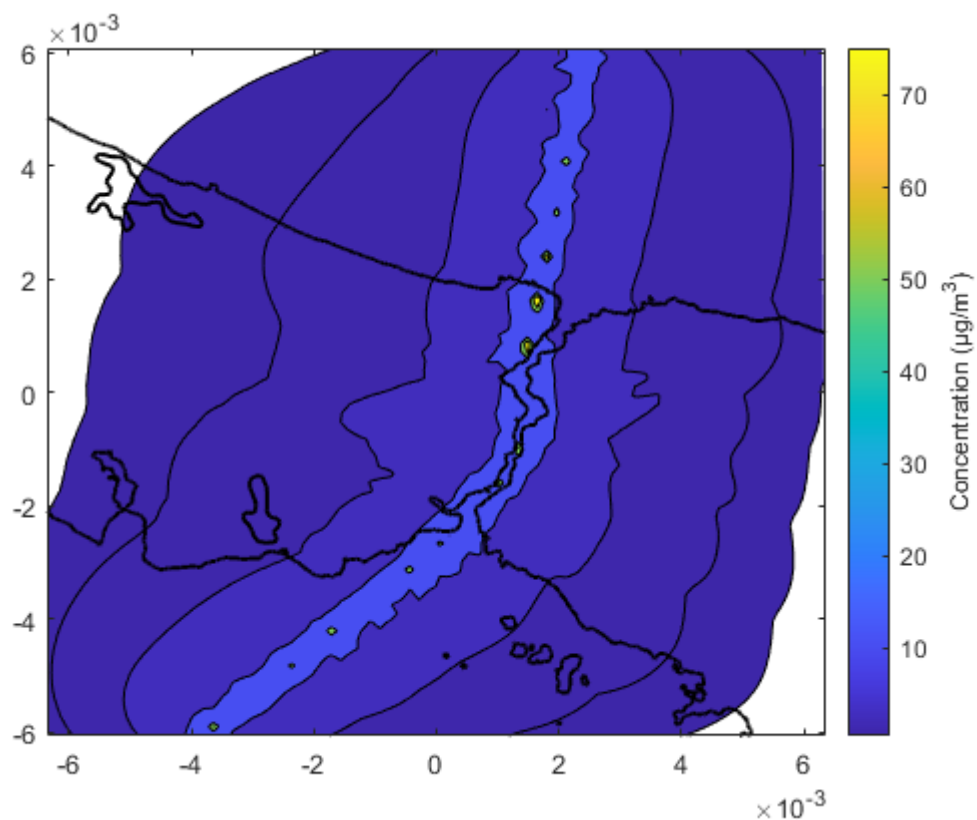Figure 5.15. Contour plot of the maximum hourly SO$_2$ concentration at each receptor.

Figure 5.16. Contour plot of the maximum 24-hour SO$_2$ concentration at each receptor.
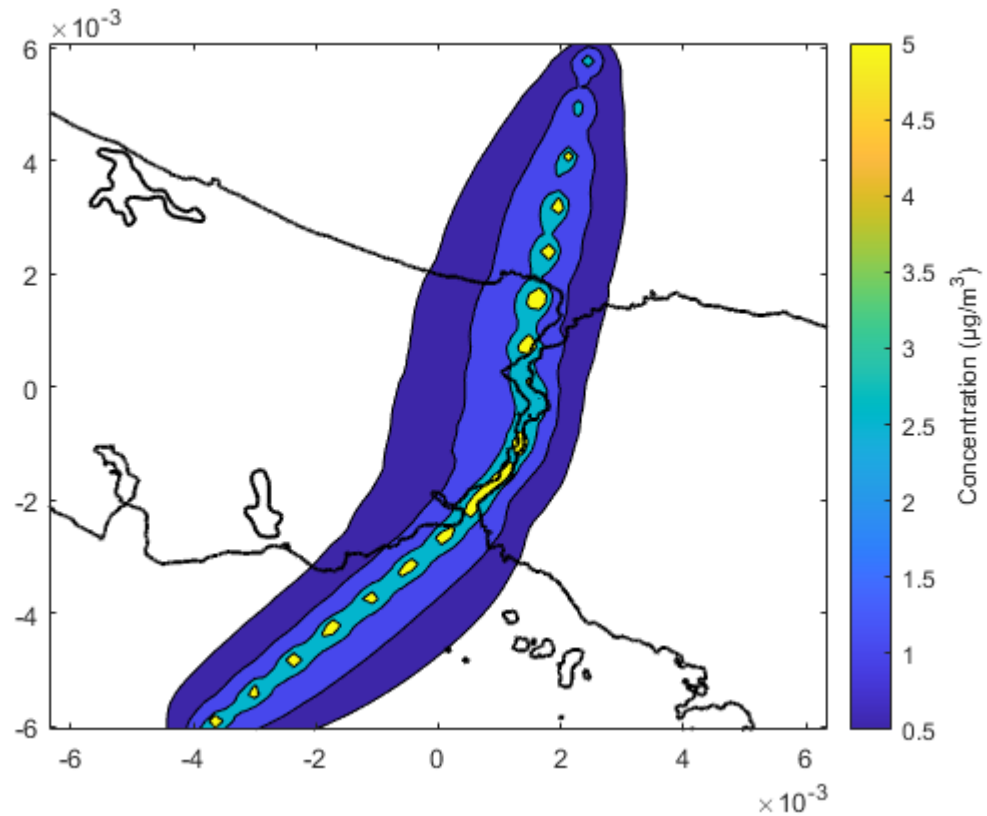
Figure 5.17. Annually averaged SO_2 concentration for year 2017.

Figures 5.15. and 5.16. show the maximum 1-hour and 24-hour SO_2 concentrations, respectively, observed at each receptor. It is observed that, the spread of the SO_2 concentration is somewhat equal on both sides of the Istanbul region, which is similar to spread pattern excepted, since the wind direction changes throughout the year. It is observed that maximum concentration of 200 µg/m^3 for the 1 hour exposure time and around 30 µg/m^3 for the 24 hour exposure time is observed on the shores of Istanbul.

Figure 5.17 presents the annual average SO_2 concentration contour. SO_2 emissions are more concentrated around the source as expected. It can be seen from the spread of the SO_2 concentration most populated parts of Istanbul are effected by the ship traffic. With values ranging from 0.5 µg/m^3 to 2.5 µg/m^3 adjacent to the source, indicating that ships are major SO_2 sources.
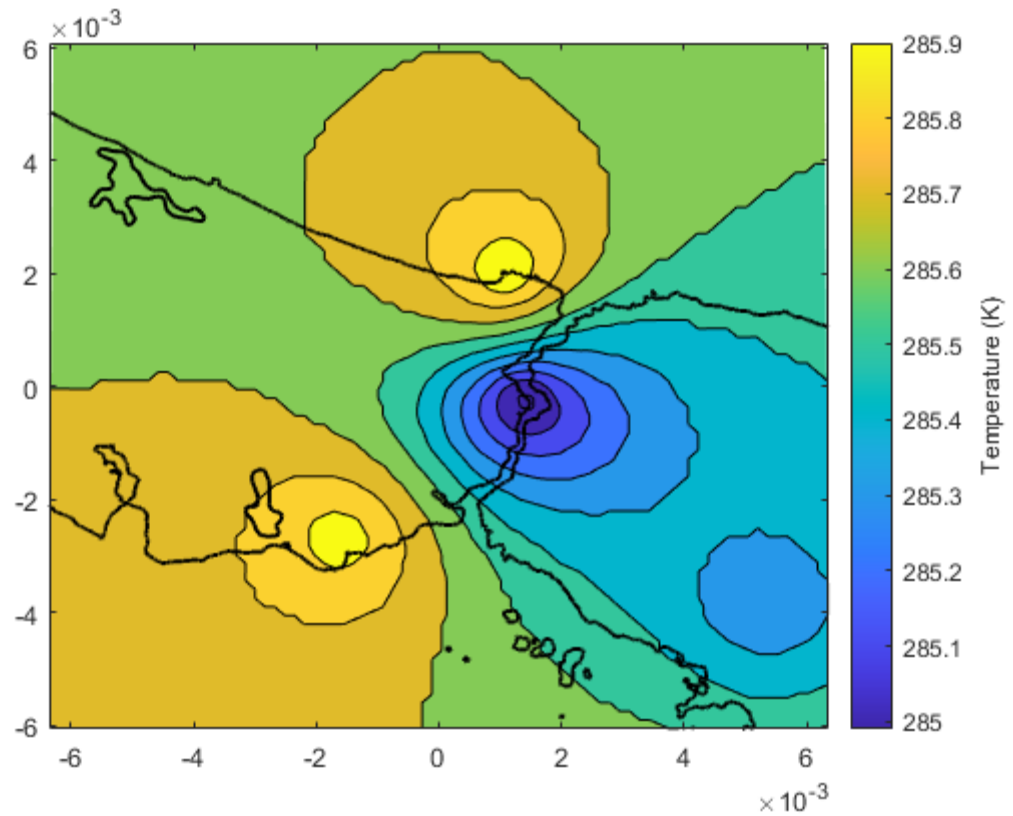
Figure 5.18. Temperature contour in the Bosphorus region, date, time: 24.04.2017, 14:00.
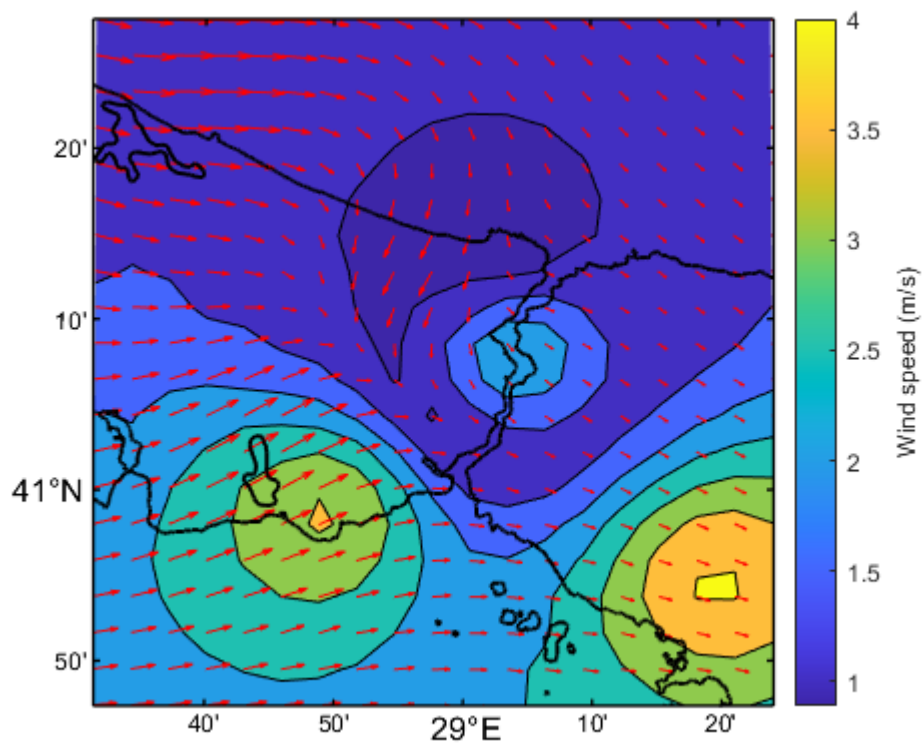

Figure 5.19. Wind plot in the Bosphorus region, date, time: 24.04.2017, 14:00.
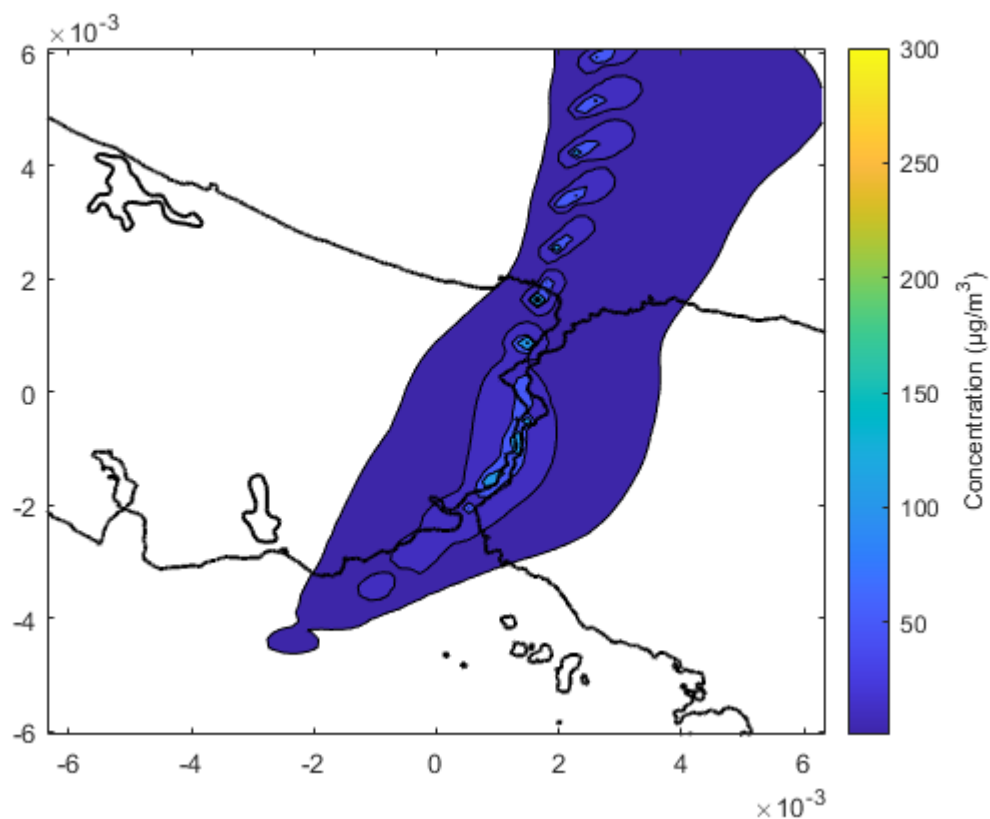
Figure 5.20. NO$_2$ contour plot at 24.04.2017 – 14:00, the time when the 18th highest hourly NO$_2$ concentration occurs.
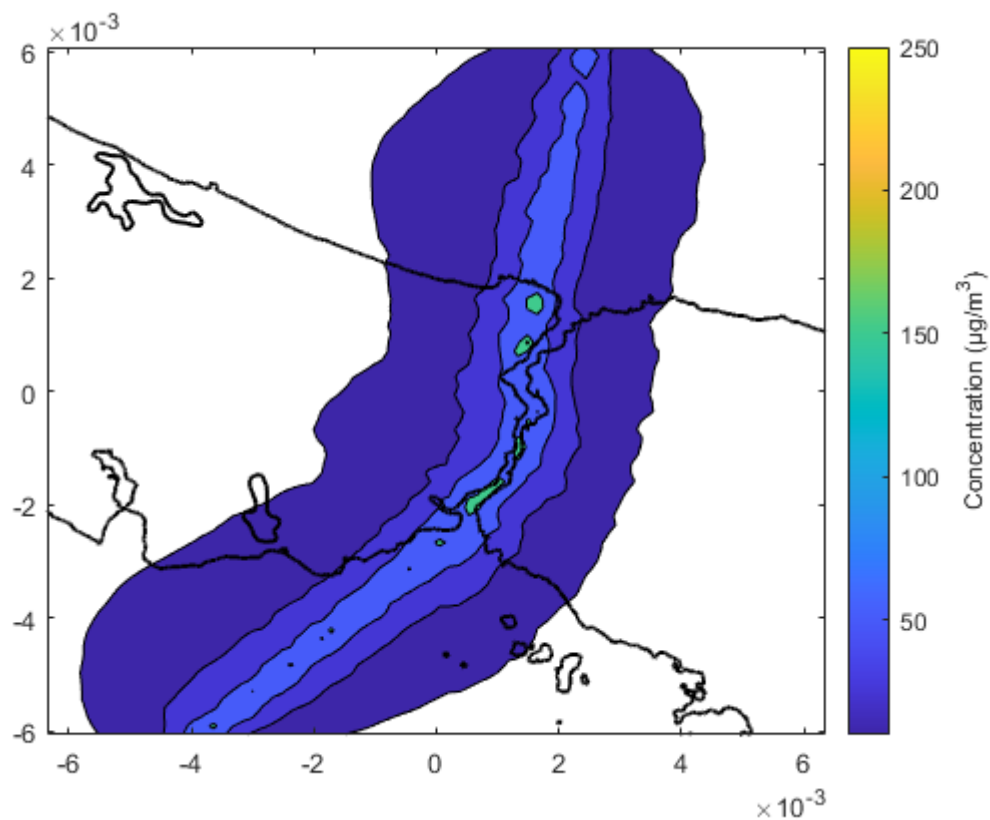

Figure 5.21. Contour plot of the 18th highest hourly NO$_2$ concentration at each receptor.

Figure 5.18 and 5.19 shows the air temperature and wind distribution on April 24, 2017 14:00, the hour when the 24th highest hourly SO_2 concentration occurs. CALMET simulation shows that winds blows from west side of the modeling area. Very low wind speed of nearly 1.5 m/s is observed at the northern part and relatively higher wind speeds of around 4 m/s was observed at the southern part of the simulated area.

Figure 5.20. shows that the highest SO_2 concentrations are observed on the Bosphorus, around the emission source as expected and with the westerly winds, spreads more on the Anotolian side of the Istanbul. Concentration spread decreases from the north to south which migt be caused by the increasing wind speed from north to south in the simulated area with mixed wind direction on the Bosphorus.

Figure 5.21. shows the 18th highest hourly NO_2 concentration at each receptor. It is observed that, the spread of NO_2 is similar on the Asian and European sides of Istanbul, since the wind direction changes throughout the year
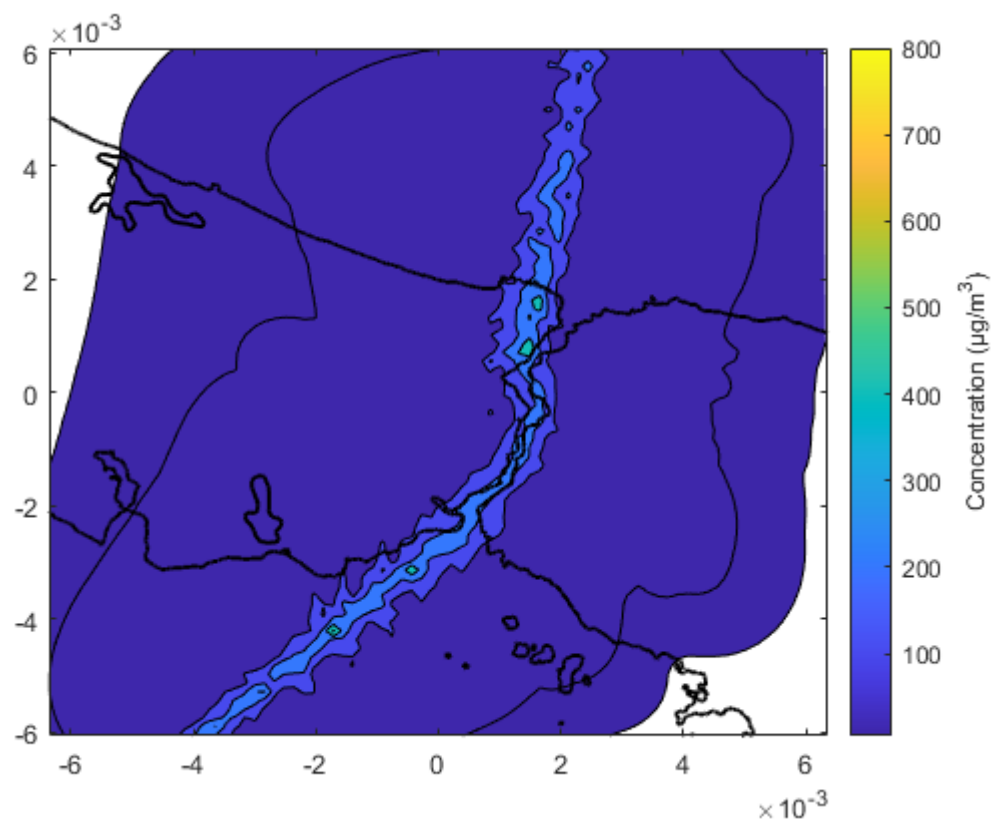
.

Figure 5.22. Contour plot of the maximum hourly NO_2 concentration at each receptor.
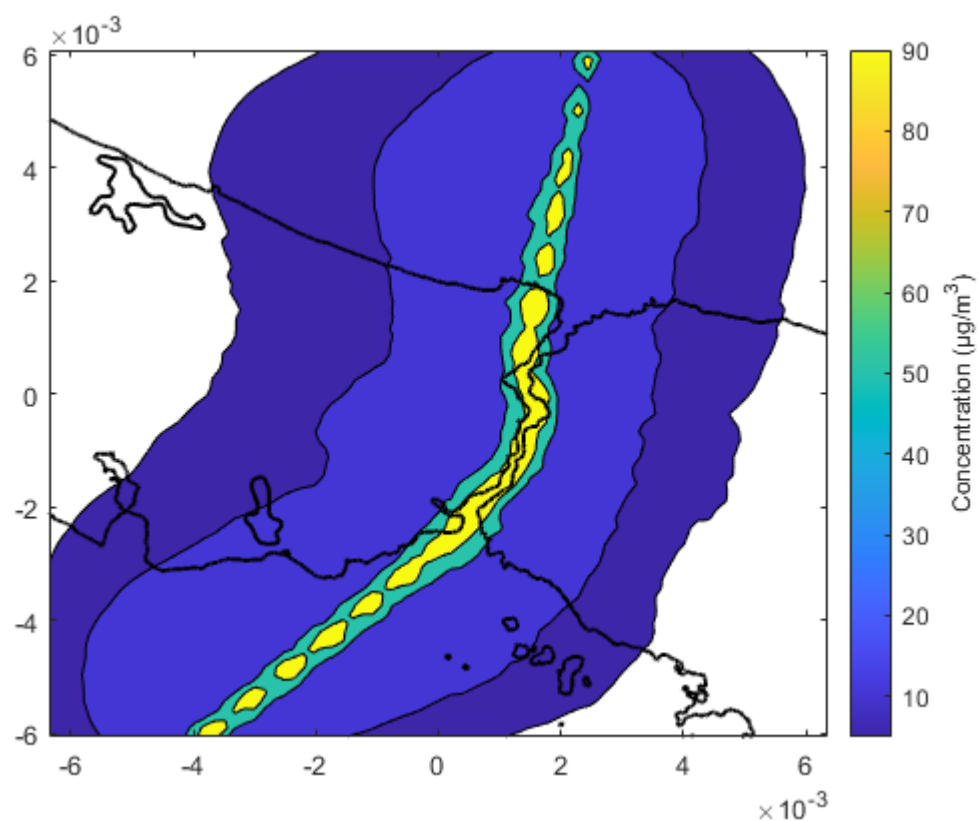
Figure 5.23. Contour plot of the maximum 24-hour NO_2 concentration at each receptor.
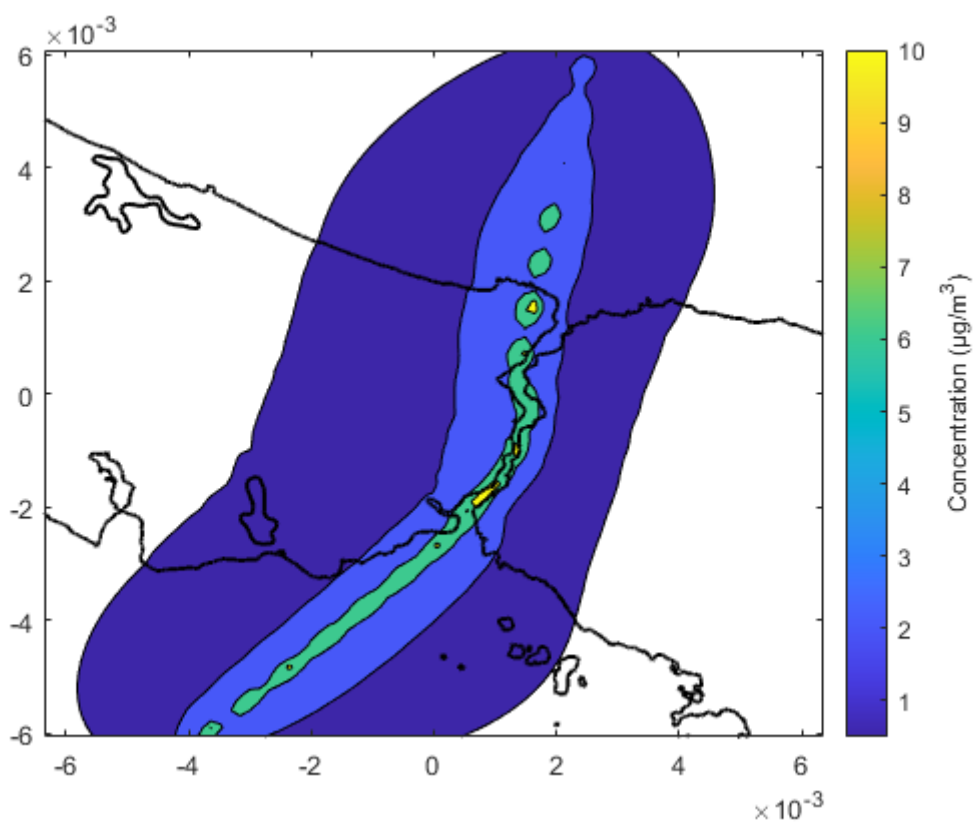

Figure 5.24. Contour plot of the annually averaged NO_2 concentration for year 2017.

Figures 5.22. and 5.23. show the maximum 1-hour and 24 hour NO_2 concentration observed at each receptor, during the simulation period. It is observed that spread of the NO2 concentration is somewhat similar on the Asian and European sides of Istanbul, since the wind direction changes throughout the year. The maximum concentration of 300 µg/m³ for the 1 hour exposure time and around 60 µg/m³ for the 24 hour exposure time is observed on the shores of Istanbul.

Figure 5.24 represents the annual average NO_2 concentration contour. NO_2 emissions are more concentrated around the source as expected. It can be seen from the spread of the NO_2 concentration most populated parts of Istanbul are effected by the ship traffic. With values ranging from 3 µg/m³ to 6 µg/m³ at around the source.

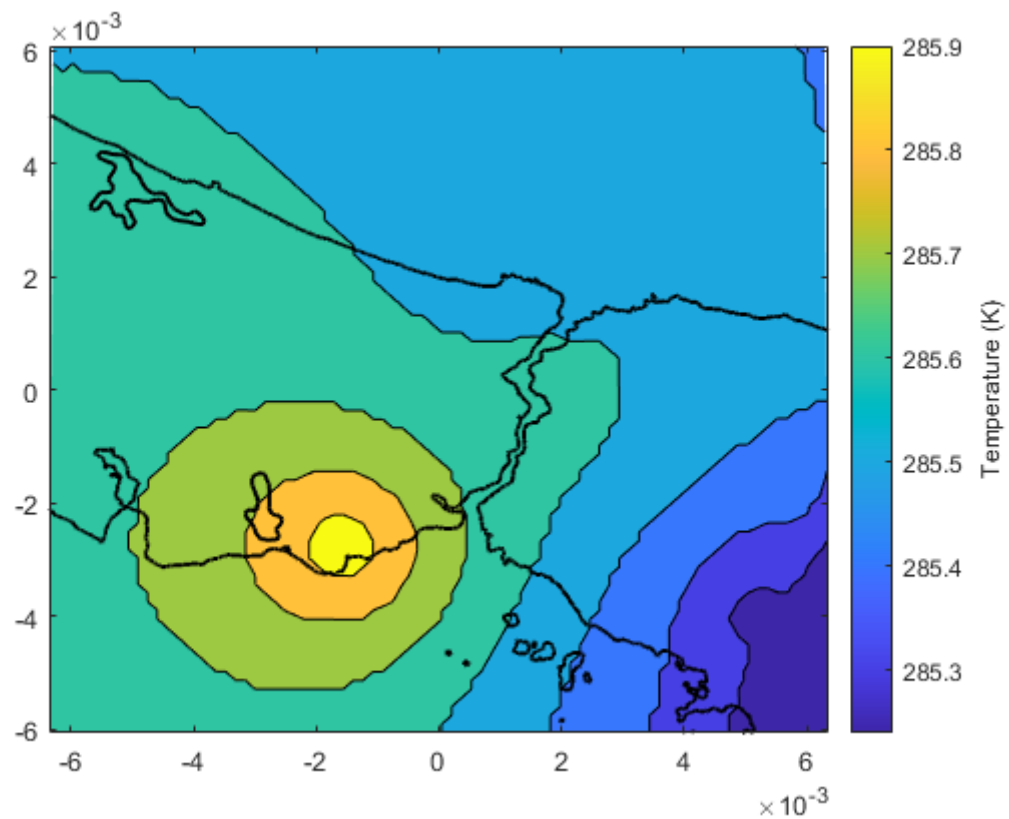Figure 5.25. Temperature contour in the Bosphorus region, date, time: 23.11.2017, 09:00.
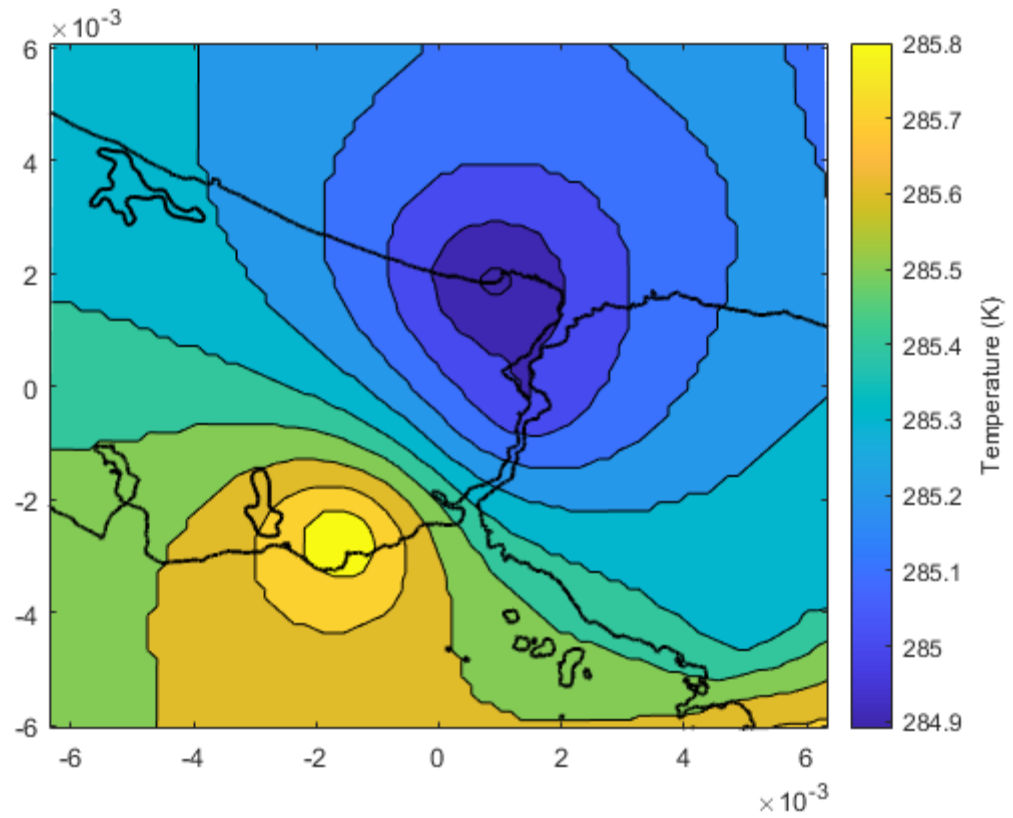
Figure 5.26. Temperature contour in the Bosphorus region, date, time: 23.11.2017, 15:00.
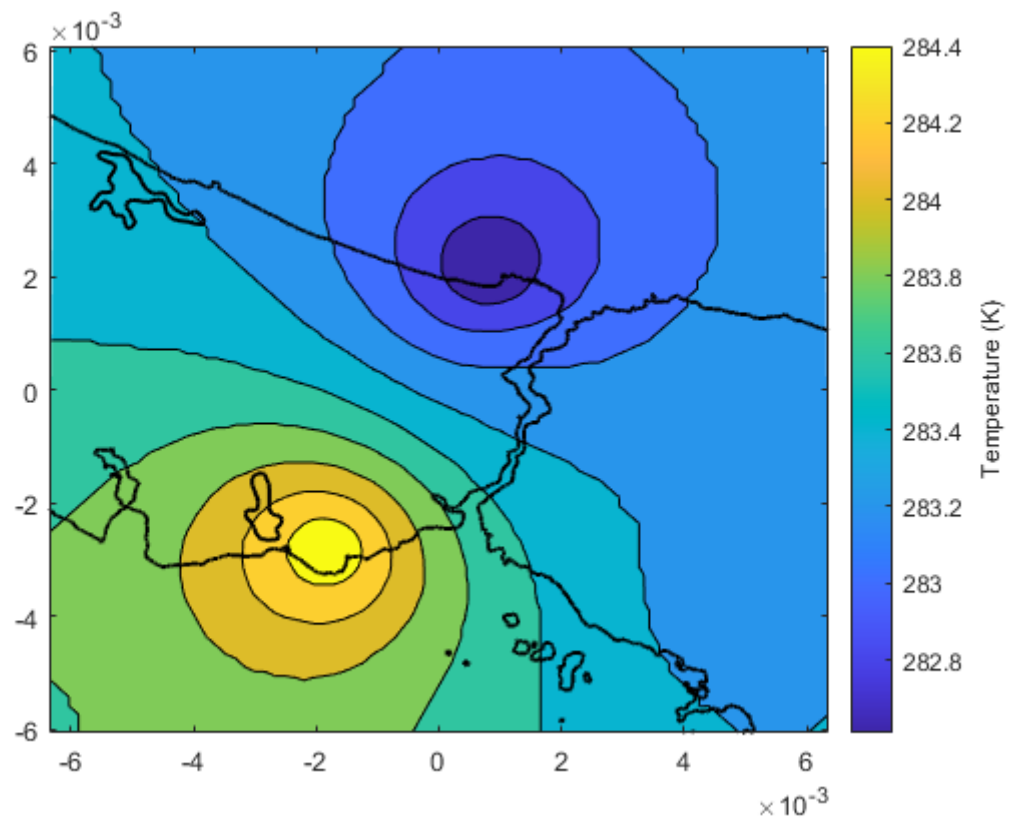
Figure 5.27. Temperature contour in the Bosphorus region, date, time: 23.11.2017, 21:00.
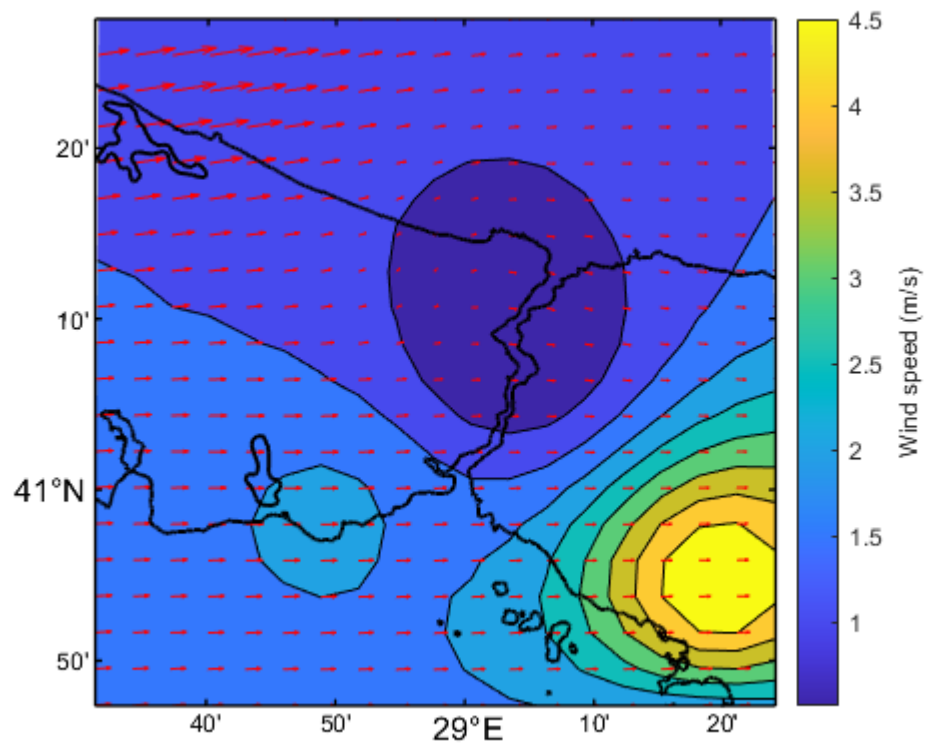
Figure 5.28. Wind plot in the Bosphorus region, date, time: 23.11.2017, 09:00.
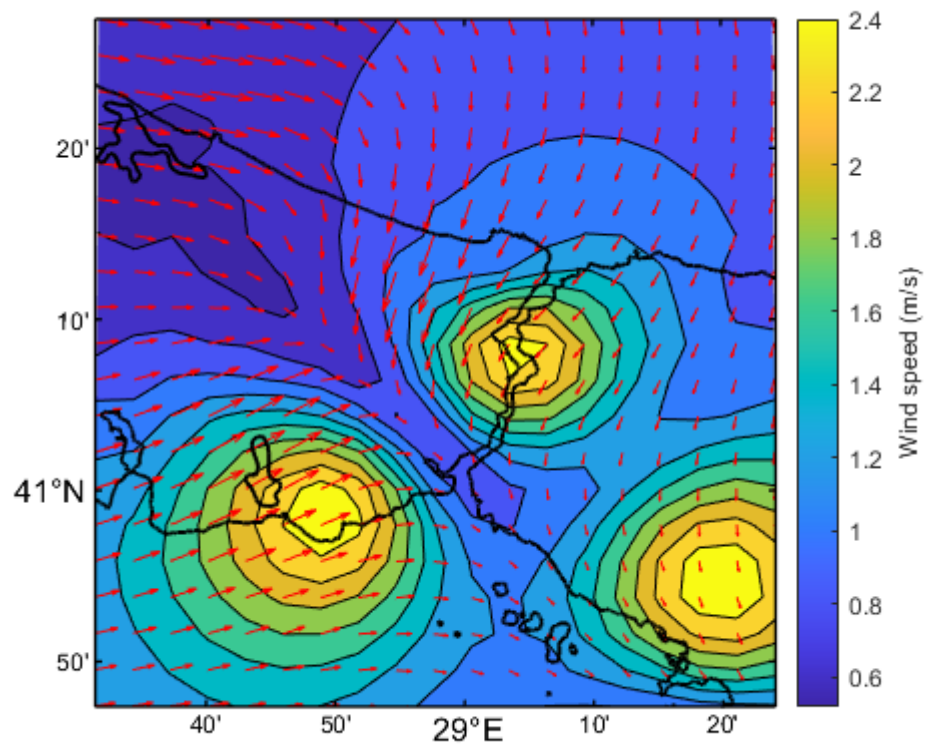
Figure 5.29. Wind plot in the Bosphorus region, date, time: 23.11.2017, 15:00.

Figure 5.30. Wind plot in the Bosphorus region, date, time: 23.11.2017, 21:00.

Figure 5.31. PM contour plot on 23.11.2017, 35th highest 24-hour primary PM_{10} concentration
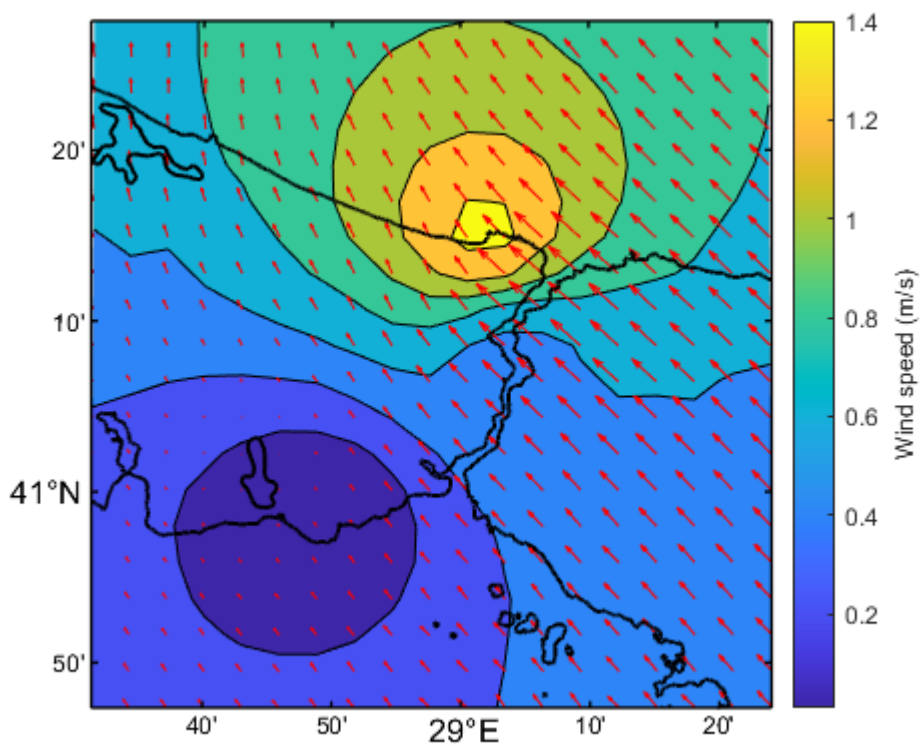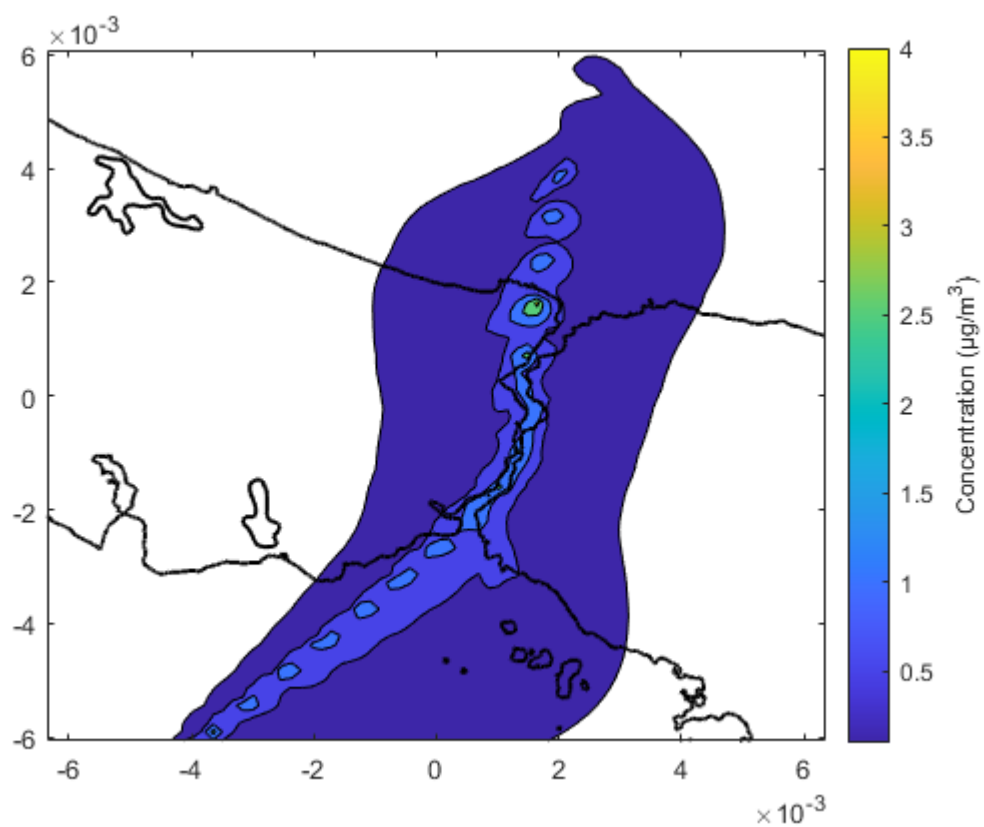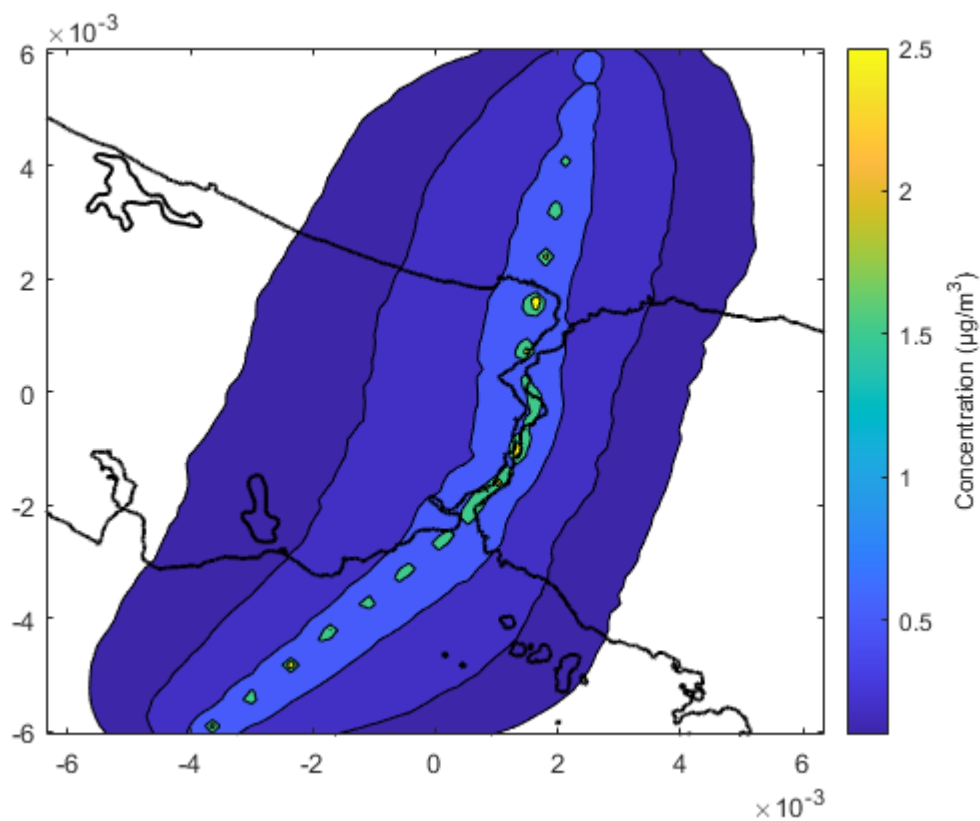
Figure 5.32. Contour Plot of the 35th highest 24-hour primary PM$_{10}$ concentration at each receptor.
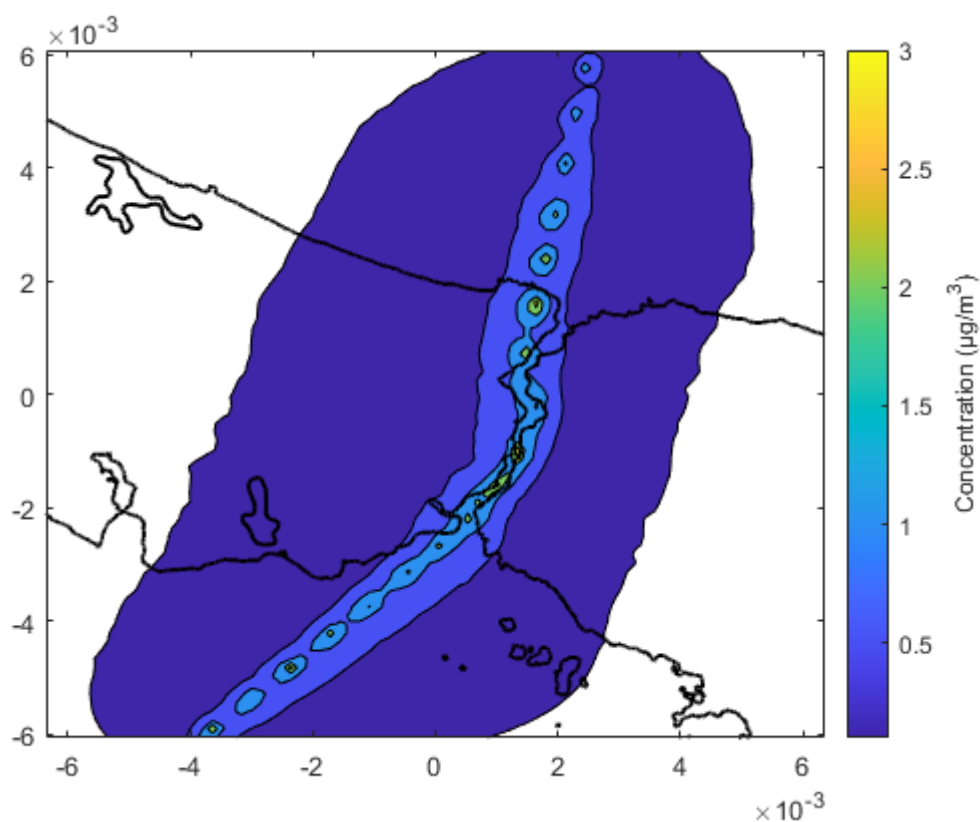
Figure 5.33. Contour plot of the 36th highest 24-hour primary PM$_{10}$ concentration at each receptor.

Figures 5.25, 5.26, 5.27, 5.28, 5.29 and 5.30 show the air temperature and wind distribution during November 23, 2017 when the 35th highest 24-hour PM_{10} concentration. CALMET simulation shows that on November 23, 2017, winds blows from west in the morning, changes direction to north-westerly in the afternoon and starts blowing from south at night. In the morning, wind speed of around 1.5 m/s and 3 m/s were observed in the north and south part of the simulated area respectively. Wind speed changes to 1.6 m/s and 0.8 m/s in the afternoon and at night respectively.

Figure 5.31. shows that the highest PM_{10} concentrations are observed on the Bosphorus, around the emission source as expected and the concentration contour for PM_{10} in the southern part of the Istanbul is observed to spread more compared to north. This might be caused by the westerly blown wind in the morning and afternoon. The spread of PM_{10} is more domaninat on the Anatolian side of the Istanbul. Concentration spread decreases from the south to north as the wind speed decreases from south to north in the simulated area only with an exception for the wind speeds at night.

Figure 5.32. and 5.33. shows the 35th and 36th highest , 24-hour average concentration of PM_{10} observed at each receptor, during the simulation period. It is observed that, the spread of PM10 is similar on the Asian and European sides of Istanbul, since the wind direction changes throughout the year.
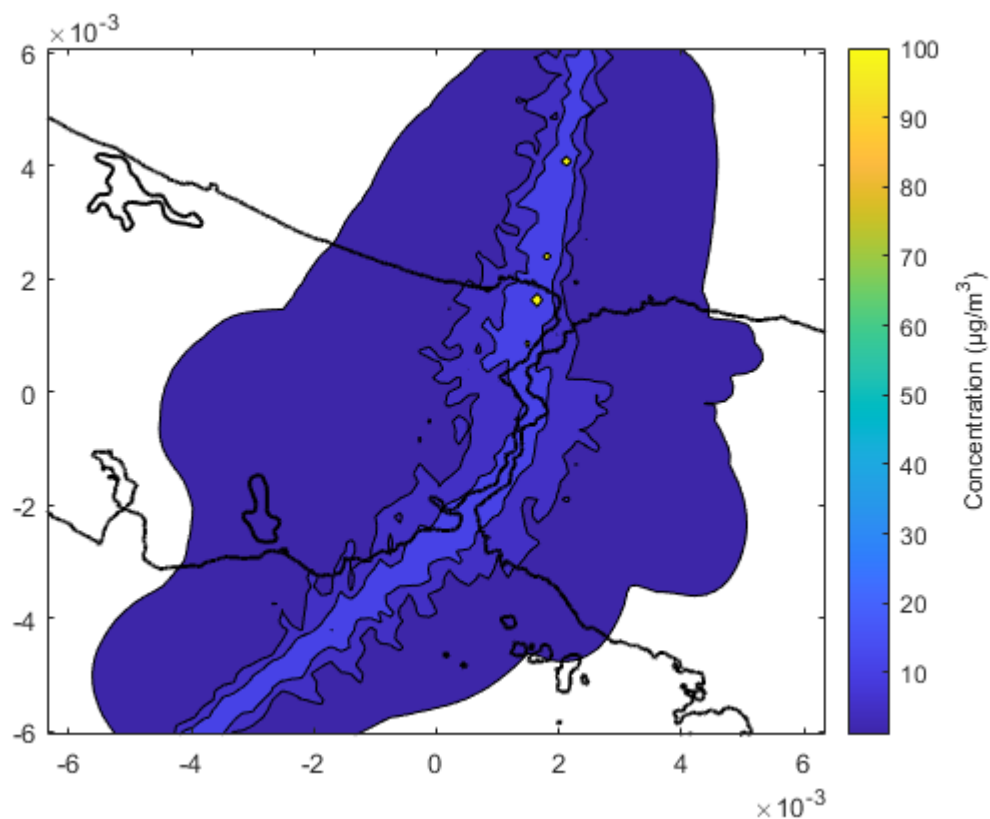
Figure 5.34. Maximum hourly primary PM$_{10}$ concentration at each grid.
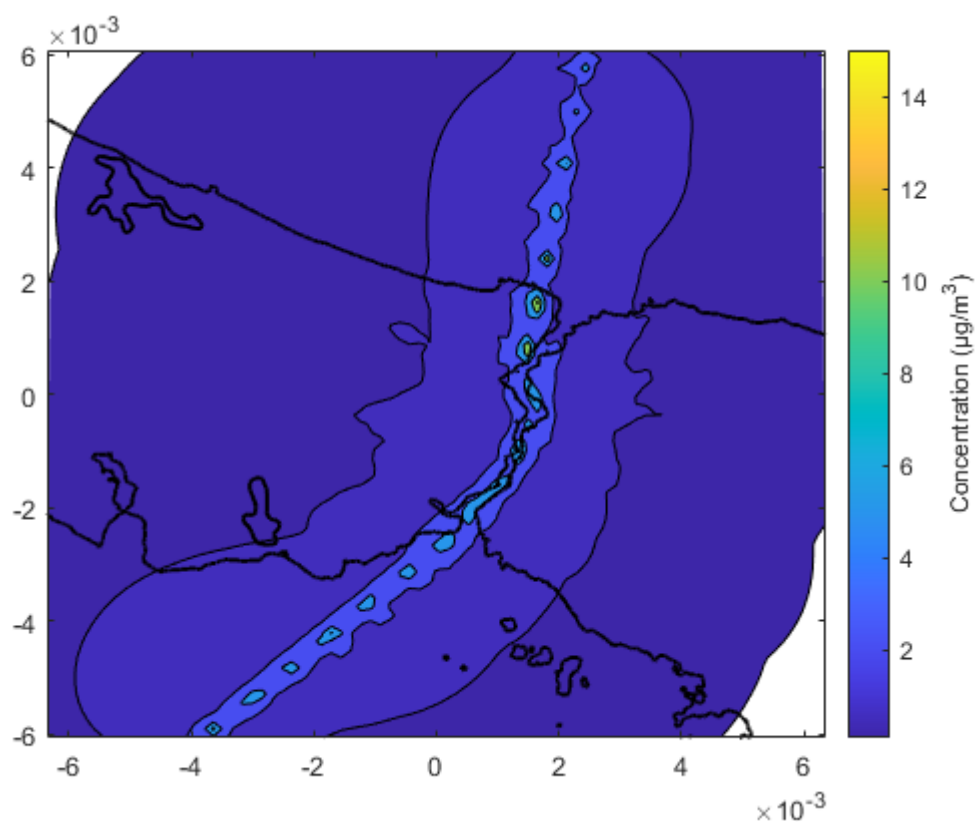
Figure 5.35. Contour plot of the maximum 24-hour primary PM$_{10}$ concentration at each receptor.
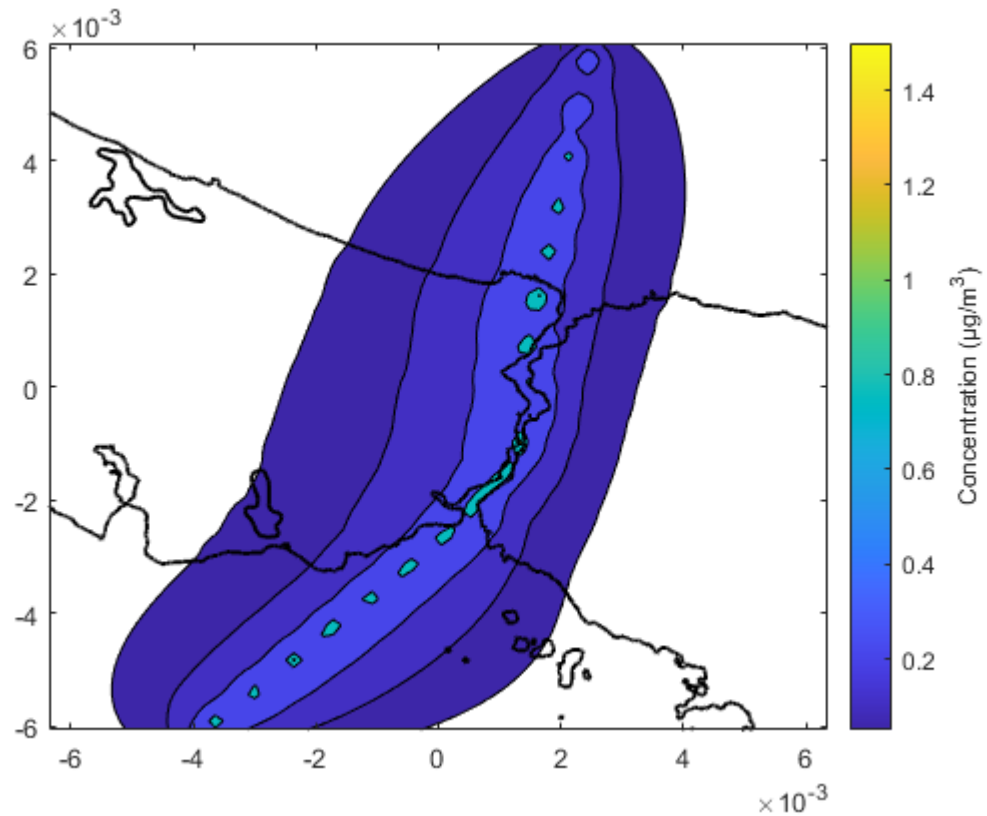
Figure 5.36. Contour plot of the Annual primary PM$_{10}$ concentration for year 2017.

Figures 5.34. and 5.35. show the maximum hourly and 24-hour PM$_{10}$ concentration observed at each receptor, respectively. It is observed that, the spread of PM$_{10}$ concentration is somewhat equal on both sides of Istanbul, since the wind direction changes throughout the year. The maximum observed concentration is 20 µg/m^3 for the 1-hour exposure time and around 6 µg/m^3 for the 24 hour exposure time. The highest conentratinos are located along the Bosphorus coastline.

Figures 5.36 presents the annually averaged PM$_{10}$ concentration contour plot. PM$_{10}$ emissions are more concentrated around the source as expected. It can be seen from the spread of the NO$_2$ concentration that the most populated parts of Istanbul are effected by the ship traffic. Also, it is observed that the European side of the Istanbul is effected more by PM$_{10}$, with values ranging from 0.6 µg/m^3 to 0.4 µg/m^3 at around the source.

Figure 5.37. Contour Plot of the annual secondary PM concentration for year 2017.

Figure 5.38. Contour of the total annual $PM_{2.5}$ concentration for year 2017.

Figure 5.37 presents the annually averaged secondary PM concentration contour plot. Secondary PM is defined as summation of NO_3 and SO_4 c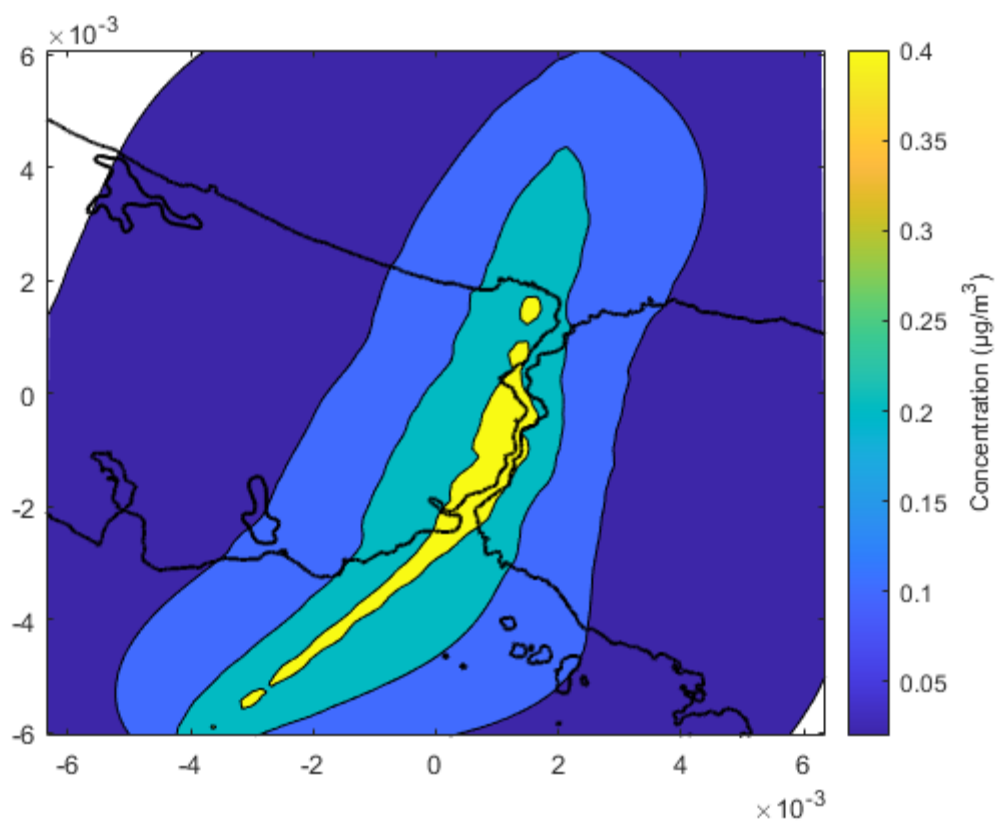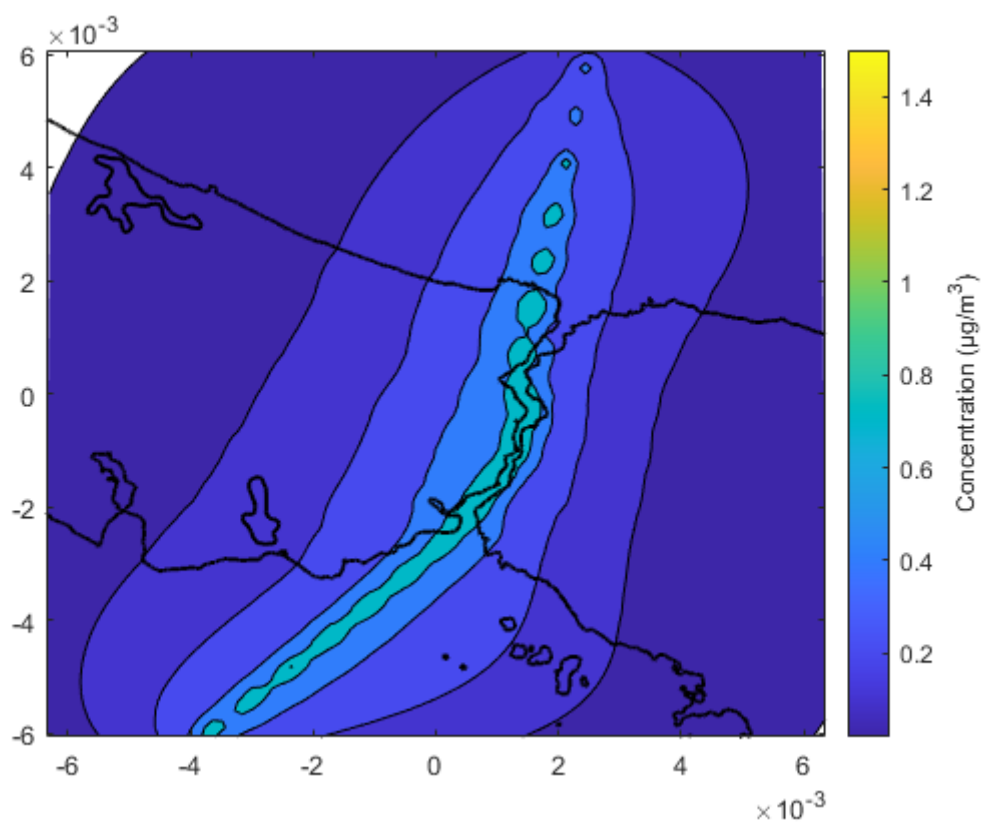oncentrations. PM emissions are more concentrated around the source as expected. It can be seen from the spread of the secondary PM concentration that the most populated parts of Istanbul are effected by the ship traffic. It is observed that the European side of the Istanbul is effected more by secondary PM, with values 0.4 µg/m^3 at European side and 0.25 µg/m^3 at Anatolian side.

Figure 5.38 presents the annually averaged $PM_{2.5}$ concentration contour plot. $PM_{2.5}$ emission is assumed to be equal to sum of 67 % of PM_{10} and all of the secondary PM. The concentration contour for $PM_{2.5}$ in the southern part of the Istanbul is observed to spread more compared to north. The spread of PM_{10} is more domaninat on the European side of the Istanbul. Concentration spread decreases from the south to north. Concentration of $PM_{2.5}$ is at around 0.4 µg/m^3 at European side and at around 0.25 µg/m^3 at Anatolian side.

Table 5.2. Comparison of the simulation results with the Turkish regulations.

Result Summary Table				
Pollutant	**Exposure Period**	**Regulation (µg/m^3)**	**Maximum Concentrations (a) due to Ship Traffic (µg/m^3)**	**% Contribution of Ship Traffic to Air Quality Standards**
SO$_2$	1 hour	350	217	61.97
	24 hours	125	69	55.18
	Annual	20	12	61.74
NO$_2$	1 hour	200	277	138.74
	Annual	40	14	34.01
PM$_{10}$	24 hours	50	4	7.13
	Annual	70	3.56	2.55
Remarks: (a) Taking into account the allowable number of exceedances (See Table 5.1)				

Table 5.2 summarizes the maximum pollutant concentrations for different exposure times predicted by The CALPUFF model and how they compared with the Turkish air quality standards. It can be seen from the results that, ships have major effect on the overall air quality in the vicinity of the Bosphorus. The impact of the ship emissions are up to 60 % of the SO_2 annual air quality standard (20 µg/m^3), nearly 35 % of the NO_2 annual air quality standard (20 µg/m^3), and approximately 2.5 % of the PM_{10} annual air quality standards (70 µg/m^3). The study shows that significance of the maritime traffic through the Bsphorus on the city's air quality, particularly on the bosphorus shores which is a common reacreational area of the city.

In order to observe the variation of the simulated concentrations with distance from the Bosphorus strait where the emission source is located, sectional annual concentration plots are presented below. The location of the selected section is shown in Figure 5.39.
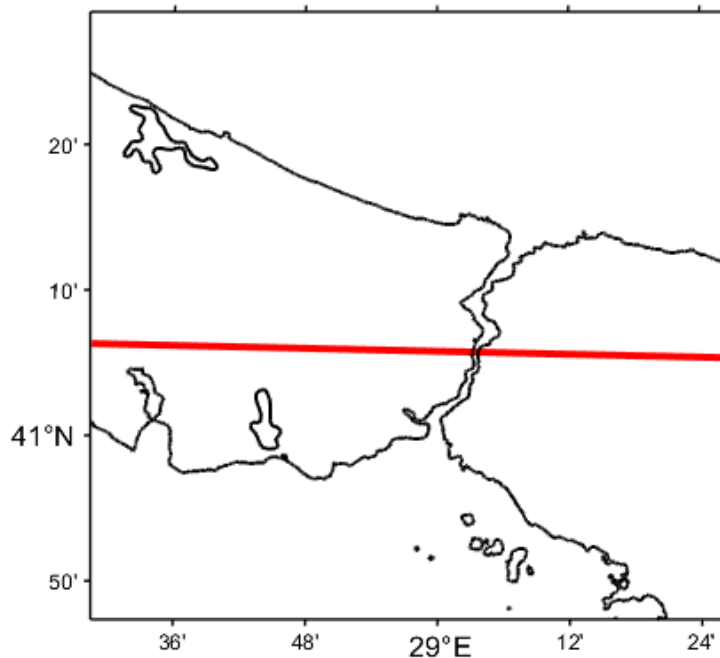
Figure 5.39. Selected section across the Bosphorus.
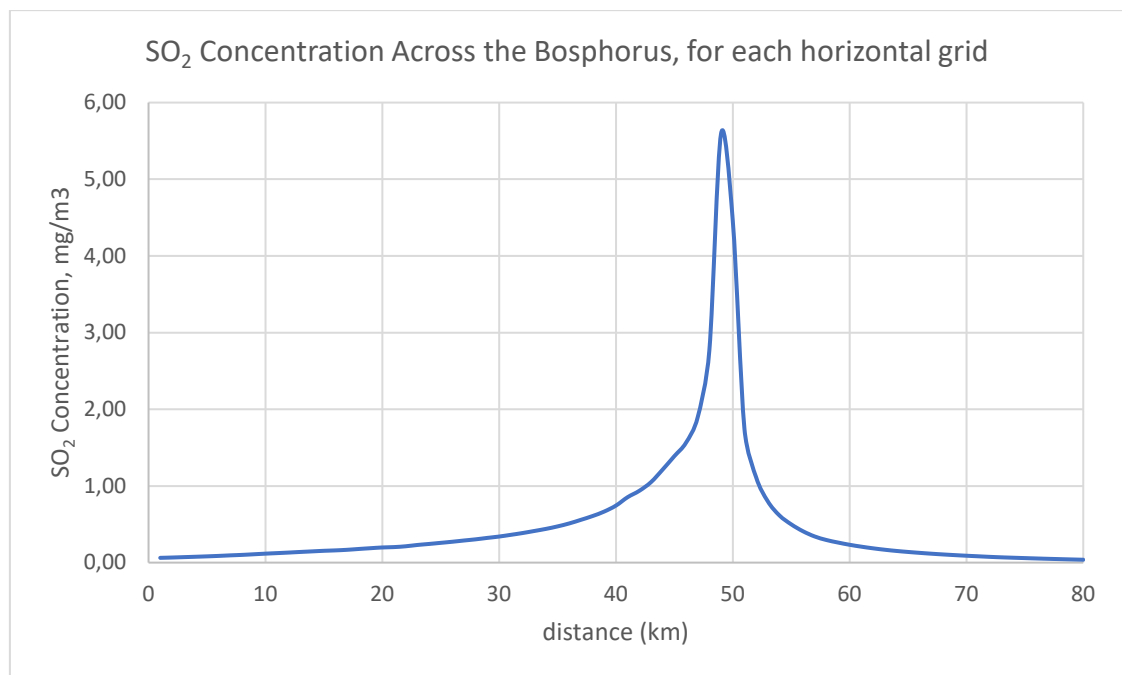
Figure 5.40. Annual SO$_2$ concentration along section perpendicular to the Bosphorus.
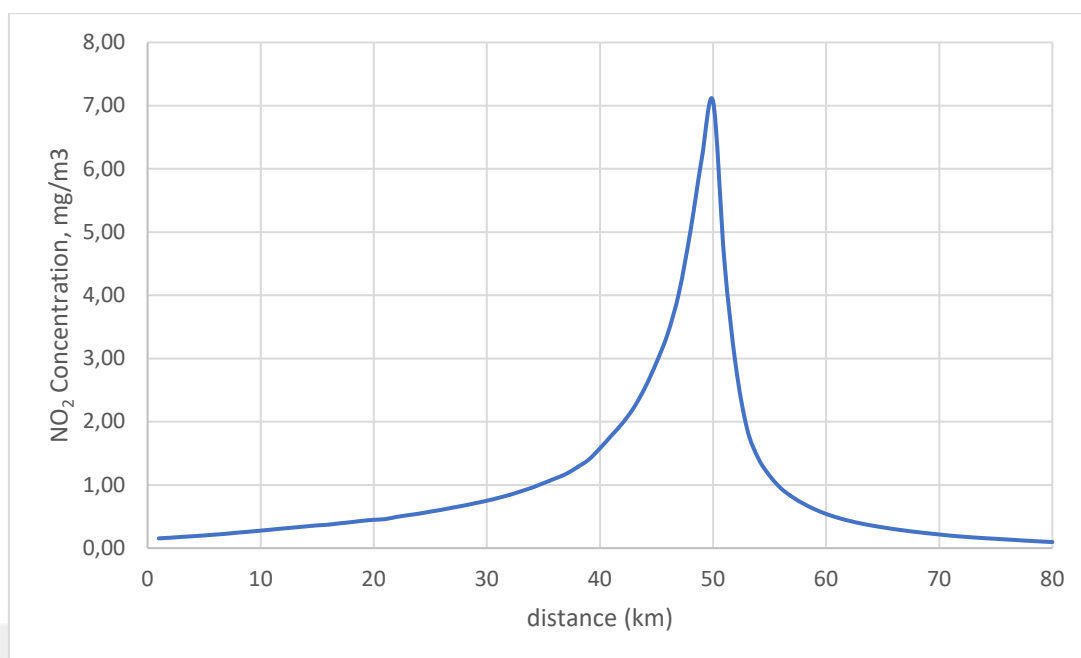
Figure 5.41. Annual NO$_2$ concentration along section perpendicular to the Bosphorus.
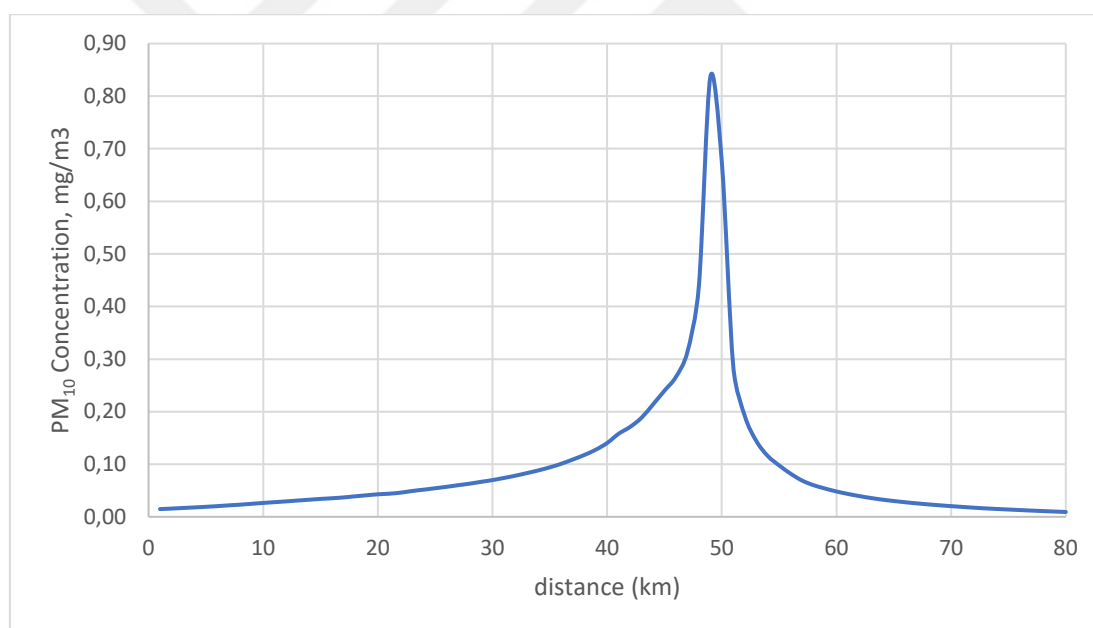
Figure 5.42. Annual PM$_{10}$ concentration along section perpendicular to the Bosphorus.
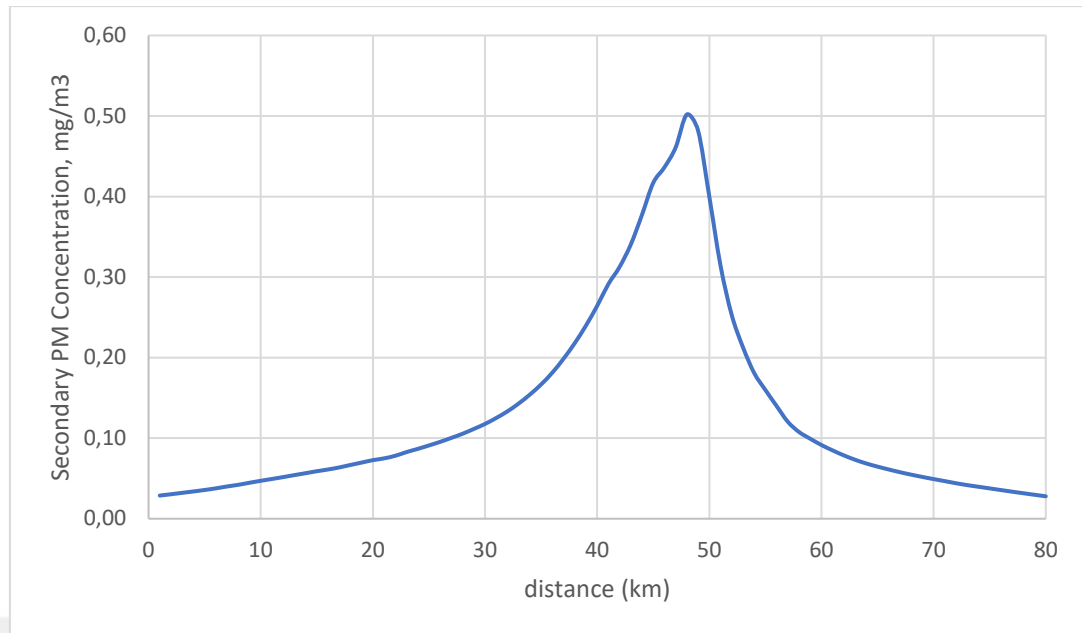
Figure 5.43. Annual Secondary PM concentration along section perpendicular to the Bosphorus.
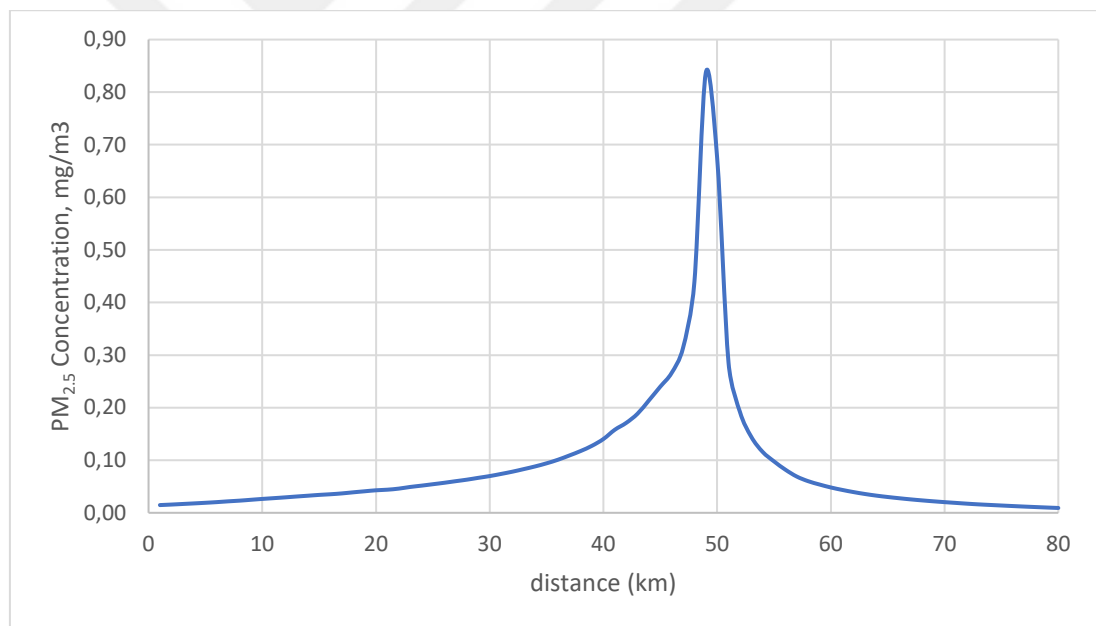
Figure 5.44. Annual total PM$_{2.5}$ concentration along section perpendicular to the Bosphorus.

Figures 5.39. to 5.44 show the annually average pollutant concentrations along the selected selection perpendicular to the Bosphorus. It can be seen from the plots that SO$_2$, NO$_2$, PM10 and PM2.5 concentrations rapidly decrease with distance from the source. However, change in the secondary PM is less compared to other pollutants. This is attributed to the fact that the secondary PM are not released at the emission source along the Bosphorus but are formed through a series of atmospheric reactions from the NO$_2$ and SO$_2$ emissions with the background ammonia and ozone

concentrations. It can be seen from the plots that, even though decay in the concentraions for all the pollutants very fast, still dense populated areas allong the coast are effected by the released emissions.

5.2. Health Impacts

Human health impacts and the external costs are calculated using EVA method and the annually averaged pollutant concentrations from the CALPUFF model for the year 2017. Table 5.2. shows simulated annual concentration of pollutant in each district in Istanbul. TurkStat, address-based population for the year 2017, was used for each neighborhood population. A total of 964 neighborhoods population were taken into account for exposure calculations covering the entire city of Istanbul. Exposure-response coefficients are taken from the EVA model (Brandt et al., 2013). Figures 5.45, 5.46, 5.47 and 5.48 present the concentration of the pollutants, SO_2, NO_2, primary PM, secondary PM and $PM_{2.5}$ at the 39 district in Istanbul. These plots were calculated from the concentrations of individual neighbourhoods within each district.
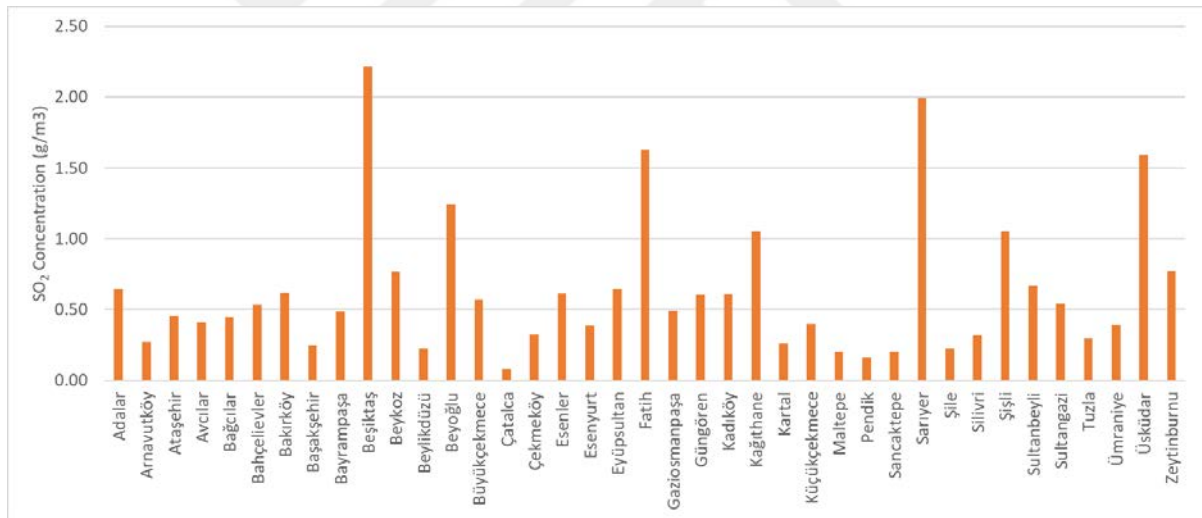
Figure 5.45. Annual SO2 concentration at each district in Istanbul for 2017.
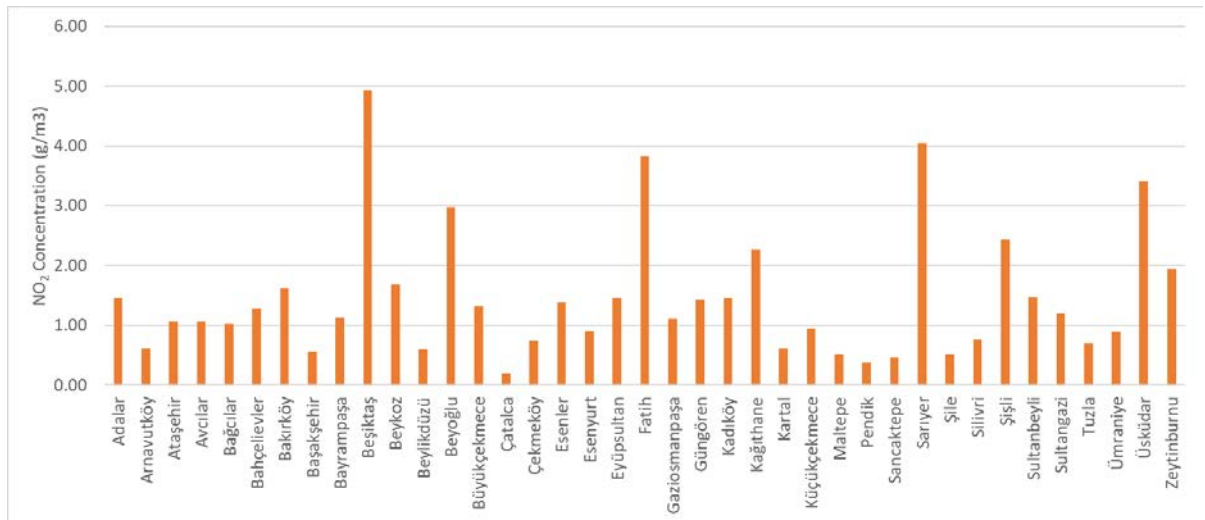
Figure 5.46. Annual NO2 concentration at each district in Istanbul for 2017.
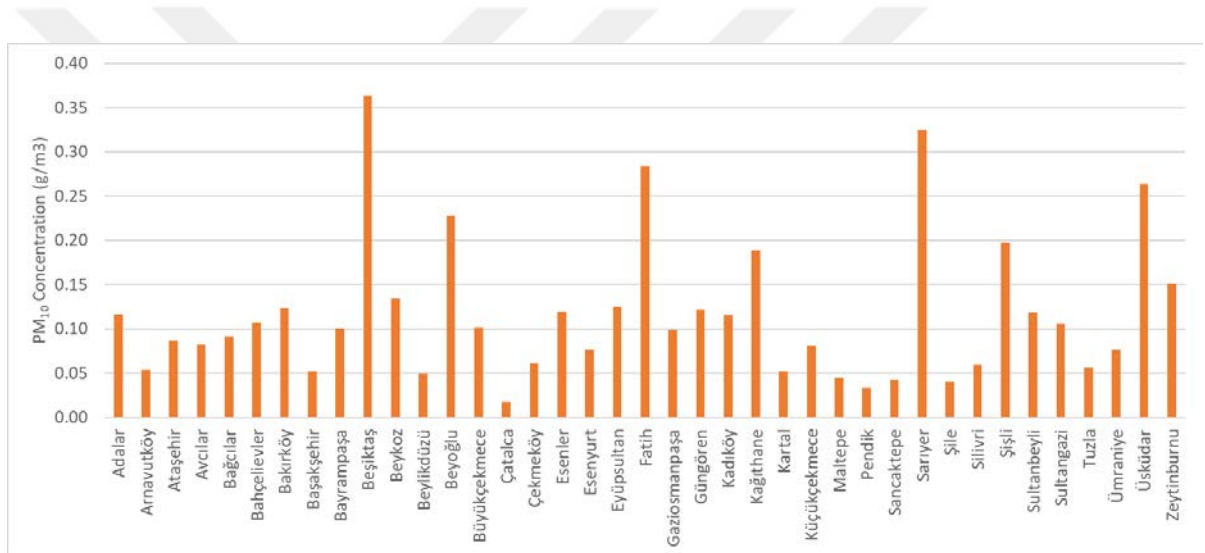
Figure 5.47. Annual primary PM concentration at each district in Istanbul for 2017.
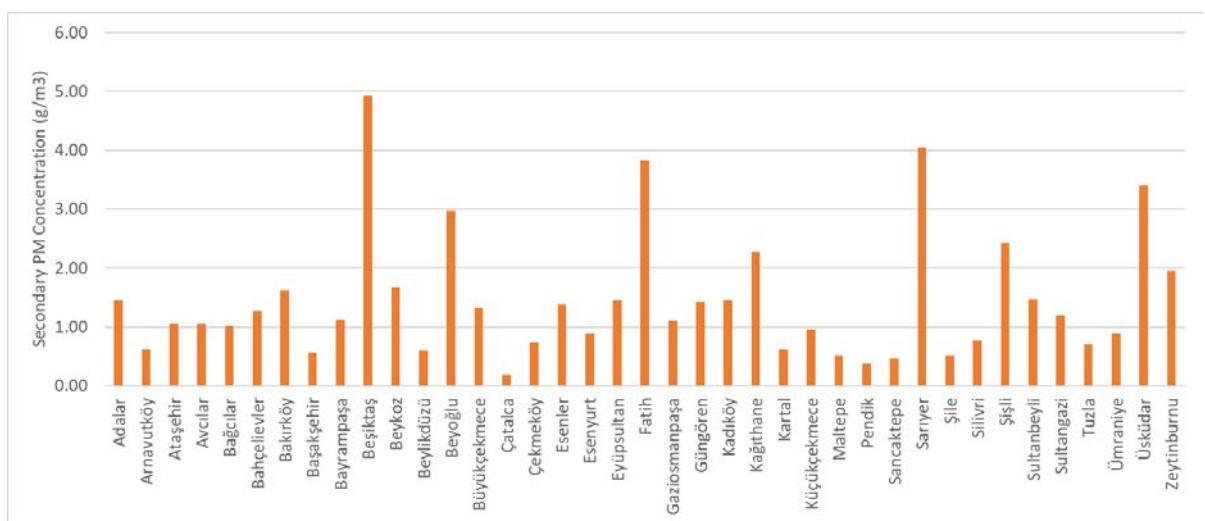
Figure 5.48. Annual secondary PM concentration at each district in Istanbul for 2017.

It is observed that Beşiktaş, Sarıyer, Üsküdar, Beyoğlu, Şişli and Kadıköy districts located along the Bosphorus shore have the highest concentration of pollutants. These districts also have very dense population, and this makes study of health effect and health-related external costs very important since the large populations are exposed to pollutants. Silivri, Şile, Çatalca and Kartal are some of the districts that are exposed least to pollutants because of this relatively distant location from the Bosphorus. Table 5.3 lists the average annual concentrations for each district.
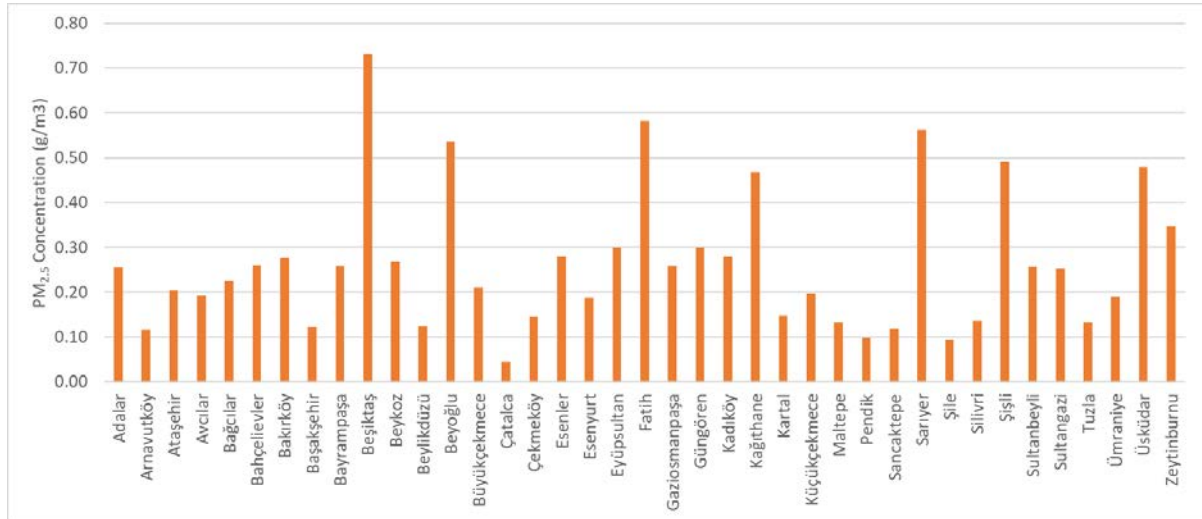
Figure 5.49. Annual total PM$_{2.5}$ concentration at each district in Istanbul for 2017.

Table 5.4. presents the estimated number of cases for different health impacts of air pollution caused by transit ship traffic in Istanbul for year 2017. There were total number of 2,500,000 health-related cases estimated. The vast majority of these cases are asthma due to PM exposure. Among the asthma cases, nearly 35 % of cases are children of aged less than 14, and 65 % are adults aged more than 15. When age groups examined, asthma has more impact on children compared to adults where the nearly 19 % of the children population suffers from asthma compared to around 16 % among the adults population. Nearly half of the asthma cases suffered from coughing, followed by bronchodilator use with 34 % of the overall asthma cases and lower respiratory symptoms with 17 % where the majority of cases are adults. The number of restricted activity days estimated was 1995. Another important health impact is the number of lung cancer caused by ship emission; it is estimated that PM caused 47 cases in 2017 while SO$_2$ caused 69 cases.

The total health-related external costs caused by transit ship emission are presented in Figure 5.4. Estimated total external costs were 83.1 million EUR in 2017. Nearly 75 % of the overall costs were contributed by years of life lost from acute mortality caused by SO$_2$ and years of life lost from

chronic mortality caused by PM. Cost of asthma, observed among adults and children combined, caused by PM pollution follows with total of 9 % percent share in the overall cost when combined.

Table 5.3. Simulated annual concentration for each district in Istanbul.

District	SO2 µg/m3	NO2 µg/m3	Primary PM µg/m3	Secondary PM µg/m3	PM2.5 µg/m3
Adalar	0.64	1.46	0.12	0.18	0.26
Arnavutköy	0.27	0.61	0.05	0.08	0.12
Ataşehir	0.46	1.06	0.09	0.15	0.20
Avcılar	0.41	1.06	0.08	0.14	0.19
Bağcılar	0.45	1.02	0.09	0.16	0.23
Bahçelievler	0.53	1.27	0.11	0.19	0.26
Bakırköy	0.62	1.63	0.12	0.19	0.28
Başakşehir	0.24	0.56	0.05	0.09	0.12
Bayrampaşa	0.49	1.13	0.10	0.19	0.26
Beşiktaş	2.22	4.93	0.36	0.49	0.73
Beykoz	0.77	1.68	0.13	0.18	0.27
Beylikdüzü	0.22	0.60	0.05	0.09	0.12
Beyoğlu	1.24	2.98	0.23	0.38	0.54
Büyükçekmece	0.57	1.32	0.10	0.14	0.21
Çatalca	0.08	0.19	0.02	0.03	0.04
Çekmeköy	0.32	0.74	0.06	0.11	0.15
Esenler	0.61	1.39	0.12	0.20	0.28
Esenyurt	0.38	0.90	0.08	0.14	0.19
Eyüpsultan	0.65	1.46	0.13	0.22	0.30
Fatih	1.63	3.83	0.28	0.39	0.58
Gaziosmanpaşa	0.49	1.10	0.10	0.19	0.26
Güngören	0.60	1.42	0.12	0.22	0.30
Kadıköy	0.61	1.46	0.12	0.20	0.28
Kağıthane	1.05	2.27	0.19	0.34	0.47
Kartal	0.26	0.61	0.05	0.11	0.15
Küçükçekmece	0.40	0.95	0.08	0.14	0.20
Maltepe	0.20	0.51	0.04	0.10	0.13
Pendik	0.16	0.38	0.03	0.08	0.10
Sancaktepe	0.20	0.47	0.04	0.09	0.12
Sarıyer	2.00	4.04	0.32	0.35	0.56
Şile	0.22	0.51	0.04	0.07	0.09
Silivri	0.32	0.77	0.06	0.10	0.14
Şişli	1.06	2.43	0.20	0.36	0.49
Sultanbeyli	0.67	1.48	0.12	0.18	0.26
Sultangazi	0.54	1.20	0.11	0.18	0.25
Tuzla	0.30	0.70	0.06	0.10	0.13
Ümraniye	0.39	0.89	0.08	0.14	0.19
Üsküdar	1.59	3.41	0.26	0.30	0.48
Zeytinburnu	0.77	1.95	0.15	0.25	0.35

Table 5.4. Health impacts of the air pollution caused by the ship traffic in Istanbul, 2017.

Health impact		Number cases in Istanbul
Morbidity	Chronic Bronchitis (PM)	238
	Restricted Activity Days (PM)	2011
	Congestive Heart Failure (PM)	117
	Lung Cancer (PM)	48
Hospital Admissions	Respiratory (PM)	13
	Respiratory (SO2)	18
	Cerebrovascular (PM)	32
Asthma, children <15 yr	Bronchodilator use (PM)	115230
	Cough (PM)	398393
	Lower respiratory symptoms (PM)	153640
Astma, adults ≥15 yr	Bronchodilator use (PM)	788737
	Cough (PM)	811936
	Lower respiratory symptoms (PM)	292877
Mortality	Acute Mortality SO2	68
	Chronic Mortality years of life lost (PM)	2274
	Infant Mortality (PM)	0

Table 5.5. External costs of the air pollution caused by the ship traffic in Istanbul, 2017.

Health impact		The total external costs in Euros
Morbidity	Chronic Bronchitis (PM)	2405332
	Restricted Activity Days (PM)	50327
	Congestive Heart Failure (PM)	367333
	Lung Cancer (PM)	193082
Hospital Admissions	Respiratory (PM)	19880
	Respiratory (SO2)	26593
	Cerebrovascular (PM)	61287
Asthma, children <15 yr	Bronchodilator use (PM)	506207
	Cough (PM)	4489491
	Lower respiratory symptoms (PM)	469525
Astma, adults ≥15 yr	Bronchodilator use (PM)	3464923
	Cough (PM)	9149701
	Lower respiratory symptoms (PM)	895031
Mortality	Acute Mortality SO2	27248961
	Chronic Mortality years of life lost (PM)	33522517
	Infant Mortality (PM)	251421

6. CONCLUSION

Air pollution has become a major concern as a result of the rapid growth of cities. Worldwide, the majority of the human population is living in cities where the main sources of air pollution are concentrated such as energy consumption, industrial activities and traffic. Exposure to air pollution, increases the risk of diseases such as, chronic bronchitis, congestive heart failure and lung cancer. Air pollution is not only associated with health risks, it also has an economic burden by causing productivity losses and healthcare costs. In this study, the contribution of transit marine traffic through the Bosphorus (Istanbul Strait) on the air quality of Istanbul is to evaluated.

EPA-approved CALMET Meteorological Model and CALPUFF atmospheric dispersion modelling computer programs were used to simulate the air pollutant concentration distributions resulting from maritime traffic for the year 2017. Hourly SO_2, NO_2, SO_4, NO_3 and PM_{10} concentrations were calculated in the model domain. Then the corresponding health impacts and related health costs due to emissions from maritime traffic is estimated using the EVA (Economic Valuation of Air pollution) methodology for the year 2017.

The results show that, the yearly average impact due to ship emissions is upto 60 % of the SO_2 Turkish air quality standard, nearly 35 % of the NO_2 Turkish air quality standard and approximately 2.5 % of the PM_{10} Turkish air quality standard. Primary pollutant concentrations however tend to decrease rapidly with distance from the Bosphorus. Hoever, secondary pollutant sources sucha s secondary PM tend to spread more over the city because they formed in the atmosphere due to various chemical reactions. The corresponding health impacts expressed in morbidity and premature mortality estimates as significant. It is estimated the the maritime traffic through the bosphorus is causing about 2,500,000 adverse health incidents, the vast majority are asthma. More severe morbidity impacts include 47 cases of lung cancer and 116 cases of congestive heart failure. The model also estimates 68 cases of acute death and 2255 of YOLL. The total associated health-related costs are estimated to be 83.1 million euros.

As a conclusion, given the proximity of large populations to the Bosphorus strait and the large volume of maritime traffic that passes thorugh it, there is a need to impose stricter standards on ship stack emissions. CALPUFF Modeling system can be used to estimate the concentrations originating from ship emissions for impact assessment and management purposes. Future reseach can examine how pollutant level calculations can be improved. Since the strait is very narrow in some sections,

smaller grids can be used for better estimation. Also, no overwater surface meteorological data was available, numerical weather prediction systems such as WRF (Weather Reseach and Forecasting) Model can be used for a more accurate wind field calculation. Future reseach could also consider similar studies to other coastal areas of Turkey or the world where martime traffic is concentrated.

REFERENCES

Akkoyunlu, A., and Erturk, F. (2002). Evaluation of air pollution trends in Istanbul. International Journal of Environment and Pollution, 18. https://doi.org/10.1504/IJEP.2002.003735.

Allwine, J., and Whiteman, C. D. (1985). MELSAR: a mesoscale air quality model for complex terrain. Volume 1. Overview, technical description and user's guide. https://doi.org/10.2172/5899806.

Altan, Y. C. (2017). Analysis and Modelig of Maritime Traffic and Ship collision in the Strait of Istanbul Based on Automatic Vessel Tracking System. Boğaziçi University.

Bennett, M. J., Yansura, M. E., Hornyik, I. G., Nall, J. M., Caniparoli, D. G., and Ashmore, C. G. (2002, June 23). Evaluation of the CALPUFF Long-range Transport Screening Technique by Comparison to Refined CALPUFF Results for Several Power Plants in Both the Eastern and Western United States. Presented at the Proceedings of the Air and Waste Management Association's 95th Annual Conference.

Benson, P. E. (1992). A review of the development and application of the CALINE3 and 4 models. Atmospheric Environment. Part B. Urban Atmosphere, 26(3), 379–390. https://doi.org/10.1016/0957-1272(92)90013-I.

Bey, I., Jacob, D. J., Yantosca, R. M., Logan, J. A., Field, B. D., Fiore, A. M., … Schultz, M. G. (2001). Global modeling of tropospheric chemistry with assimilated meteorology: Model description and evaluation. Journal of Geophysical Research: Atmospheres, 106(D19), 23073–23095. https://doi.org/10.1029/2001JD000807.

Bozyazi, E., Incecik, S., Mannaerts, C. M., and Brussel, M. (2000). Analysis and mapping of air pollution using a GIS approach: A case study of Istanbul. Advances in Air Pollution, 8, 431–440.

Brandt, J., Mikkelsen, T., Thykier-Nielsen, S., and Zlatev, Z. (1996). The Danish Rimpuff and Eulerian accidental release model (the DREAM). Physics and Chemistry of the Earth, 21(5–6), 441–444. https://doi.org/10.1016/S0079-1946(97)81139-1.

Brandt, J., Silver, J. D., Christensen, J. H., Andersen, M. S., Bønløkke, J. H., Sigsgaard, T., … Frohn, L. M. (2013). Contribution from the ten major emission sectors in Europe and Denmark to the health-cost externalities of air pollution using the EVA model system – an integrated modelling approach. Atmospheric Chemistry and Physics, 13(15), 7725–7746. https://doi.org/10.5194/acp-13-7725-2013.

Brandt, Jørgen, Frohn, L., Christensen, J., Andersen, M., Hertel, O., Geels, C., … Skjøth, C. (2013). Assessment of health-cost externalities of air pollution at the national level using the EVA model system.

Brandt, Jørgen, Silver, J. D., Frohn, L., Geels, C., Gross, A., Hansen, A., … Christensen, J. (2012). An integrated model study for Europe and North America using the Danish Eulerian Hemispheric Model with focus on intercontinental transport of air pollution. Atmospheric Environment, 53, 156–176. https://doi.org/10.1016/j.atmosenv.2012.01.011.

Byun, D., and Schere, K. L. (2006). Review of the Governing Equations, Computational Algorithms, and Other Components of the Models-3 Community Multiscale Air Quality (CMAQ) Modeling System. Applied Mechanics Reviews, 59(2), 51–77. https://doi.org/10.1115/1.2128636.

Carruthers, D. J., Holroyd, R. J., Hunt, J. C. R., Weng, W. S., Robins, A. G., Apsley, D. D., … Smith, F. B. (1994). UK-ADMS: A new approach to modelling dispersion in the earth's atmospheric boundary layer. Journal of Wind Engineering and Industrial Aerodynamics, 52, 139–153. https://doi.org/10.1016/0167-6105(94)90044-2.

Carson, D. J. (1973). The development of a dry inversion-capped convectively unstable boundary layer. Quarterly Journal of the Royal Meteorological Society, 99(421), 450–467. https://doi.org/10.1002/qj.49709942105.

Chen, D., Zhao, Y., Nelson, P., Li, Y., Wang, X., Zhou, Y., … Guo, X. (2016). Estimating ship emissions based on AIS data for port of Tianjin, China. Atmospheric Environment, 145, 10–18. https://doi.org/10.1016/j.atmosenv.2016.08.086.

Christensen, J. H. (1997). The Danish eulerian hemispheric model—A three-dimensional air pollution model used for the arctic. Atmospheric Environment, 31(24), 4169–4191. https://doi.org/10.1016/S1352-2310(97)00264-1.

Cimorelli, A. J., Perry, S. G., Venkatram, A., Weil, J. C., Paine, R. J., Wilson, R. B., … Brode, R. W. (2005). AERMOD: A Dispersion Model for Industrial Source Applications. Part I: General Model Formulation and Boundary Layer Characterization. Journal of Applied Meteorology, 44(5), 682–693. https://doi.org/10.1175/JAM2227.1.

Crank, J. (1975). The mathematics of diffusion (2d ed). Oxford, [Eng]: Clarendon Press.

Danielson, J. J., and Gesch, D. B. (2011). Global multi-resolution terrain elevation data 2010 (GMTED2010) (Report No. 2011–1073). https://doi.org/10.3133/ofr20111073.

DiCristofaro, D. C., and Hanna, S. R. (1991). The Offshore and Coastal Dispersion (OCD) Model: Revisions and Evaluations. In H. van Dop and D. G. Steyn (Eds.), Air Pollution Modeling and Its Application VIII (pp. 759–768). https://doi.org/10.1007/978-1-4615-3720-5_88.

Douglas, S., and Kessler, R. (1988). User's guide to the diagnostic wind field model (Version 1.0) (p. 48). San Rafael, CA: Systems Applications, Inc.

Elbir, T., Mangır, N., and Kara, M. (2015). Air quality dispersion modeling in the city of Istanbul by CALMET/CALPUFF modeling system. Presented at the 18th ISERD International Conference, Tokyo, Japan.

Elbir, Tolga, Mangir, N., Kara, M., Simsir, S., Eren, T., and Ozdemir, S. (2010). Development of a GIS-based decision support system for urban air quality management in the city of Istanbul. Atmospheric Environment, 44(4), 441–454. https://doi.org/10.1016/j.atmosenv.2009.11.008.

Endresen, Ø., Sørgård, E., Behrens, H. L., Brett, P. O., and Isaksen, I. S. A. (2007). A historical reconstruction of ships' fuel consumption and emissions. Journal of Geophysical Research: Atmospheres, 112(D12). https://doi.org/10.1029/2006JD007630.

Erturk, F. (1986). Investigation of strategies for the control of air pollution in the Golden Horn region, Istanbul, using a simple dispersion model. Environmental Pollution Series B, Chemical and Physical, 11(3), 161–168. https://doi.org/10.1016/0143-148X(86)90021-2.

Eyring, V., Köhler, H. W., van Aardenne, J., and Lauer, A. (2005). Emissions from international shipping: 1. The last 50 years. Journal of Geophysical Research: Atmospheres, 110(D17). https://doi.org/10.1029/2004JD005619.

Gesch, D. B., Verdin, K. L., and Greenlee, S. K. (1999). New land surface digital elevation model covers the Earth. Eos, Earth and Space Science News, 80(6), 69–70. https://doi.org/10.1029/99EO00050.

Gosman, A. D., and loannides, E. (1983). Aspects of Computer Simulation of Liquid-Fueled Combustors. Journal of Energy, 7(6), 482–490. https://doi.org/10.2514/3.62687.

Holtslag, A. A. M., and Van Ulden, A. P. (1983). A Simple Scheme for Daytime Estimates of the Surface Fluxes from Routine Weather Data. Journal of Climate and Applied Meteorology, 22(4), 517–529. Retrieved from JSTOR.

Jalkanen, J.-P., Brink, A., Kalli, J., Pettersson, H., Kukkonen, J., and Stipa, T. (2009). A modelling system for the exhaust emissions of marine traffic and its application in the Baltic Sea area. Atmospheric Chemistry and Physics, 9(23), 9209–9223. https://doi.org/10.5194/acp-9-9209-2009.

Jones, A., Thomson, D., Hort, M., and Devenish, B. (2007). The U.K. Met Office's Next-Generation Atmospheric Dispersion Model, NAME III. In C. Borrego and A.-L. Norman (Eds.), Air Pollution Modeling and Its Application XVII (pp. 580–589). Boston, MA: Springer US.

Jones, R., Lehr, W., Simecek-Beatty, D., and Reynolds, R. M. (2013). ALOHA® (Areal Locations Of Hazardous Atmospheres) 5.4.4: Technical Documentation (p. 96). Retrieved from https://response.restoration.noaa.gov/sites/default/files/ALOHA_Tech_Doc.pdf.

Kalhor, M., and Bajoghli, M. (2017). Comparison of AERMOD, ADMS and ISC3 for incomplete upper air meteorological data (case study: Steel plant). Atmospheric Pollution Research, 8(6), 1203–1208. https://doi.org/10.1016/j.apr.2017.06.001.

Leelőlssy, Á., Molnár, F., Izsák, F., Havasi, Á., Lagzi, I., and Mészáros, R. (2014). Dispersion modeling of air pollutants in the atmosphere: A review. Central European Journal of Geosciences, 6(3), 257–278. https://doi.org/10.2478/s13533-012-0188-6.

Levy, J. I., Spengler, J. D., Hlinka, D., Sullivan, D., and Moon, D. (2002). Using CALPUFF to evaluate the impacts of power plant emissions in Illinois: Model sensitivity and implications. Atmospheric Environment, 36(6), 1063–1075. https://doi.org/10.1016/S1352-2310(01)00493-9.

Liu, M.-K., and Yocke, M. A. (1980). Siting of Wind Turbine Generators in Complex Terrain. Journal of Energy, 4(1), 10–16. https://doi.org/10.2514/3.62455.

Lockwood, F. C., and Naguib, A. S. (1975). The prediction of the fluctuations in the properties of free, round-jet, turbulent, diffusion flames. Combustion and Flame, 24, 109–124. https://doi.org/10.1016/0010-2180(75)90133-9.

Miola, A., and Ciuffo, B. (2011). Estimating air emissions from ships: Meta-analysis of modelling approaches and available data sources. Atmospheric Environment, 45(13), 2242–2251. https://doi.org/10.1016/j.atmosenv.2011.01.046.

NCDC TD3505 Integrated Surface Hourly Data. (2005). Retrieved from http://rda.ucar.edu/datasets/ds463.3/.

O'Brien, J. J. (1970). A Note on the Vertical Structure of the Eddy Exchange Coefficient in the Planetary Boundary Layer. Journal of the Atmospheric Sciences, 27(8), 1213–1215. https://doi.org/10.1175/1520-0469(1970)027<1213:ANOTVS>2.0.CO;2.

Perry, S. G. (1992). CTDMPLUS: A Dispersion Model for Sources near Complex Topography. Part I: Technical Formulations. Journal of Applied Meteorology, 31(7), 633–645. https://doi.org/10.1175/1520-0450(1992)031<0633:CADMFS>2.0.CO;2.

Perry, S. G., Burns, D. J., Adams, L. H., Paine, R. J., and Strimaitis, D. G. (1989). User's guide to the Complex-Terrain Dispersion Model Plus Algorithms for Unstable Situations (CTDMPLUS): Volume 1. Model description and user instructions.

Piedelièvre, J. P., Musson-Genon, L., and Bompay, F. (1991). Media: An Eulerian Model of Atmospheric Dispersion Validation on the Chernobyl Release. In H. van Dop and D. G. Steyn (Eds.), Air Pollution Modeling and Its Application VIII (pp. 597–599). https://doi.org/10.1007/978-1-4615-3720-5_55.

Pozorski, J., and Minier, J.-P. (1998). On the Lagrangian turbulent dispersion models based on the Langevin equation. International Journal of Multiphase Flow, 24(6), 913–945. https://doi.org/10.1016/S0301-9322(98)00016-0.

Scire, J. S., Insley, E. M., and Yamartino, R. J. (1990). Model formulation and user's guide for the CALMET meteorological model. Concord, MA: Sigma Research Corporation.

Seinfeld, J. H., and Pandis, S. N. (2006). Atmospheric chemistry and physics: From air pollution to climate change (2nd ed). Hoboken, N.J: J. Wiley.

Shearer, A. J., Tamura, H., and Faeth, G. M. (1979). Evaluation of a Locally Homogeneous Flow Model of Spray Evaporation. Journal of Energy, 3(5), 271–278. https://doi.org/10.2514/3.62437.

Shuen, J.-S., Chen, L.-D., and Faeth, G. M. (1983). Evaluation of a stochastic model of particle dispersion in a turbulent round jet. AIChE Journal, 29(1), 167–170. https://doi.org/10.1002/aic.690290127.

Snyder, W. H., Thompson, R. S., Eskridge, R. E., Lawson, R. E., Castro, I. P., Lee, J. T., … Ogawa, Y. (1985). The structure of strongly stratified flow over hills: Dividing-streamline concept. Journal of Fluid Mechanics, 152, 249–288. https://doi.org/10.1017/S0022112085000684.

Stein, A. F., Draxler, R. R., Rolph, G. D., Stunder, B. J. B., Cohen, M. D., and Ngan, F. (2015). NOAA's HYSPLIT Atmospheric Transport and Dispersion Modeling System. Bulletin of the American Meteorological Society, 96(12), 2059–2077. https://doi.org/10.1175/BAMS-D-14-00110.1.

Stockie, J. M. (2011). The Mathematics of Atmospheric Dispersion Modeling. SIAM Review, 53(2), 349–372. https://doi.org/10.1137/10080991X.

Stohl, A., Forster, C., Frank, A., Seibert, P., and Wotawa, G. (2005). Technical note: The Lagrangian particle dispersion model FLEXPART version 6.2. Atmospheric Chemistry and Physics, 5(9), 2461–2474. https://doi.org/10.5194/acp-5-2461-2005.

Stohl, A., Hittenberger, M., and Wotawa, G. (1998). Validation of the lagrangian particle dispersion model FLEXPART against large-scale tracer experiment data. Atmospheric Environment, 32(24), 4245–4264. https://doi.org/10.1016/S1352-2310(98)00184-8.

Suh, K.-S., Han, M.-H., Jung, S.-H., and Lee, C.-W. (2009). Numerical simulation for a long-range dispersion of a pollutant using Chernobyl data. Mathematical and Computer Modelling, 49(1), 337–343. https://doi.org/10.1016/j.mcm.2008.01.008.

Trozzi, C. (2010). Emission estimate methodology for maritime navigation. Türk Boğazları Gemi Geçiş İstatistikleri. (2017). Retrieved from https://atlantis.udhb.gov.tr/istatistik/gemi_gecis.aspx.

United States Geological Survey. (n.d.). United States Geological Survey: Land Cover Products. Retrieved from https://www.usgs.gov/centers/eros/science/usgs-eros-archive-land-cover-products-global-land-cover-characterization-glcc?qt-science_center_objects=0#qt-science_center_objects.

van der Gon, H. D., and Hulskotte, J. (2010). Methodologies for estimating shipping emissions in the Netherlands. Netherland Environmental Assessment Agency.

Venkatram, A. (1980). Estimating the Monin-Obukhov length in the stable boundary layer for dispersion calculations. Boundary-Layer Meteorology, 19(4), 481–485. https://doi.org/10.1007/BF00122347.

Whall, C., Scarbrough, T., and Stavrakaki, A. (2010). Defra UK ship emissions inventory. Final report. London: Entec UK Limited.

Williams, M., and Yamada, T. (1990). A Microcomputer-based Forecasting Model: Potential Applications for Emergency Response Plans and Air Quality Studies. Journal of the Air and Waste Management Association, 40(9), 1266–1274. https://doi.org/10.1080/10473289.1990.10466781.

Yamada, T., Bunker, S., and Moss, M. (1992). Numerical Simulations of Atmospheric Transport and Diffusion over Coastal Complex Terrain. Journal of Applied Meteorology, 31(6), 565–578. https://doi.org/10.1175/1520-0450(1992)031<0565:NSOATA>2.0.CO;2.

Zhou, Y., Levy, J. I., Hammitt, J. K., and Evans, J. S. (2003). Estimating population exposure to power plant emissions using CALPUFF: a case study in Beijing, China. Atmospheric Environment, 37(6), 815–826. https://doi.org/10.1016/S1352-2310(02)00937-8.